# UNCLASSIFIED

## REPORT DOCUMENTATION PAGE

*Form Approved OMB No. 0704-0188*



| 1. AGENCY USE ONLY *(Leave blank)* | 2. REPORT DATE | 3. REPORT TYPE AND DATES COVERED |
|---|---|---|
| | 89-11-29 | technical |

**4. TITLE AND SUBTITLE**

Self-Calibrating Apparatus To Find Dynamic Compressibility of Organic Solids

**5. FUNDING NUMBERS**

ARL:UT Independent Research and Development Program

**6. AUTHORS**

David E. Edmonds

**7. PERFORMING ORGANIZATION NAME(S) AND ADDRESS(ES)**

Applied Research Laboratories
The University of Texas at Austin
P.O. Box 8029
Austin, Texas 78713-8029

**8. PERFORMING ORGANIZATION REPORT NUMBER**

ARL-TR-89-53

**9. SPONSORING / MONITORING AGENCY NAME(S) AND ADDRESS(ES)**

Applied Research Laboratories
The University of Texas at Austin
P.O. Box 8029
Austin, Texas 78713-8029

**10. SPONSORING / MONITORING AGENCY REPORT NUMBER**

**11. SUPPLEMENTARY NOTES**

**12a. DISTRIBUTION / AVAILABILITY STATEMENT**

Approved for public release; distribution is unlimited.

**12.b. DISTRIBUTION CODE**

**13. ABSTRACT** *(Maximum 200 words)*

A self-calibrating apparatus has been developed to measure the adiabatic dynamic compressibility of organic solids. The test chamber is a small cavity where bulk cyclic compression is accomplished and monitored with piezoelectric transducers (simple disks). This chamber is different from other chambers of similar design in that it can be re-calibrated at each data point without changing static pressure, opening the chamber, or using a calibration sample. Self-calibration is accomplished using a chamber cavity which is divided into a *main* chamber and two *side-chambers*. One side-chamber contains the sample suspended in pressure fluid; the other contains only pressure fluid. The main chamber contains transducers and a remotely operated *door*. The door may close off either side-chamber or be left open, allowing the three measurement conditions required to calibrate the chamber. This eliminates two sources of error associated with making separate runs to calibrate the chamber: the reproducibility of the re-assembly process, and the effect of pressure history on the transducer's calibration. The ranges of the equipment are: pressure 0-70 MPa (10,000 psi), temperature 0-80°C, and frequencies generally below 2000 Hz. Much of the measurement process is monitored or controlled by a Hewlett-Packard HP-85 desktop computer through DC control voltages or an HPIB bus. Data were taken in isothermal runs at pressures stepped down from 8000 or 10,000 psi in 2000, 1000, or 500 psi increments. Poly(vinyl acetate) (PVAc), and polytetrafluoroethylene (Teflon) were tested and the results compared to data obtained by other researchers using other means. This comparison showed that the apparatus yields reliable, useful data.

| 14. SUBJECT TERMS | | | 15. NUMBER OF PAGES |
|---|---|---|---|
| adiabatic dynamic compressibility | dynamic compressibility | polymer | 86 |
| lumped element method | polytetrafluoroethylene | Teflon | 16. PRICE CODE |
| poly(vinyl acetate) | di(2 ethyl hexyl)sebacate | pressure tests | |

| 17. SECURITY CLASSIFICATION OF REPORT | 18. SECURITY CLASSIFICATION OF THIS PAGE | 19. SECURITY CLASSIFICATION OF ABSTRACT | 20. LIMITATION OF ABSTRACT |
|---|---|---|---|
| UNCLASSIFIED | UNCLASSIFIED | UNCLASSIFIED | SAR |



# UNCLASSIFIED

## TABLE OF CONTENTS

## LIST OF TABLES

## LIST OF FIGURES

## FOREWORD

This report is an adaptation of the thesis of the same title written by David E. Edmonds. Mr. Edmonds was enrolled in the Department of Mechanical Engineering at The University of Texas at Austin for his graduate work, and received a degree of Master of Science in Engineering in August 1989.

The work was an Independent Research and Development project at Applied Research Laboratories, The University of Texas at Austin, and was performed between September 1986 and September 1989.

A. W. Nolle
Supervisor

# CHAPTER 1

## Introduction

*Adiabatic Dynamic Compressibility* is a material property that is important in some organic solids' applications. *Compressibility* is as much as it says: the ability of a material to be compressed from all sides. It is numerically equal to the inverse of bulk modulus:

$$\beta = \frac{1}{K} \quad ,$$

where $\beta$ is compressibility and K is bulk modulus. The units used for $\beta$ throughout this report will be $cm^2$/dyne. *Dynamic* compressibility implies small amplitude, finite frequency, repetitive loading of the material. Note that static pressure and frequency are variables in dynamic compressibility. *Adiabatic* dynamic compressibility is dynamic compressibility measured at a high enough frequency that no heat transfer occurs as the material is compressed cyclically—the temperature may go up and down during a cycle, but the heat energy contained in the sample stays the same. From now on in this report, we will use "dynamic compressibility" or simply "compressibility" to mean "adiabatic dynamic compressibility". Finally, in addition to the normal storage of energy implied by static compressibility, cyclic loading produces mechanical hysteresis-like losses (the sample absorbs or dissipates some energy each time it is compressed and allowed to expand again). Typically the magnitude of the loss part is only a few percent of the magnitude of the storage part of compressibility. Mathematically, and for the electronic analogy, we find it convenient to express compressibility as a complex number where the real part represents storage and the (negative) imaginary part represents loss. Dynamic compressibility, then, is written as a phasor:

$$\vec{\beta} = \beta_{(r)} + \mathring{\imath}\,\beta_{(\mathring{\imath})}$$

where the subscript '$_{(r)}$' denotes 'real,' '$_{(\mathring{\imath})}$' denotes 'imaginary,' and $\mathring{\imath}$ stands for $\sqrt{-1}$.

For *linear isotropic* materials (materials whose material properties do not change as they are mechanically stressed, and whose properties are the same in all directions), we need three complex parameters to describe their behavior under all types of mechanical stress. Often these parameters are bulk modulus K (or dynamic compressibility), sheer modulus G, and Young's modulus Y (other parameters can be described as a function of these). The speed of sound in a 3-dimensional medium (i.e., the *bulk wave speed*) is found using[1]

$$c_o = \left( \frac{K + \frac{4}{3}G}{\rho} \right)^{\frac{1}{2}} \qquad (1.1)$$

where $\rho$ is density. For rubberlike materials (including many organic polymers) G is very small compared to K and a useful lower limit of sound speed can be found using $\beta$ (=1/K) and $\rho$:

$$c_o \geq \sqrt{\frac{1}{\beta\rho}} \ .$$

For this project, we aimed at developing an apparatus to easily measure dynamic compressibility of the organic compounds used in sonar electroacoustic transducers. Sonar transducers are typically made with silver plated piezoelectric materials which, of course, cannot be put in seawater without some sort of coating. Often the transducers are constructed by mechanically isolating the active piezoelectric elements using corprene and/or stencil paper, then potting the result in polyurethane. Sonar designers choose isolating and potting materials based partially on their storage and loss compressibility under the conditions at which the sonar will operate. These conditions are a wide range of temperature, pressure, and frequency. Table 1.1 contains a summary of the desired ranges along with the specifications for our equipment. Notice that our equipment is limited to lower frequency tests. This limit is a function of the geometry of the chamber and the lumped element method we use to make our measurements. Several methods are available to measure dynamic compressibility (Figure 1.1). We have defined compressibility as a *bulk* parameter (1/K) which means compression must be from all directions, rather than along a single axis. This constraint almost necessitates fluid encasement of the sample. Cyclic compression of a fluid can be achieved by three related methods: traveling compression and rarefaction (sound) waves, standing sound waves, or bulk cyclic compression of fluid in a cavity. Traveling waves (Figure 1-1(A)) could be directed from a source, through the sample, and detected. The effects of the fluid and transducers could be subtracted out by superposition to find the effects of the sample. Singh and Nolle[2] measured absorption and approximate sound velocity in polyisobutalene

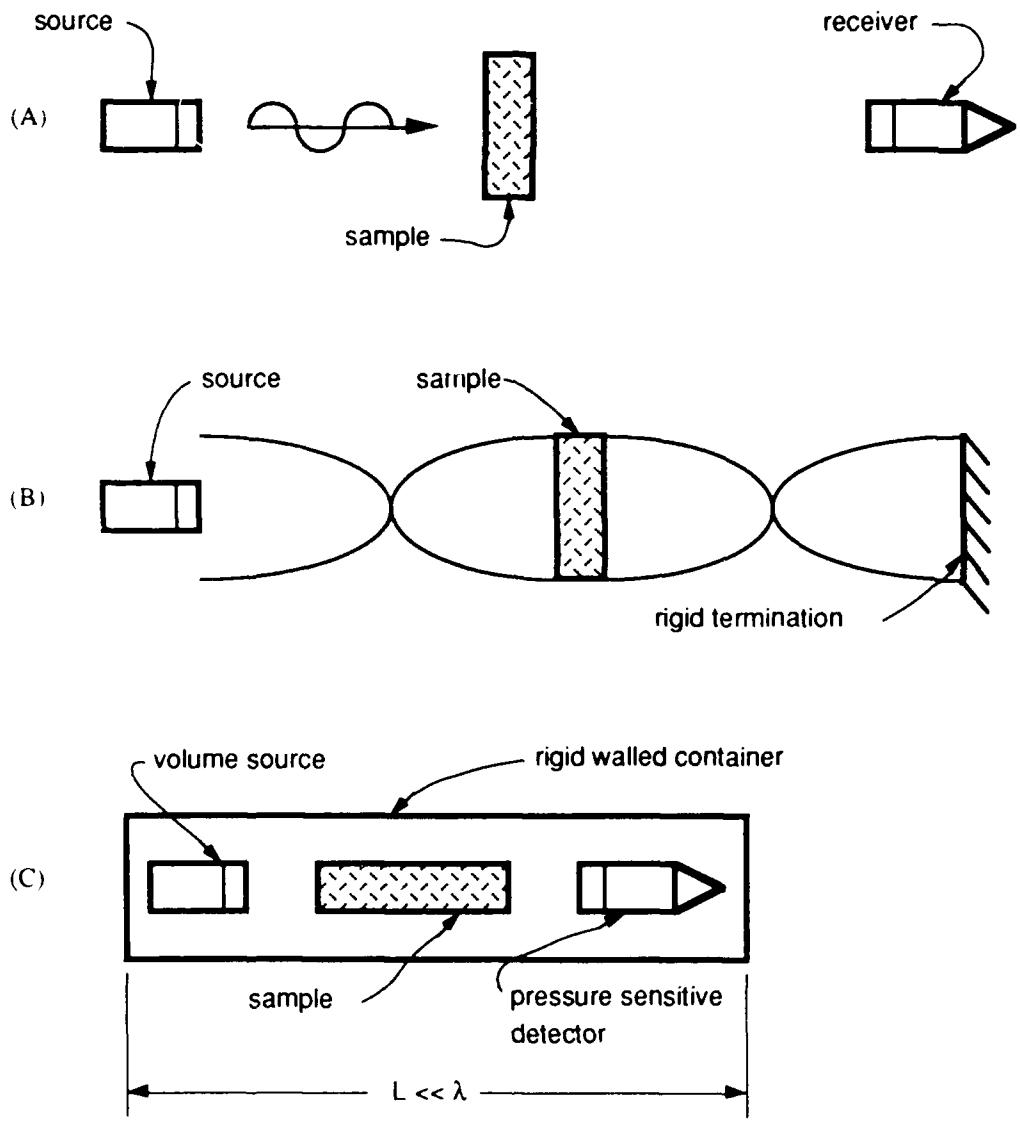


**Figure 1.1** THREE METHODS TO MEASURE DYNAMIC COMPRESSIBILITY: (A) WITH TRAVELING WAVES, (B) WITH STANDING WAVES, AND (C) BULK COMPRESSION OF FLUID AND SAMPLE. THE APPARATUS IN THIS REPORT USES METHOD (C).

AS-89-1525

with such an apparatus in 1959. A standing wave with the sample placed at a pressure antinode can also be used (Figure 1 1(B)). An approximation must be made that the dynamic pressure is constant throughout the sample; thus the sample must be only a small fraction of a wavelength thick. The mathematics would involve the change in resonant frequency versus the change in wavelength of the standing wave with and without the sample present in a particular standing wave field. Finally, if the chamber containing fluid, sample, and transducers is very small compared to the wavelength, a bulk cyclic compression of the fluid can be achieved (Figure 1 1(C)). This *lumped element method* invites the use of an electrical analogy where, say, pressure is analogous to voltage, and all the objects in the chamber are connected in parallel. We employ this method with our apparatus, as do many others (Refs. 3, 4, 5, 6, and 13). It is quite similar to the method pioneered by McKinney, Edelman, and Marvin[4] in 1956.

Our chamber is similar to that of McKinney, Edelman, and Marvin, but has an important difference: it is *self-calibrating*. Other chambers employing this method[3,4,5,6] consist basically of two small transducers and a space for a sample. Tests must be made with the chamber empty and again with a sample whose compressibility is known in order to calibrate the chamber before the unknown sample can be tested. Adding known and unknown samples requires depressurizing and taking apart the chamber. Inaccuracies creep in as the transducers' calibration may change with pressure history, and as the process to remove air from the chamber is imperfect. (The size and amount of small air bubbles left in the chamber is slightly different for each assembly.) In addition, the whole operation can take a few days if the chamber takes a while to come to thermal equilibrium after it is assembled. Our version of the chamber, by contrast, employs two *side-chambers*. These side-chambers share a door that can be moved to acoustically hide either side-chamber or can be left 'open'. With the sample placed in one side-chamber, and the other side-chamber left empty (containing only pressure fluid), we can

Table 1 1 DESIRED RANGES FOR CONDITIONS, AND RANGES FOR THE APPARATUS IN THIS REPORT.

| *condition* | *range desired* | *range for this equip.* |
|---|---|---|
| pressure | 0-10,000 psi | 0-10,000 psi |
| temperature | ≐0-80C | ≐0-80C |
| frequency | (as wide as possible) | ≐200-1400 Hz |

make the calibration measurements and the unknown measurement by simply moving the door. This method requires opening the chamber only to change unknown samples, needs no calibration sample, and, once set up, yields data points at 2 to 3 minute intervals.

The rest of this report explains the function of our chamber and gives a sample of our results compared to the results of others. Chapter 2 focuses on theory—the lumped element approximation and electronic analogies in general, then their application to this chamber. Chapter 3 contains extensive notes on the chamber's design, materials, construction, supporting apparatus, and computer hard and software. Chapter 4 presents and compares results for poly(vinyl acetate) (PVAc) and polytetrafluoroethylene (PTFE, or Teflon) to those of McKinney, Edelman, and Marvin,[4] Lin,[3] and others. Chapter 5 is a list of recommendations for work to be done that would improve the current equipment. Chapter 6 is a summary of the bulk of the material in this report.

# CHAPTER 2

# Theory

## 2–1 Overview of Dynamic Compressibility in Polymers

In this section we briefly present parts of a few theories which endeavor to explain the behavior of dynamic compressibility. We do this simply to help the reader visualize the happenings inside the sample as it is compressed. These succinct and conceptual notes are by no means a reliable authority on polymers or the free volume concept. For a detailed explanation of the basics of polymers, see Ralls, Courtney, and Wulff[8] (Chapters 6, and 18.8); for explanations of the free volume concept see Ferry;[9] and to learn about the free volume concept applied to dynamic compressibility, see the papers by McKinney and Belcher,[7] Liu,[3] or Burns *et al.*,[6] as well as the text by Ferry.[9] The following explanation draws repeatedly from each of these references.

*Organic compounds* are those derived from living or once living sources (e.g., fossil fuels). They are characterized by the fact that they are based in molecular carbon. The majority of these carbon compounds are, or behave like, polymers. *Polymers* consist of large molecules made up of many repetitions of a building block called a *monomer*. Monomers contain at least one carbon atom and a few other atoms (usually hydrogen). The important fact is that the carbon atoms in a monomer can bond to the carbon atoms of other monomers and form a chain—much like train cars or pop-beads. The chains can be straight, bent, branched, or even linked to themselves in places, and can be of any length. The length, the presence and orientation of other atoms in the monomers, the bonds, and other factors all determine the material properties of the polymer. The simplest 'poly'mer, ethane ($C_2H_6$), is a gas at room temperature, while the longer though still simple octane ($C_8H_{18}$), a constituent of gasoline, is a highly volatile liquid. A rubber tire, on the other hand, can be considered one huge polymer molecule twisted and connected to itself through a process called *vulcanizing*. The organic solids we deal with in this report are polymers which are solid at the

ranges of temperatures and pressures we address.

Polymers that are solid usually consist of molecules much too large to be gaseous, and too large and/or too tangled up with each other to be truly liquid. The solids are either rubbery or (for even larger and/or more tangled up molecules that are rubbery at higher temperatures) glassy. The temperature at which a particular polymer becomes glassy is called its *glass transition temperature*, $T_g$. The glass transition is marked by a sharp change in some mechanical properties, most notably a great increase in thermal expansivity above $T_g$ (see Ref. 9). Some solid polymers have crystal-like regions where molecules or parts of molecules have aligned themselves with each other or have wrapped around one another (forming *spherulites*). The crystallinity of a polymer depends on its make-up, shape, size, and the process by which it was manufactured. Because of the size of most polymer molecules, a polymer is almost never completely crystalline. The fact that two chemically equal polymers can have different amounts of crystallinity means that even different samples of the "same" polymer can have different properties.

Now that we have a glimpse of what a solid polymer is like, we would like to compress our solid polymer. A solid polymer's huge molecules, where they are not crystalline, can be thought of as like a huge plate of spaghetti with each strand wiggling due to thermal kinetic energy. Just as there is air trapped in amongst the noodles of spaghetti, there is empty space amongst the molecules of a polymer. This empty space is the polymer's *free volume*. Below $T_g$ the amount of free volume per molecule is usually quite small, but above $T_g$ free volume increases rapidly. (Recall that above its $T_g$, a polymer's thermal expansivity increases greatly. Most of this increase in expansivity is due to the increase of free volume in amongst the molecules.) Let us take a non-crystalline, solid polymer sample above its $T_g$. If we compress our sample hydraulically (i.e., from all sides), and quasi-statically (i.e., at an infinitesimal frequency), pieces of the molecules will bend around to take up less space. Simplistically, if a polymer molecule happens to be conveniently oriented next to a large enough free volume, it may move there, and our sample would get smaller at the expense of that free volume. The free volume concept is often applied to liquids in this way. In this case of a rubbery polymer, however, the molecules are so large that only segments of the molecules bend to re-pack into free volume spaces. If we had first cooled our sample below its $T_g$ it would have much less free volume and generally would not be able to compress by rearranging molecules or parts of molecules. Polymers below their $T_g$ are usually less compressible than polymers above their $T_g$. Similarly, crystalline regions have very little free volume (crystals are packed rather efficiently) and are less compressible than rubbery regions. At finite frequencies even polymers

above their $T_g$ may not have time to rearrange their molecules and will act glassy. The result is that at very low frequencies a polymer in its rubbery state may compress by using free volume as a liquid might, while at very high frequencies the same polymer may act like a glass. Since the compression mechanism changes as frequency becomes finite, the dynamic compressibility changes as a function of frequency. This is part of what makes static and dynamic compressibility differ. The range of frequencies where a sample acts not-quite-like-a-liquid but not-quite-like-a-glass is often referred to as the *dispersion region.* Finally, when the pressure is released (at any frequency), molecules return to their unstressed state. The free volume packing, and the twisting and stretching of chemical bonds requires some energy. When pressure is lowered, most of the energy is returned (constituting the storage part of dynamic compressibility), and the rest is lost as heat (constituting the loss part of dynamic compressibility). Typically, measurements are performed on a sample at some given hydrostatic pressure with relatively tiny dynamic hydraulic pressure variations superimposed (this is why dynamic compressibility is given at a particular temperature *and* pressure).

There is one other point worth mentioning at this time. If a sample undergoes a sudden temperature change, especially if it is close to its $T_g$, the amount of free volume present becomes very dependent on the new temperature and how long it has been at the new temperature. After anywhere from several minutes to hundreds of hours the free volume reaches the equilibrium value predicted by the thermal expansivity. The length of time depends on the new temperature relative to $T_g$ (less time for temperatures slightly above $T_g$), on the size of the temperature jump, and on the polymer. A similar phenomenon occurs for sudden changes in hydrostatic pressure. As a result even the temperature and pressure history of a sample can have some effect on its material properties (through the changes in free volume).

With these simple tools, we can now imagine what we would expect from a polymer under different conditions. At higher static pressures and/or lower temperatures (especially at temperatures below $T_g$) the molecules will typically be closer together and compressibility will be small. Similarly, at lower pressures/higher temperatures (especially at temperatures above $T_g$) compressibility will be large. A sample which has just undergone a sudden decrease in hydrostatic pressure (or rise in temperature) may be less compressible than one which has been at that static pressure (or temperature) for a while. And, at a given temperature and pressure, the compressibility will usually decrease with increasing frequency--especially in the dispersion region. In the interest of brevity, we will not deal with different frequencies in the data presented in this report.

## 2–2 Lumped Element Method Applied to Chamber

In this section we apply the lumped element method (mentioned in the introduction, on page 4) to our chamber. A *lumped element method* is one in which we assume that changes happening to a certain object (element) are happening to the whole object simultaneously, regardless of its size or shape (i.e., each *element* is a changing, homogeneous *lump*, homogeneous but changing with respect to temperature, pressure, velocity, etc.). In our case we wish to assume that the *pressure* is the same everywhere in the chamber, though our measurements involve finite frequency (therefore finite wavelength) pressure oscillations. This requires, first of all, that the chamber and all the objects inside of it be very small compared to a wavelength. For example, if the sound speed in the fluid is 1500 meters per second, and the frequency is 1000 hertz, the wavelength is 1.5 meters. As a result, the shape of the fluid should have dimensions less than 15 centimeters to avoid danger of the appearance of phenomena associated with wave motion. The smaller the dimensions, the more accurate our assumption. A further requirement is that there are no pressure drops due to viscosity or inertia where the fluid moves through constrictions. (A pressure drop may occur across a constriction regardless of frequency.) If the chamber and the objects inside of it are small compared to a wavelength, the system may be modeled as a collection of lumped elements, and if there are no pressure drops due to constrictions, all the elements in the chamber will be at the same pressure.

We now apply this method to our chamber. A schematic of the chamber appears in Figure 2–1. The chamber is as small as practical in order that the highest frequency possible may be used, but not so small that samples which contain suspended particles or crystal-like regions cease to act homogeneous. It contains places for the two transducers and a place for the sample. The input transducer acts as a volume expander (it is a small piezoelectric disk) to cyclically change the pressure, and the output transducer (another small piezoelectric disk) detects the pressure changes in the chamber due to the expander. We will explore the upper frequency limit of the chamber in Section 2–5, but for now let us assume that the frequency is low enough to let us treat all the objects in the chamber as lumped elements, and that the effects of any constrictions are negligible. The lumped element model lends itself to an analogy between the physical lumped elements and lumped electrical circuit components. (Even the effects of constrictions may be modeled as circuit elements if they are quantifiable, as we will see in Section 2–5.) This analogy, addressed in the next section, will involve three complex unknowns. Since there are three unknowns, three measurements must be taken under three different conditions to develop three simultaneous

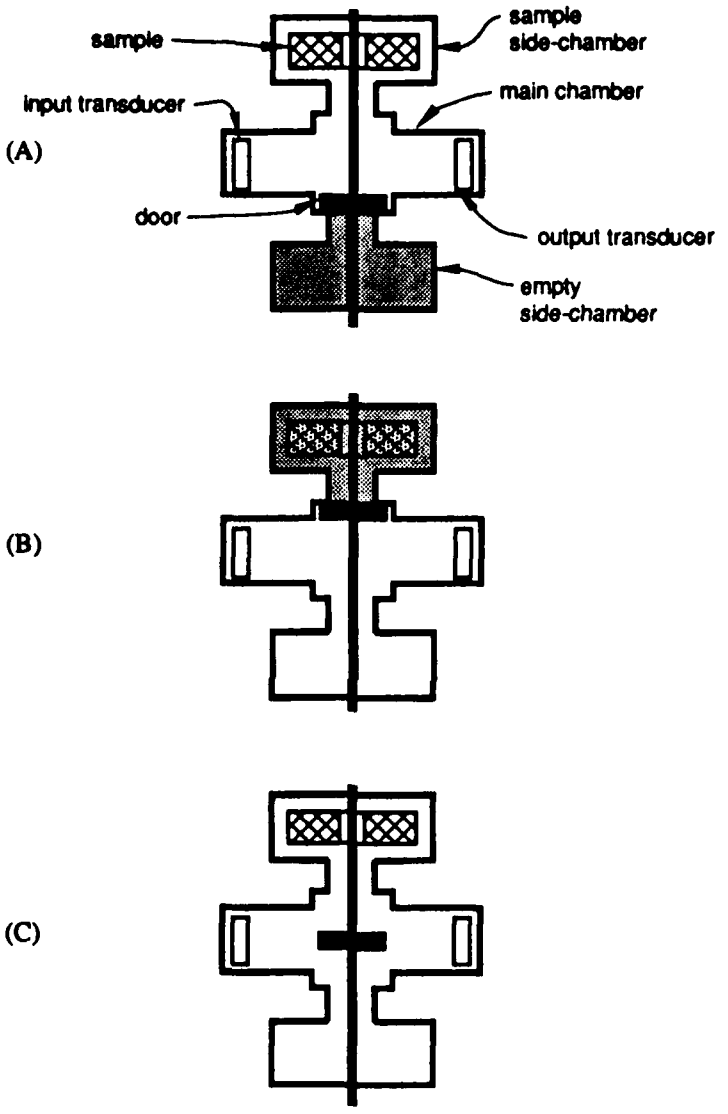


**Figure 2 1** A WORKING SCHEMATIC OF THE CHAMBER SHOWING THE THREE POSITIONS OF THE DOOR: (A) SAMPLE ONLY, (B) NO SAMPLE, (C) BOTH SIDE CHAMBERS PRESENT. OVERALL DIMENSIONS ARE APPROXIMATELY 2.0 INCHES (5.1 CM) BY 1.6 INCHES (4.2 CM) (DRAWING IS APPROXIMATELY TO SCALE).

AS-89-1526

equations. This is where we use the advantage of side-chambers and a door (see Figure 2–1). As seen in the figure, the door between the side chambers allows the creation of three different measurement conditions: (A), "sample only," where the main chamber and the side-chamber containing the sample are present while the empty side-chamber is acoustically hidden by the door; (B), "no sample," where the sample side-chamber is hidden, as if the sample were taken out; and (C), "both side-chambers present," similar to condition (A) except the total volume of the chamber is increased.

With the lumped element theory and the three measurement conditions for the chamber explained, we are now ready to draw the electrical analogy.

## 2–3 Electrical Analogy

In this section we make an analogy between the chamber (shown schematically in Figure 2–1) and an electric circuit. From this analogy we can write equations involving the dynamic compressibility of the polymer sample. The first step is to define the assumptions and symbols we will use. We apply several assumptions:

- **Low frequency**—this is required to implement the lumped element assumptions.
- **Side-chambers have rigid walls**—we leave the impedance of the main chamber as an unknown since it contains transducers, wires to mount the transducers, teflon seals, etc. The side-chambers, though, are rooms two and a half centimeters in diameter and one centimeter deep surrounded by several centimeters of stainless steel. Rigidity is a safe assumption.
- **Fluid is lossless**—liquids used in this chamber have loss compressibilities approximately two orders of magnitude below that of most polymer samples, and well below the level of scatter in the data, so their losses can be neglected.
- **No losses due to side-chambers**—the side-chambers have rigid walls and are filled with lossless fluid; therefore no losses should occur except due to the sample in the sample side-chamber. There is, however, a constriction at the opening between the side-chamber and the main chamber as depicted in Figure 2–1. There may be viscous losses as fluid moves in and out of this constriction. This loss is assumed insignificant, though Section 2–5.3 explores the actual significance of these *neck losses*.

We also need analogous tools and symbols from electric circuit theory. In this analogy pressure, $P$, is analogous to voltage, $E$. Accordingly: fluid volume velocity is analogous to current; the energy dissipation (acoustic resistance) is analogous to electric resistance; the ability of a lumped volume of matter to store energy through motion is like inductance; energy stored in a compressed lumped volume is like energy stored in a capacitor; and combinations of energy storing and/or dissipating elements are impedances. These quantities and their units are summarized in Table 2-1. Symbols with arrows over them are *complex vectors* (or *phasors*). Notice that many of the acoustic symbols are the same as traditional

**Table 2-1** SYMBOLS USED IN ELECTRICAL ANALOGY. (CGS UNITS ARE USED SO THAT RESULTS MAY BE COMPARED TO THOSE IN OTHER PAPERS WHERE COMPRESSIBILITY IS OFTEN REPORTED IN $CM^2$/DYNE.)

| *Acoustic* | | | *Electrical* | | |
|---|---|---|---|---|---|
| *symbol* | *name* | *units* | *symbol* | *name* | *units* |
| $P$ | pressure | dyne/cm$^2$ | $E$ | potential | volt |
| $v$ | decrease in volume | cm$^3$ | $q$ | charge | coulomb |
| $\dot{v}$ | rate of dec. vol. | cm$^3$/s | $i$ | current | amp |
| $C$ | ac. capacitance | cm$^5$/dyne | $C_E$ | capacitance | farad |
| $L$ | ac. inductance | s$^2$dyne/cm$^5$ | $L_E$ | inductance | nenry |
| $R$ | ac. resistance | s dyne/cm$^5$ | $R_E$ | resistance | ohm |
| $\vec{Z}$ | ac. impedance | s dyne/cm$^5$ | $\vec{Z}_E$ | impedance | ohm |
| $\vec{C}$ | complex ac. cap. | cm$^5$/dyne | $\vec{C}_E$ | complex cap. | farad |

electric symbols, while the electric symbols are subscripted. We do this simply for neatness in our equations since the only truly electrical quantity we use is potential, $E$.

*Acoustic Capacitance* is very important in this analogy. We take a moment now to thoroughly define it and complex capacitance—a quantity which at first may seem odd. By definition bulk modulus, K, is the pressure required for a differential volume strain:

$$\mathrm{K} = \frac{P}{-\mathrm{d(V)/V}}$$

where V is the volume of the object being strained, and d(V) has a negative sign since a positive pressure leads to a decrease in volume. If $v$, the decrease in

volume due to compression, is very small, then

$$\mathrm{K} \cong \frac{P}{v/\mathrm{V}}$$

or

$$P \cong \mathrm{K}\frac{v}{\mathrm{V}} \tag{2-3.1}$$

where $v$ is the (positive) decrease in volume and V is the volume of the object being strained. Also by definition, electrical capacitance $C_E$ is the stored charge $q$ per unit of potential $E$ on a given capacitor:

$$C_E = \frac{q}{E}$$

or

$$E = \frac{q}{C_E} \,. \tag{2-3.2}$$

According to our basic assumption, $E$ is like $P$, and $q$, the charge is like $v$, the decrease in volume. With this in mind, comparing Equations 2-3.1 and 2-3.2 leads us to conclude that

$$\frac{1}{C_E} \sim \frac{\mathrm{K}}{\mathrm{V}} \quad ;$$

therefore

$$C = \mathrm{V}\beta \,, \tag{2-3.3}$$

where $\beta$ is compressibility, defined by 1/K. The quantity we pursue is complex dynamic compressibility, $\vec{\beta}_s$ (defined in the introduction):

$$\vec{\beta}_s = \beta_{(storage)} + \mathring{\imath}\,\beta_{(loss)} \,,$$

where $\mathring{\imath} = \sqrt{-1}$. Since it is much easier to solve equations which yield $\vec{\beta}_s$ directly, we define a complex capacitance

$$\vec{C} = \mathrm{V}\vec{\beta}$$

so that

$$\vec{Z}_s = \frac{1}{\mathring{\imath}\,\omega\vec{C}_s} = \frac{1}{\mathring{\imath}\,\omega(\mathrm{V}_s\vec{\beta}_s)} \,, \tag{2-3.4}$$

where $\vec{Z}_s$ is the acoustic impedance of the sample, $\vec{\beta}_s$ is the dynamic compressibility of the sample, and $\mathrm{V}_s$ is the sample volume. The alternative is to solve

$$\vec{Z}_s = R_s + \frac{1}{\mathring{\imath}\,\omega C_s} \tag{2-3.5}$$

(where $R_s$ is the resistance of the sample and $C_s$ is the non-lossy capacitance) for $\vec{\beta}_s$. Note that solving Equation 2-3.5 with $\vec{\beta}_s$ from Equation 2-3.4 yields:

$$R_s = \frac{-\beta_{s(\overset{\circ}{i})}}{\omega V_s(\beta^2_{s(r)} + \beta^2_{s(\overset{\circ}{i})})}, \tag{2-3.6}$$

and

$$C_s = \frac{V_s(\beta^2_{s(r)} + \beta^2_{s(\overset{\circ}{i})})}{\beta_{s(r)}}, \tag{2-3.7}$$

where the subscripts $s$ are for "sample," (r) for "real" (storage), and $(\overset{\circ}{i})$ for "imaginary" (loss), and $\omega$ is the angular frequency. This shows us that $\beta_{s(\overset{\circ}{i})}$ must be negative to constitute a loss.

Now that we have all the tools from the lumped element assumptions through the circuit elements, we can build an analogous circuit. Since each di-

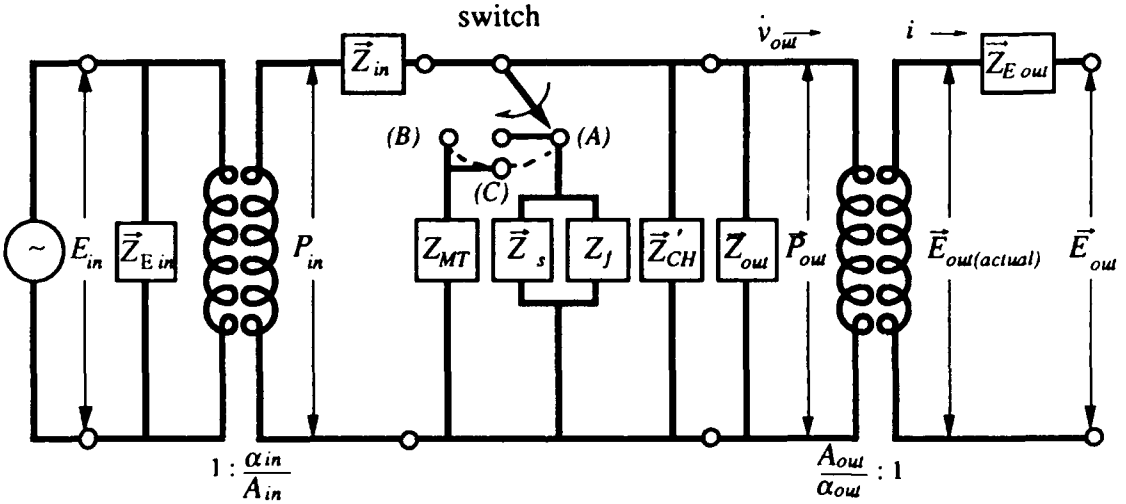


**Figure 2 2** AN ANALOGOUS CIRCUIT FOR THE CHAMBER. THE SWITCH IS ANALOGOUS TO THE DOOR IN THE ACTUAL CHAMBER. IN POSITION (A) (SHOWN) ONLY THE SAMPLE SIDE-CHAMBER IS ON LINE, (B) ONLY THE EMPTY SIDE-CHAMBER IS ON LINE, AND (C) BOTH CHAMBERS CONTACT THE SWITCH AND ARE ON LINE.

AS-89-1527

mension in the chamber will be much less than a wavelength, and we have assumed there are no effects due to constrictions, geometry is not a factor in making the analogous circuit. With this in mind, the simplest model is to have all the objects in the chamber in parallel where it is easy to see the pressure is the same

everywhere. Figure 2–2 shows such a circuit. Notice that the transducers are parallel elements as a whole, but appear as two-port equivalents which are made of parallel and series parts. Let us examine each element of Figure 2–2. From left to right we see:

- **Function generator** (extreme left)—supplies a sinusoidal voltage to the transducer.
- **Input transducer**—appears as a "transformer" two-port transforming voltage, $E$, into pressure, $P$, similar to the model developed by Mason.[11]
  - $\vec{Z}_{E\,in}$—the electrical input impedance. It is irrelevant since it appears in parallel and we measure the voltage $E_{in}$.
  - **"Perfect transformer"**—transforms potential into pressure. The value of the "effective turns ratio" $\alpha_{in}$ and the area of the transducer $\mathrm{A}_{in}$ are unimportant since they will cancel later. However, we need to remember that the input pressure $P_{in}$ is related to $E_{in}$ by

    $$\frac{\alpha_{in}}{\mathrm{A}_{in}} E_{in} = P_{in}.$$

    Notice $E_{in}$ and $P_{in}$ are real since we define phase changes relative to these quantities.
  - $\vec{Z}_{in}$ —the input transducer's internal "acoustic" impedance. This can be approximately calculated using properties of the transducer material and the geometry of the transducer, but, since properties may change with age and pressure history, and geometry may change or not be exactly known (e.g., a piece of silver plating flaking off thus lessening the total effective area), $\vec{Z}_{in}$ is left as an *unknown*.
- $Z_{MT}$—the impedance of the empty chamber. Recall that we assume there are no losses and that the walls of the chamber are rigid. As a result this impedance is due only to the fluid, so that

  $$Z_{MT} = \frac{1}{\overset{\circ}{\imath}\,\omega\,\mathrm{V}_{MT}\,\beta_f}$$

  where $\mathrm{V}_{MT}$ is the volume of the empty side-chamber, and $\beta_f$ is the compressibility of the fluid, which is known. Notice that since $\beta_f$ has no loss component, it is a real quantity.

- $\vec{Z}_s$—the *unknown* complex impedance of the sample, related to $\beta_s$ by Equation 2–3.4.

- $Z_f$—the impedance of the fluid which surrounds the sample in the sample side-chamber. The volumes of the two side-chambers are equal, so the volume of this fluid is $V_{MT} - V_s$. $Z_f$ is described by:

$$Z_f = \frac{1}{\overset{\circ}{\imath}\,\omega\,(V_{MT} - V_s)\,\beta_f}\,.$$

- $\vec{Z}'_{CH}$—the impedance of the main chamber as a whole including the fluid, transducer mounts, electrical connections, and any small undissolved bubbles of air which might be present. This is *unknown*.

- **Output transducer**—again similar to Mason's model except the "transformer" two-port is formed with the parallel element $\vec{Z}_{out}$ on the pressure side, and the series element $\vec{Z}_{E\,out}$ on the electrical side. Since $\vec{Z}_{out}$ is in parallel with the unknown $\vec{Z}'_{CH}$, it can be accounted for in the measured calibration as part of $\vec{Z}'_{CH}$. We measure $\vec{E}_{out}$ with a very high-impedance meter (lock-in amplifier) so that the current $i$ in the output transducer is essentially zero. With no current, $\vec{Z}_{E\,out}$ is irrelevant and $\vec{E}_{out(actual)}$ is equal to $\vec{E}_{out}$ so, as with the input transducer,

$$\frac{\alpha_{out}}{A_{out}} E_{out} = P_{out}.$$

  Recall from elementary circuit theory that a two-port equivalent for a transformer usually replaces the ideal transformer with a current controlled current source and a voltage controlled voltage source. In the version of Mason's model for the output transducer here, we would have a current controlled volume-velocity source, and a pressure controlled voltage source. These elements differ slightly from the mere transformers shown in the drawings. The end result is that when the current $i$ is zero, the volume velocity through the "perfect transformer," $\dot{v}_{out}$, is also zero and the parts of the transducer to the right of $\vec{Z}_{out}$ are an open circuit. These manipulations of the "transformer" two-port yield the circuit shown in Figure 2–3. Note that:

$$\vec{Z}_{CH} = \frac{1}{\frac{1}{\vec{Z}'_{CH}} + \frac{1}{\vec{Z}_{out}}}.$$

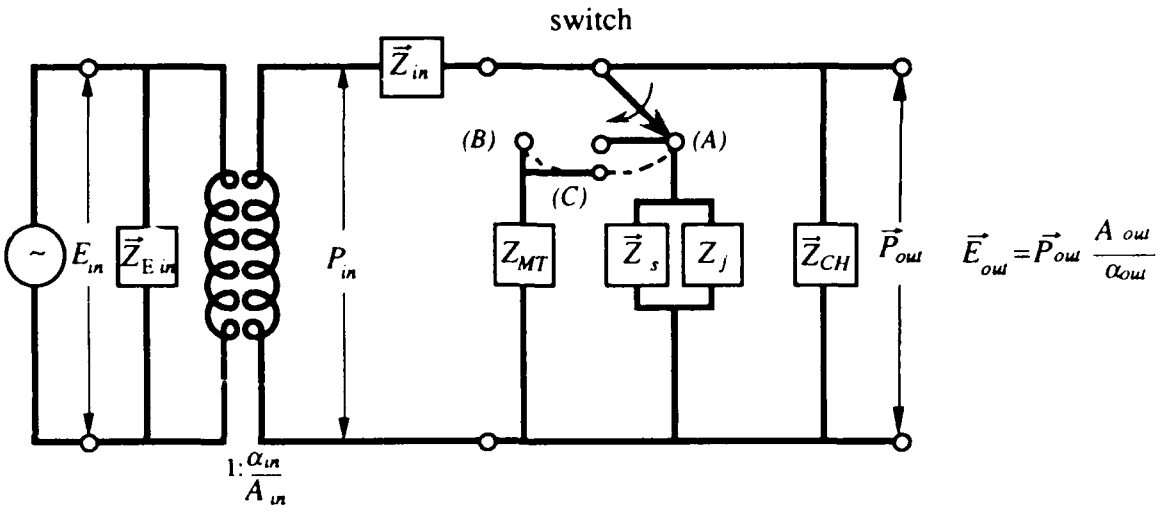


**Figure 2-3** FINAL ANALOGOUS CIRCUIT FOR THE CHAMBER

AS-89-1528

- **The switch.** The switch is the electric analog to the door in Figure 2-1. With the "switch" we make three different circuits: position (A), sample only; (B), no sample; and (C), both side-chambers present, and solve for our three unknowns ($\vec{Z}_{in}$, $\vec{Z}_{CH}$, and $\vec{Z}_s$) by finding the ratios:

$$\left(\frac{\vec{E}_{out}}{E_{in}}\right)_x$$

for each $x$ ((A), (B), or (C)).

## 2-4 Solution to Equations

We now only need to write equations and solve them for $\vec{\mathcal{Z}}_s$ in terms of the known quantities $\mathcal{Z}_f$, $V_{MT}$, $V_s$, and $(\vec{E}_{out}/E_{in})_x$. We start by deriving the relation $\vec{P}_{out}/P_{in}$ for each switch position as portrayed in Figure 2-3. For position (A), sample side chamber only, the resulting (simplified) circuit is shown in Figure 2-4. In our analogy Ohm's Law appears as

$$\vec{P} = \vec{v}\,\vec{Z}\ .$$

Applying Ohm's Law directly (adding the series and parallel elements properly)

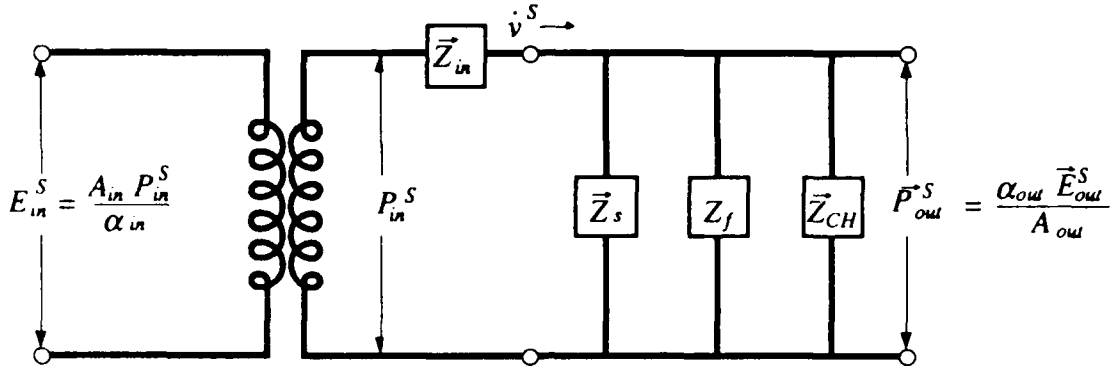


**Figure 2 4** ANALOGOUS CIRCUIT FOR SWITCH POSITION (A), SAMPLE SIDE-CHAMBER ONLY (DENOTED IN EQUATIONS BY SUPERSCRIPT *S*). NON-ESSENTIAL PARTS HAVE BEEN REMOVED.

AS-89-1529

we can obtain two independent equations:

$$P^S_{in} = \vec{v}^S \left\{ \vec{Z}_{in} + \left[ \frac{1}{\vec{Z}_s} + \frac{1}{Z_f} + \frac{1}{\vec{Z}_{CH}} \right]^{-1} \right\} \qquad (2\text{-}4.1)$$

for $P^S_{in}$ where the *superscript S* stands for the condition where the *sample* side-chamber only is on line, and

$$\vec{P}^S_{out} = \vec{v}^S \left[ \frac{1}{\vec{Z}_s} + \frac{1}{Z_f} + \frac{1}{\vec{Z}_{CH}} \right]^{-1} \qquad (2\text{-}4.2)$$

for $\vec{P}^S_{out}$. Finally, the ratio of $\vec{P}^S_{out}/P^S_{in}$ is proportional to the desired ratio $\vec{E}^S_{out}/E^S_{in}$:

$$\frac{\vec{P}^S_{out}}{P^S_{in}} = \frac{1}{\vec{Z}_{in}} \left[ \frac{1}{\vec{Z}_s} + \frac{1}{Z_f} + \frac{1}{\vec{Z}_{CH}} + \frac{1}{\vec{Z}_{in}} \right]^{-1} = \frac{A_{in}\, \alpha_{out}\, \vec{E}^S_{out}}{A_{out}\, \alpha_{in}\, E^S_{in}} , \qquad (2\text{-}4.3)$$

where the constant of proportionality ,

$$\frac{A_{in}\, \alpha_{out}}{A_{out}\, \alpha_{in}} ,$$

will cancel later. Figure 2-5 is the (simplified) circuit for the switch position in which the *empty* side-chamber only is on line, denoted now by *superscript T*. This similar circuit yields similar equations and a ratio similar to Equation 2-4.3:

$$\frac{\vec{P}^T_{out}}{P^T_{in}} = \frac{1}{\vec{Z}_{in}} \left[ \frac{1}{Z_{MT}} + \frac{1}{\vec{Z}_{CH}} + \frac{1}{\vec{Z}_{in}} \right]^{-1} = \frac{A_{in}\, \alpha_{out}\, \vec{E}^T_{out}}{A_{out}\, \alpha_{in}\, E^T_{in}} . \qquad (2\text{-}4.4)$$

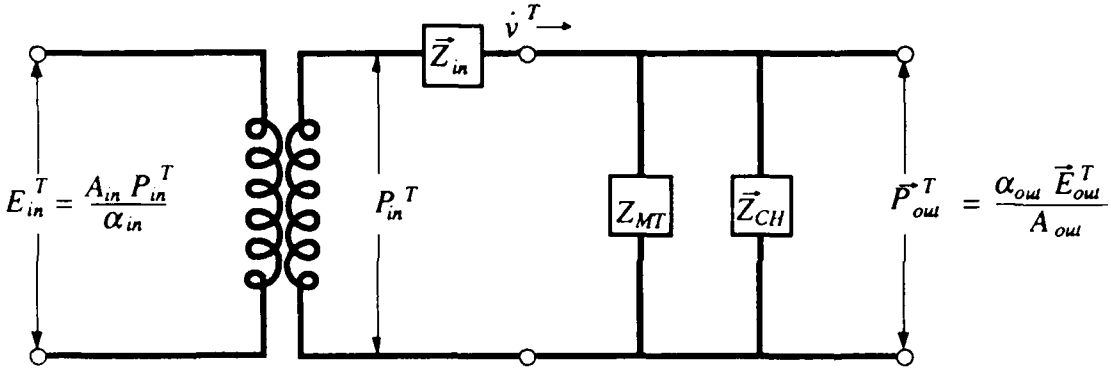


**Figure 2–5** ANALOGOUS CIRCUIT FOR SWITCH POSITION (B), EMPTY SIDE-CHAMBER ONLY (DENOTED IN EQUATIONS BY SUPERSCRIPT $T$). NON-ESSENTIAL PARTS HAVE BEEN REMOVED.

AS-89-1530

Finally, with *both* side-chambers on line (this condition denoted now by *superscript B*), another similar circuit results (not shown), and a third ratio results in the third simultaneous equation:

$$\frac{\vec{P}_{out}^B}{P_{in}^B} = \frac{1}{\vec{Z}_{in}} \left[ \frac{1}{Z_{MT}} + \frac{1}{\vec{Z}_s} + \frac{1}{Z_f} + \frac{1}{\vec{Z}_{CH}} + \frac{1}{\vec{Z}_{in}} \right]^{-1} = \frac{A_{in}\, \alpha_{out}\, \vec{E}_{out}^B}{A_{out}\, \alpha_{in}\, E_{in}^B} . \qquad (2\text{-}4.5)$$

Now we have three equations, but apparently seven unknowns: $\vec{Z}_s$, $\vec{Z}_{in}$, $\vec{Z}_{CH}$, and $A_{in}$, $A_{out}$, $\alpha_{in}$, and $\alpha_{out}$. Later in the derivation we will find ratios of Equations 2-4.3, 2-4.4, and 2-4.5 which will enable us to cancel the four "extra" unknowns. Until then, let us abbreviate the far right side of Equations 2-4.3, 2-4.4, and 2-4.5 with the letter $\vec{F}^x$ defined as

$$\vec{F}^x = \frac{A_{in}\, \alpha_{out}\, \vec{E}_{out}^x}{A_{out}\, \alpha_{in}\, E_{in}^x} . \qquad (2\text{-}4.6)$$

First we solve Equation 2-4.4 to find an expression for $\vec{Z}_{CH}$:

$$\frac{1}{\vec{Z}_{CH}} = \frac{1}{\vec{F}^T \vec{Z}_{in}} - \frac{1}{\vec{Z}_{in}} - \frac{1}{Z_{MT}} . \qquad (2\text{-}4.7)$$

Substitute Equation 2-4.7 into Equations 2-4.3 and 2-4.5 to eliminate $\vec{Z}_{CH}$:

$$\vec{F}^S = \frac{1}{\vec{Z}_{in}} \left[ \frac{1}{\vec{F}^T \vec{Z}_{in}} - \frac{1}{Z_{MT}} + \frac{1}{Z_f} + \frac{1}{\vec{Z}_s} \right]^{-1} \qquad (2\text{-}4.8)$$

$$\vec{F}^B = \frac{1}{\vec{Z}_{in}} \left[ \frac{1}{\vec{F}^T \vec{Z}_{in}} + \frac{1}{Z_f} + \frac{1}{\vec{Z}_s} \right]^{-1} . \qquad (2\text{-}4.9)$$

then subtract the reciprocal of Equation 2-4.9 from that of Equation 2-4.8 to (temporarily) eliminate $\vec{Z}_s$:

$$\frac{1}{\vec{F}^B} - \frac{1}{\vec{F}^S} = \vec{Z}_{in} \left[\frac{1}{Z_{MT}}\right]. \tag{2-4.10}$$

This gives us an expression for $\vec{Z}_{in}$:

$$\vec{Z}_{in} = Z_{MT} \left[\frac{1}{\vec{F}^B} - \frac{1}{\vec{F}^S}\right]. \tag{2-4.11}$$

Finally we substitute Equation 2-4.11 into Equation 2-4.9 to solve for $\vec{Z}_s$:

$$\vec{Z}_s = \frac{Z_{MT}\left[\frac{1}{\vec{F}^B} - \frac{1}{\vec{F}^S}\right]}{\frac{1}{\vec{F}^B} - \frac{1}{\vec{F}^T} - \frac{Z_{MT}}{Z_f}\left[\frac{1}{\vec{F}^B} - \frac{1}{\vec{F}^S}\right]}. \tag{2-4.12}$$

Equation 2-4.12 can be simplified by noting two things. First of all, the factor $1/\vec{F}^x$ is in each term on the top and bottom of this expression which allows us to cancel the common factor

$$\frac{A_{in}\,\alpha_{out}}{A_{out}\,\alpha_{in}}.$$

The resulting equation is:

$$\vec{Z}_s = \frac{Z_{MT}\left[\frac{E^B_{in}}{\vec{E}^B_{out}} - \frac{E^S_{in}}{\vec{E}^S_{out}}\right]}{\frac{E^B_{in}}{\vec{E}^B_{out}} - \frac{E^T_{in}}{\vec{E}^T_{out}} - \frac{Z_{MT}}{Z_f}\left[\frac{E^B_{in}}{\vec{E}^B_{out}} - \frac{E^S_{in}}{\vec{E}^S_{out}}\right]}.$$

Finally, if the input potential $E^x_{in}$ can be kept constant for all three measurements (a safe assumption, since the three measurements can be made in as little as five minutes with the apparatus in its current form—not enough time for the function generator to drift), then the common factor $E^x_{in}$ $(= E^S_{in} = E^B_{in} = E^T_{in})$ can be canceled also. The result is Equation 2-4.13:

$$\vec{Z}_s = \frac{Z_{MT}\left[\frac{1}{\vec{E}^B_{out}} - \frac{1}{\vec{E}^S_{out}}\right]}{\frac{1}{\vec{E}^B_{out}} - \frac{1}{\vec{E}^T_{out}} - \frac{Z_{MT}}{Z_f}\left[\frac{1}{\vec{E}^B_{out}} - \frac{1}{\vec{E}^S_{out}}\right]}. \tag{2-4.13}$$

Now we solve the equations in terms of $\vec{\beta}_s$. Recall

$$\vec{Z}_s = \frac{1}{i\,\omega\,V_s\,\vec{\beta}_s},$$

$$Z_{MT} = \frac{1}{\mathring{\imath}\ \omega\, \mathrm{V}_{MT}\, \beta_f}\ ,$$

and

$$Z_f = \frac{1}{\mathring{\imath}\ \omega\, (\mathrm{V}_{MT} - \mathrm{V}_s)\, \beta_f}\ .$$

After substituting into Equation 2-4.13, algebra yields:

$$\vec{\beta}_s = \beta_f \left\{ 1 - \frac{\mathrm{V}_{MT}}{\mathrm{V}_s} \left[ \frac{(1/\vec{E}^T_{out}) - (1/\vec{E}^S_{out})}{(1/\vec{E}^B_{out}) - (1/\vec{E}^S_{out})} \right] \right\} \qquad (2\text{-}4.14)$$

where now $\vec{\beta}_s$ is in terms of immediately measurable quantities.

Reducing Equation 2-4.14 to its real and imaginary parts requires a great deal of elementary complex algebra. We will leave out the steps, but the results follow. First let us note that

$$\vec{E}^x_{out} = E^x_{out\,(r)} + \mathring{\imath}\, E^x_{out\,(\mathring{\imath})}.$$

To save subscripts, let us define

$$\vec{E}^x_{out} \doteq R^x + \mathring{\imath}\, I^x$$

where $R^x = E^x_{out\,(r)}$, and $I^x = E^x_{out\,(\mathring{\imath})}$. To save space let us also define the following quantities to be used in the final equations:

$$A = \frac{(R^B)^2 + (I^B)^2}{(R^T)^2 + (I^T)^2}$$

$$B = \left[ \left( (R^T)^2 + (I^T)^2 - R^T R^S - I^T I^S \right) * \left( (R^B)^2 + (I^B)^2 - R^S R^B - I^S I^B \right) \right]$$

$$+ \left[ \left( R^T I^S - R^S I^T \right) * \left( R^B I^S - R^S I^B \right) \right]$$

$$D = \left[ \left( (R^B)^2 + (I^B)^2 - R^S R^B - I^S I^B \right) * \left( R^T I^S - R^S I^T \right) \right]$$

$$+\left[\left((R^T)^2+(I^T)^2-R^SR^T-I^SI^T\right)*\left(R^BI^S-R^SI^B\right)\right]$$

$$F=\left[(R^B)^2+(I^B)^2-R^SR^B-I^SI^B\right]^2+\left[R^BI^S-R^SI^B\right]^2 \quad .$$

The final equations for the real and imaginary parts of $\vec{\beta}_s$ are:

$$\beta_{s(r)}=\beta_f\left[1\ -\ \frac{V_{MT}}{V_s}\,A\,\frac{B}{F}\right]\ , \tag{2-4.15}$$

and

$$\beta_{s(i)}=\beta_f\left[-\frac{V_{MT}}{V_s}\,A\,\frac{D}{F}\right]\ , \tag{2-4.16}$$

where $A$, $B$, $D$, and $F$ are defined above.

## 2–5 Upper Frequency Limit and the Effects of Constrictions

*We modeled the working equations derived above on a lumped element* analogy. Within this analogy, the complex compressibility of an element in the chamber determined its effective complex capacitance. However, we modeled the side-chambers as simple capacitances by assuming pressure drops due to inertial and viscous effects of the fluid in the neck (the constriction between side- and main chambers) were negligible. These simplifications—the assumption that the effects of the neck are negligible as well as the lumped element approximations—are valid only for lower frequencies. The *upper frequency limit*, $f_{max}$, is the highest frequency at which we may operate the chamber and still consider our assumptions valid. In this section we first find $f_{max}$ as dictated by the assumption that elements in the chamber are small compared to the wavelength of sound in them. Next we revise $f_{max}$ to safeguard our assumption that the inertial (inductive) effects of the neck are negligible. Finally we investigate the viscous (resistive, or lossy) effects of the neck.

### 2-5.1 Limit as Imposed by Lumped Element Assumptions

In general lumped element assumptions break down when the wavelengths involved approach the order of magnitude of the largest linear dimension of any object modeled as a lump. By far the largest object in the chamber is

the fluid. The largest in-line dimension of the fluid is the distance between the walls behind each transducer (left and right ends of main chamber in Figure 2–1), approximately 4.2 cm. There is no clear-cut line between where an object can be considered lumped or not lumped. However, a common rule of thumb is that for an element to be considered "lumped", the minimum wavelength must be at least ten times the largest in-line dimension. To be conservative, let us make the minimum wavelength no less than 20 times the length of the chamber:

$$\lambda_{min} = 0.84\ m,$$

where $\lambda_{min}$ is the minimum wavelength. Therefore a rough estimate of the maximum frequency is:

$$f_{max} = \frac{c_o(\frac{m}{s})}{0.84\ m} = 1.2\, c_o\ \text{Hz} \qquad (2\text{–}5.1)$$

where $c_o$ is the linear adiabatic phase velocity in meters per second, and the units for $f_{max}$ are hertz (Hz). For the results in Chapter 4, we used Di(2 ethyl hexyl)sebacate (abbreviated DiSebacate) as the fluid in the chamber. In Appendix A we estimate the minimum sound speed in the current range of the equipment is approximately 1200 m/s. By Equation 2–5.1,

$$f_{max} = 1450\ \text{Hz}\ .$$

Notice this is the worst case scenario. At higher pressures, and/or lower temperatures, where the sound speed in DiSebacate can reach over 1700 m/s, frequencies over 2000 Hz may be used. Changing to a different fluid could change the maximum frequency depending on the new fluid's sound speed. We will revise this rough estimate when we account for the (frequency dependent) neck inductance, $L_n$.

### 2–5.2 Limit Imposed by Neck Inductance, $L_n$

The side-chambers, with their relatively small necks, act like helmholtz resonators. The inductance associated with these necks increases with frequency and can only be neglected at frequencies significantly below resonance.

#### Helmholtz Resonance:

First let us calculate the helmholtz resonance frequency, $f_H$, as it will be useful both now in defining $f_{max}$ and later when we estimate the effective neck loss. *Helmholtz resonance* is a lumped element phenomenon involving a cavity

with a constriction (neck) at its opening. Consider the fluid in the neck of a side-chamber as a lumped mass. This is inductive, while the remaining volume of the side-chamber is still capacitive. (Let us focus on the empty chamber for simplicity, though these arguments may easily be adapted to the sample side-chamber.) As many common texts explain,[1] neck inductance is represented by:

$$L_n = \frac{\rho_o V_n}{S_n^2} = \frac{\rho_o l'}{S_n}$$

where $\rho_o$ is the at-rest density of the fluid, $S_n$ is the cross-sectional area of the neck (tube), $l'$ is the effective length of the neck, and $V_n = S_n \times l'$ is the effective volume of the neck. We will find it convenient to define density with the relation between adiabatic bulk modulus, density, and linear sound speed for non-lossy, homogeneous fluids:[11]

$$\beta = \frac{1}{\rho_o c_o^2} \text{ or } \rho_o = \frac{1}{\beta c_o^2} ,$$

(this can be calculated from Equation 1-.1 since G $\cong$ 0 for liquids). So:

$$L_n = \frac{l'}{\beta c_o^2 S_n} . \qquad (2\text{-}5.2)$$

The impedance of the side-chamber, then, is really the sum of a capacitive part and an inductive part. Figure 2-6 depicts this modified view of the empty side-chamber. In a standard helmholtz resonator, the capacitance is considered due only to the volume of the body of the chamber and does not include the neck. In Figure 2-6, $C'_{MT}$ is the capacitance of the side-chamber volume *minus* the volume of the neck, and $L_n$ is the inductance of the neck. (Notice that $C_{MT}$ (without the prime) is the capacitance of the whole chamber *including* the neck. It is the correct value in the working equations, where $L_n$ is ignored.) Later we will see this modified side-chamber model as part of a modified model of the whole chamber. We will use this later model to estimate the effective resistance in the neck (see Section 2-5.3, especially Figure 2-8). The impedance of the side-chamber as modeled in Figure 2-6 is:

$$Z_{MT} = \frac{1}{\overset{\circ}{\imath}\omega C'_{MT}} + \overset{\circ}{\imath}\omega L_n . \qquad (2\text{-}5.3)$$

Resonance occurs when the impedance adds to zero. Solving Equation 2-5.3 for a resonance in terms of cyclical resonant frequency, $f_H$, and substituting Equations 2-5.2 and 2-3.3 for $L_n$ and $C'_{MT}$, respectively, we find:

$$f_H = \frac{c_o}{2\pi}\sqrt{\frac{S_n}{l' V'_{MT}}} \qquad (2\text{-}5.4)$$

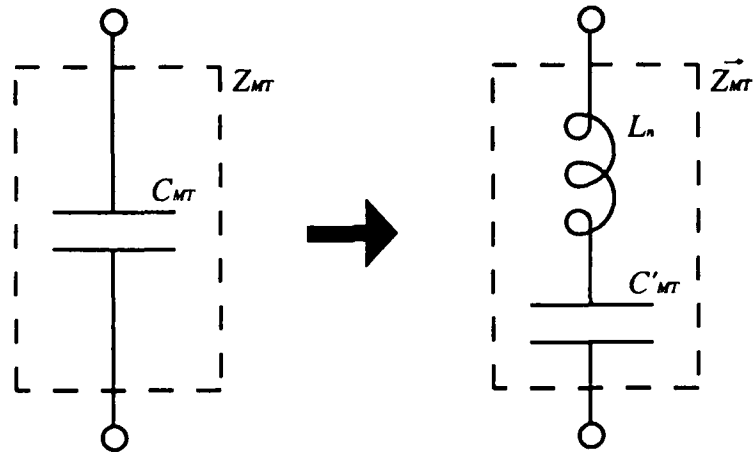


**Figure 2–6** ADDING AN INDUCTIVE PART TO THE EMPTY SIDE-CHAMBER

AS-89-1531

where $S_n$ is the cross sectional area of the neck, $V'_{MT}$ is the volume of the cavity (in this case the volume of the sample cavity portion of the side-chamber (see Figure 2–7)), and $l'$ is the effective neck length. The effective neck length is typically the physical length plus a small end correction proportional to the neck radius a:

$$l' = l + ma$$

where $m$ is a function of the neck geometry. Values for $m$ are typically in the range of 0.6 (for an unflanged opening with no end correction on the inside of the resonator) to 1.7 (for a flanged end correction on each side of the neck)[1] and it may be argued that the end correction should be smaller if the resonator resonates into a finite volume. Additionally, the neck, as defined in Figure 2–7, is not clearly flanged—it opens to a *plateau* where the door rests when the chamber is shut. As a result, we will consider a range for $m$:

$$0 < m < 1.7 \quad .$$

From the dimensions in Figure 2–7 (more details on the dimensions are in Chapter 3), we see

$$S_n = 0.416 \text{ cm}^2$$

$$V'_{MT} = 5.07 \text{ cm}^3$$

$$l = 0.66 \text{ cm}$$

$$a = \frac{5}{32} \text{ in } (0.397\text{cm})$$

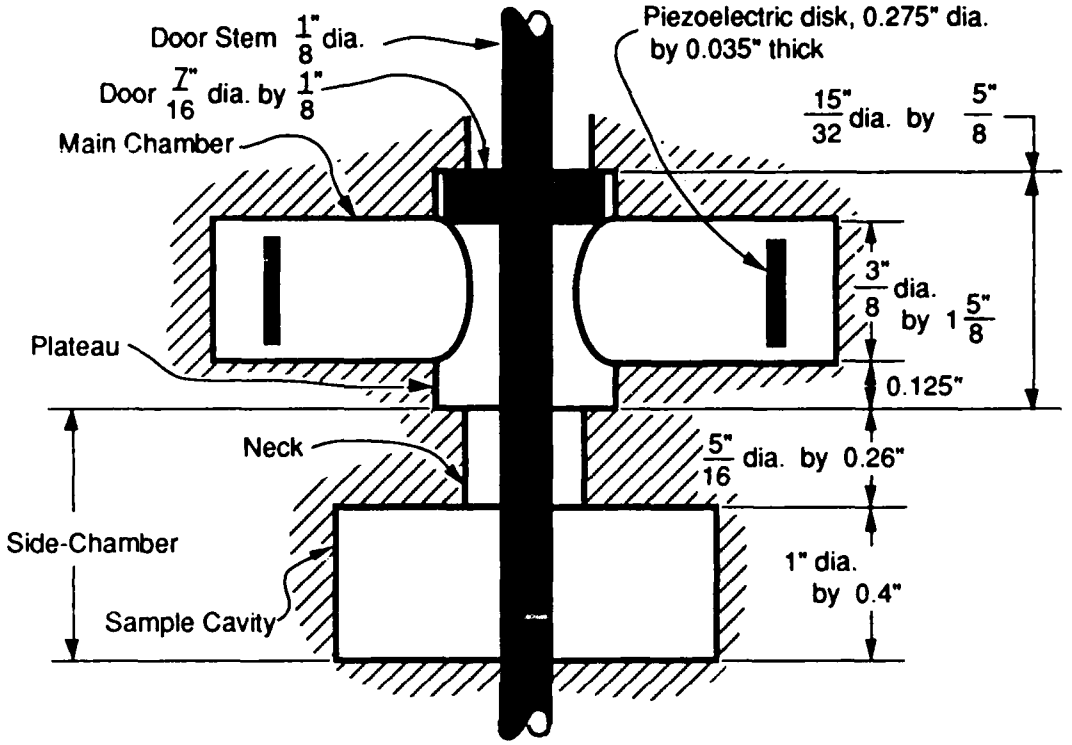


**Figure 2–7** SOME DIMENSIONS OF A SIDE-CHAMBER.

AS-89-1532

$$l = 0.66\text{cm} < l' < 1.33\text{ cm} = l + 1.7\text{a}\,.$$

Equation 2–5.4 yields:

$$4.0\,c_o < f_H < 5.6\,c_o \text{ Hz.} \qquad (2\text{–}5.5)$$

As an example, at 21°C and 1000 psig, the data in Appendix A gives a $c_o$ of approximately 1460 m/s. With this, Equation 2–5.5 yields:

$$5800\text{ Hz} < f_H < 8200\text{ Hz.}$$

Experimental data (which appears in Figure 2–9) gives:

$$f_H \cong 6100\text{ Hz.}$$

**Frequency Limit:**

Now that we have impedances and the helmholtz frequency quantified, we can employ them in a definition of an upper frequency limit which considers the neck impedance. In our working equations we assume the neck impedance is insignificant. To assume the neck impedance is insignificant is to assume that

$$Z_{MT} = \frac{1}{\mathring{i}\omega C_{MT}} \cong \frac{1}{\mathring{i}\omega C'_{MT}} + \mathring{i}\omega L_n \, .$$

This is so if

$$\left| \frac{\mathring{i}\omega L_n}{(\mathring{i}\omega C'_{MT})^{-1}} \right| \ll 1 \, .$$

Substituting Equations 2-5.2 for $L_n$ and 2-3.3 for $C'_{MT}$, and reducing, we find

$$\left| \frac{\mathring{i}\omega L_n}{(\mathring{i}\omega C'_{MT})^{-1}} \right| = \frac{\omega^2}{c_o^2} \left( \frac{l' \, \mathrm{V}'_{MT}}{\mathrm{S}_n} \right) \, . \qquad (2\text{-}5.6)$$

Substituting in the square of Equation 2-5.4, we see:

$$\left| \frac{\mathring{i}\omega L_n}{(\mathring{i}\omega C'_{MT})^{-1}} \right| = \left( \frac{f}{f_H} \right)^2 \, ,$$

where we have replaced $(\omega/2\pi)^2$ with $f^2$. A conservative restriction is that the inductive part be less than 4% of the capacitive part:

$$\left| \frac{\mathring{i}\omega L_n}{(\mathring{i}\omega C'_{MT})^{-1}} \right|_{max} < 0.04$$

or:

$$\left( \frac{f}{f_H} \right)^2 < 0.04.$$

This gives us a practical upper frequency limit of

$$f_{max} = 0.2 f_H \, . \qquad (2\text{-}5.7)$$

According to the measured value at 21°C and 1000 psi,

$$f_{max} = 0.2 \times 6100 \text{ Hz} = 1200 \text{ Hz} \, .$$

Applying Equation 2–5.5 to Equation 2–5.7 we can estimate:

$$0.8c_o < f_{max} < 1.12c_o \text{ Hz} .$$

Notice this $f_{max}$ is lower than the one based on the effect of lumped element assumptions. **Therefore, the practical upper frequency limit is:**

$$\boldsymbol{f_{max} = 0.2 f_H} .$$

### 2–5.3 Effect of Neck Loss, $R_n$

In our working equations we neglected the viscous losses due to the fluid in the neck. Now we will add resistance to the empty side-chamber model in Figure 2–6, combine it into a simplified chamber model, and use some measured data to estimate the significance of the neck loss.

The first step is the simplified chamber model. Figure 2–8 shows the side-chamber (with added loss element, $R_n$) incorporated into a circuit model of the whole chamber. This circuit is a simplified form of Figure 2–5 on page 19. The main chamber appears as a capacitance, $C_{CH}$ (rather than $\vec{Z}_{CH}$), and the input impedance is also a capacitance $C_{in}$ (rather than $\vec{Z}_{in}$). It is reasonable to assume that the input impedance is very large compared to the other impedances in the chamber, making $C_{in}$ quite small compared to other capacitances in the system. We will show momentarily that this is a reliable approximation to the real chamber. By inspection alone, though, we can see that when $f_H$ is reached, the branch representing a side-chamber will act like a short circuit except for the small $R_n$. As a result, $\vec{P}_{out}$ will be very small. Similarly, at another frequency the side-chamber branch and the main chamber branch should react to constitute another resonance where $\vec{P}_{out}$ is a maximum. This is similar to the *tank resonance* in the tuned amplifier of an AM radio. This tank resonance corresponds physically to a state where the fluid in the chamber is 'sloshing' back-and-forth from the main chamber to the side-chamber through the neck.

Let us now calculate this tank resonance to show this proposed circuit is a realistic treatment of the neck impedance. In Figure 2–8, $P_{in}$ is the input cyclic pressure. $C_{CH}$ is the capacitance of the main chamber:

$$C_{CH} = \mathrm{V}_{CH}\beta , \qquad (2\text{–}5.8)$$

where $\mathrm{V}_{CH}$ is the volume of the main chamber, and $\beta$ is the compressibility of the fluid. Accounting for the door, doorstem, transducers, and approximately for the plateaus, $\mathrm{V}_{CH}$ is approximately 3.19 cubic centimeters. Let us assume for the

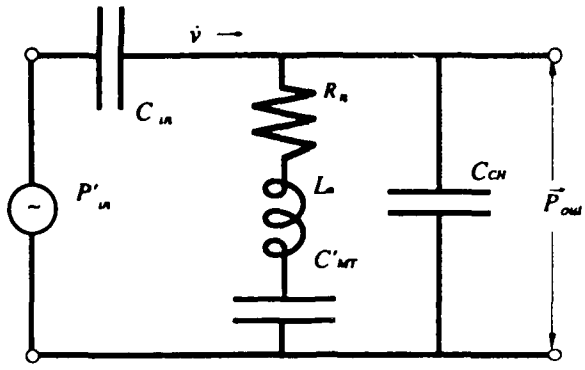


**Figure 2–8** CHAMBER MODEL SIMILAR TO A 'TANK CIRCUIT.' THE CAPACITOR $C_{CH}$ MODELS THE MAIN CHAMBER, WHILE THE PARALLEL BRANCH TO THE LEFT OF IT MODELS THE EMPTY SIDE-CHAMBER AS IN FIGURE 2–6. $C_{in}$ MODELS THE LARGE INPUT IMPEDANCE OF THE TRANSDUCER. A TANK CIRCUIT IS USED IN A TUNED AMPLIFIER.

AS-89-1533

time being the resistance in the neck, $R_n$, is negligible. We can easily write an equation for the impedance, $\vec{Z}_P$, of the parallel branches in Figure 2–8:

$$\vec{Z}_P = \left[\frac{1}{\vec{Z}_{CH}} + \frac{1}{Z_{MT}}\right]^{-1}$$

$$\cong \left[\mathring{i}\omega C_{CH} + \left[\frac{1}{\mathring{i}\omega C'_{MT}} + \mathring{i}\omega L_n\right]^{-1}\right]^{-1}$$

$$= \frac{1 - \omega^2 L_n C'_{MT}}{\mathring{i}\omega(C_{CH} + C'_{MT} - \omega^2 L_n C_{CH} C'_{MT})} \,. \qquad (2\text{–}5.9)$$

Note that $\vec{Z}_P$=0 when:

$$\omega_H = \sqrt{\frac{1}{L_n C'_{MT}}}$$

which, when we apply Equations 2–3.3 and 2–5.2, is simply the helmholtz resonance, Equation 2–5.4:

$$\omega_H = c_o\sqrt{\frac{S_n}{l' V'_{MT}}} = 2\pi f_H \,,$$

where $l'$ is the length of the neck, $S_n$ is the cross sectional area of the neck, and $V'_{MT}$ is the volume of the sample cavity part of the side-chamber. The impedance goes to zero at $f_H$ since the parallel branch representing the side-chamber acts

like a short circuit at its resonance. The tank circuit resonance occurs when $\vec{Z}_P$ goes infinite, i.e., the bottom of Equation 2-5.9 goes to 0:

$$C_{CH} + C'_{MT} - \omega_T^2 L_n C_{CH} C'_{MT} = 0$$

or:

$$\omega_T = \sqrt{\frac{1}{L_n C_{CH}} + \frac{1}{L_n C'_{MT}}}\ , \qquad (2\text{-}5.10)$$

where $\omega_T$ is the 'tank resonance.' During tank resonance the voltage across the parallel elements is a maximum. Substituting Equations 2-5.2 and 2-3.3 into 2-5.10, we find:

$$\omega_T = c_o \sqrt{\frac{S_n(V'_{MT} + V_{CH})}{l' V'_{MT} V_{CH}}}\ . \qquad (2\text{-}5.11)$$

A ratio of the tank resonance to the helmholtz resonance reduces to the rather simple relation:

$$\frac{\omega_T}{\omega_H} = \left(1 + \frac{V'_{MT}}{V_{CH}}\right)^{\frac{1}{2}} \quad .$$

This can easily be calculated and easily compared to experiment. Recall that $V'_{MT}$ and $V_{CH}$ are 5.07 cm$^3$ and 3.19 cm$^3$, respectively. Therefore

$$\frac{\omega_T}{\omega_H} = 1.61|_{calculated}\ .$$

The graph in Figure 2-9 is copied from the analog plotter plot of the magnitude of $\vec{E}_{out}$ (with $E_{in} \cong 40\ V_{p-p}$) for the empty chamber at 21°C and 1000 psig. Recall from Section 2-3 that the electrical output, $\vec{E}_{out}$, is directly proportional to the output pressure, $\vec{P}_{out}$. The near-zero at 6100 Hz corresponds to the helmholtz resonance where, except for $R_n$, the side-chamber branch in Figure 2-8 is a short circuit. The first maximum in Figure 2-9—at approximately 9500 Hz—corresponds to the tank resonance. The length of the chamber, $1\frac{5}{8}$ in. (4.13 cm), gives a half wavelength standing wave frequency of approximately 17700 Hz ($c_o$ = 1460 m/s, see Appendix A) which roughly corresponds to the second peak in Figure 2-9. The experimental ratio of frequencies is:

$$\frac{\omega_T}{\omega_H} = \frac{9500}{6100} = 1.56|_{measured}.$$

This agreement between theory and experiment shows that the proposed circuit gives a realistic treatment of the effects of neck impedance.

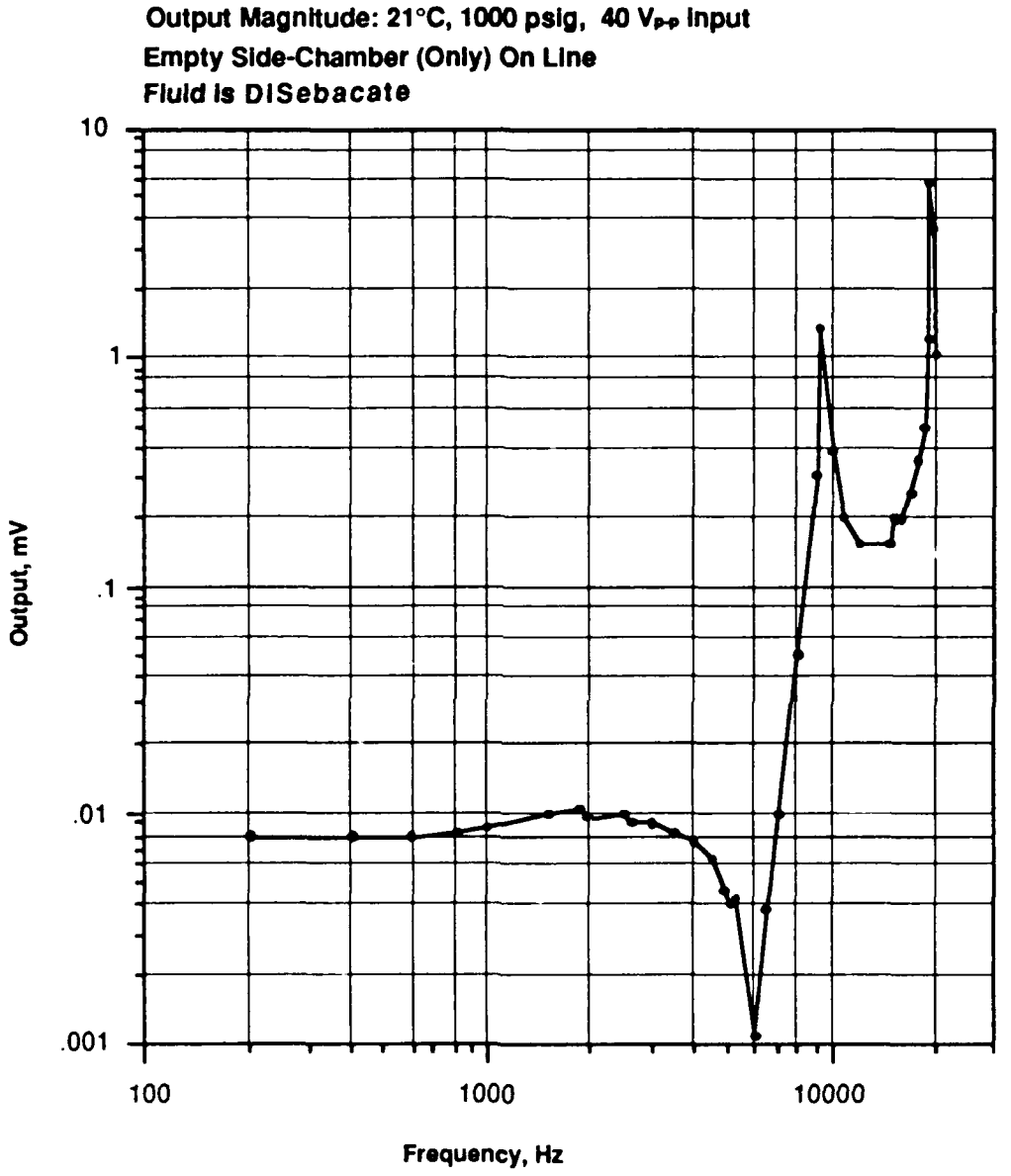


**Figure 2-9** OUTPUT VOLTAGE MAGNITUDE, $E_{out}$, AS A FUNCTION OF FREQUENCY. EMPTY SIDE-CHAMBER LEFT OPEN, SAMPLE SIDE-CHAMBER CLOSED OFF. INPUT VOLTAGE IS APPROXIMATELY 40 $V_{p-p}$, STATIC PRESSURE IS 1000 PSIG, TEMPERATURE IS 21°C. PRESSURE FLUID IS DISEBACATE.

AS-89-1534

Now that we know we may trust the simplified circuit in Figure 2-8, let us use it and the data in Figure 2-9 to finally find the significance of $R_n$. At low enough frequencies the effects of $L_n$ and $R_n$ will be small compared to the effect of $C'_{MT}$. The circuit in Figure 2-8 is simply a voltage divider based on capacitances. The magnitude of the output pressure is:

$$\vec{P}_{out}(\omega_l) = \frac{C_{in}}{C'_{MT} + C_{CH} + C_{in}} P_{in}$$

where $\omega_l$ is a low frequency. Since $C_{in}$ is small compared to $C'_{MT}$ and $C_{CH}$, let us simplify to:

$$\vec{P}_{out}(\omega_l) = \frac{C_{in}}{C'_{MT} + C_{CH}} P_{in} \quad . \tag{2-5.12}$$

This would remain constant with increasing frequency if the neck impedance were not present. However, at the helmholtz resonance the storage parts of the side-chamber's impedance go to zero and the shunt impedance (the impedance to the parallel branches) is dominated by the presumably small $R_n$. The magnitude of the output at resonance is approximately:

$$\vec{P}_{out}(\omega_H) = \frac{C_{in}}{\frac{1}{\omega_H R_n} + C_{CH}} P_{in} \ , \tag{2-5.13}$$

where $C_{in}$ has again been left out of the denominator. The magnitude of the ratio of Equation 2-5.12 to Equation 2-5.13 is:

$$\left| \frac{\vec{P}_{out}(\omega_l)}{\vec{P}_{out}(\omega_H)} \right| = \frac{\left| \frac{1}{\omega_H R_n} \right| + C_{CH}}{C'_{MT} + C_{CH}} \ . \tag{2-5.14}$$

From Figure 2-9 this ratio is approximately 8. And, since $V'_{MT} = 5.07$ cm$^3$ and $V_{CH} = 3.19$ cm$^3$,

$$C_{CH} = \frac{3.19}{5.07} C'_{MT} = 0.63 C'_{MT} \ .$$

Using this information in Equation 2-5.14 and solving for $R_n$, we find:

$$R_n \cong 0.08 \left( \frac{1}{\omega_H C'_{MT}} \right) \quad .$$

At resonance, then, the impedance due only to the capacitance of the chamber is about 12 times the loss impedance through the neck. Furthermore, since we operate at a frequency less than or equal to 0.2 $f_H$, the impedance of the chamber

is at least five times what it is at the helmholtz resonance. Therefore at working frequencies the impedance due to the capacitive side-chamber is 50 or 60 times that due to the loss in the neck. This conclusion is based on the data in Figure 2-9. $R_n$ could become significant with more viscous fluids, and will increase with viscosity at lower temperatures for DiSebacate.

In principle, corrections for $R_n$ and $L_n$ can be made at each temperature and pressure by taking measurements at several frequencies in the working range. With the satisfactory circuit model in Figure 2-8 it is possible to evaluate $R_n$ and $L_n$ using a curve-fit and then compensate for these elements in the working equations.

# CHAPTER 3

## Construction of the Apparatus

### 3–1 Introduction

In this chapter we discuss the design and construction of the chamber and its supporting apparatus. We also include a brief summary of the procedure used to take data.

### 3–2 Design Concepts

McKinney, Edelman, and Marvin introduced the concept of a small, bulk-compression chamber to measure dynamic compressibility in 1956.[4] Their chamber (as well as chambers used in subsequent measurements[3,6,7]) consisted of a short cylinder approximately 1 cm in diameter and 1 cm long containing a transducer at each end. The sample sat between the transducers as suggested by Figure 1-1(C). These chambers contained no doors; therefore they had to be taken apart and re-assembled for each set of measurements (or *run*). Typically a run would be made at various temperatures and pressures with the chamber empty, again with it containing an unknown sample, and finally with the chamber containing a calibration sample whose compressibility was known. (The calibration sample was needed because the governing equations require three measurements. Since there was no "door" to simply change the effective volume of the chamber (see Section 2-2), a third condition was obtained using a calibration sample). Each disassembly required the technician to disassemble the chamber; remove, add, or replace the sample; assemble the chamber; evacuate it; fill it with pressure fluid; and wait for the chamber to come to thermal equilibrium. This original single-chamber design presents several problems. Since the transducers change with pressure and temperature histories, empty and calibration runs must be made often (e.g., once per sample run). The transducers may even

change slightly during a run, causing errors. In addition, temperatures and pressures must be reliably reproduced in order to match up values of $\vec{E}^x_{out}$ and $E^x_{in}$ (the input and output voltages, respectively) from each run. A third problem is that the evacuation of the chamber is not perfect, and is not likely to be reproducible. If a small air bubble is present in the chamber for one run, it cannot be calibrated out (e.g., as part of $\vec{Z}_{CH}$, the chamber's acoustic impedance) if it is not present in another run. Finally, a complete set of runs for a single temperature and range of pressures (or a single pressure and a range of temperatures) may take on the order of three days.

These problems led to the concept of the current chamber: we wanted to put the unknown and calibration samples inside the chamber so they were at the right temperature and pressure, then somehow hide one, the other, or both by isolating them from the rest of the chamber. The simplest, most practical way to do this is to have one "*door*" in the main chamber which slides between two compartments (*side-chambers*)—one in either side of the main chamber. The door slides to close off either side-chamber or is left in a middle position where neither side-chamber is closed off. One side-chamber contains the sample, the other is left empty. A schematic of the chamber is in Figure 2–1. As Figure 2–1 depicts, three measurement conditions are possible without the use of a calibration sample. With this chamber, all three measurements can be made simply by moving the door—which is controllable from the outside. A new calibration is made for each data point. (Section 4–4 contains an example of the advantage of this *self-calibrating* feature.) Once the sample is placed in the chamber (changing samples requires a disassembly) data points can be obtained at intervals of approximately three minutes.

## 3–3 Chamber Design

The chamber design accommodates several desired parameters as well as several practical constraints. The chamber should operate in a range of temperatures from less than 0° to over 70°C. It has to prevent air from leaking in, or pressure fluid from leaking out, for internal pressures between near vacuum (a few micrometers of mercury) and 10,000 psi throughout the desired temperature range. The chamber must accommodate the widest frequency range possible. Therefore, since our measurement method involves lumped element approximations, a small chamber is desirable. However, the sample must be large enough that it will act homogeneous even if it contains suspended particles or large crystal-like regions. As a compromise, we designed our chamber so that cross sectional areas of the sample will have dimensions on the order of 1 cm. Corprene

(cork particles suspended in neoprene), for example, typically has particles whose dimensions are on the order of one millimeter. As a final constraint, the door must leave a constant volume in the main and side-chambers as it moves to close off side-chambers or is left open. This is not only to make the calculations easier, but to keep the pressure in the chamber constant and to avoid net hydrostatic forces on the door-stem. As a result of these constraints the door has two stems, each of which passes through the wall of a side-chamber.

An isometric view of the assembled chamber appears in Figure 3-1, while assembly cross-sections appear in Figures 3-2 and 3-3.

There are several other practical aspects to the design:

- **Transducers:** Ideally we would like free-floating (i.e., uncoupled to the walls) monopoles expanding at the desired frequency and at a reasonable amplitude. Real transducers, though, must have electrical connections to the outside world. In a closed chamber this requires electrical leads through the chamber walls which ultimately connect to the transducers. We use the electrically insulated *feed-through connectors* as positive leads and the chamber walls as a ground (see Figure 3-4). Our expander and receiver are piezoelectric disks made of silver-plated Channelite 5500 ceramic (lead zinconate-lead titanate). The disks used for the results in Chapter 4 were 0.275 *in. in diameter, and* 0.035 *in. thick. They were soldered* (using low melting point (136°C) Cadmium solder) to a piece of springy wire bent in the shape of a "handlebar moustache" (see Figure 3-4). This wire suspended the disk so it would not couple directly with the walls, and also served as the ground for the transducer. We soldered the positive face of the disk to a short piece of wire which we in turn soldered to the insulated feed-through. The short pieces of wire involved were springy enough not to permanently deform as the transducer plug was screwed into place. The natural frequency of these springs soldered to the mass of the transducer was far above the working frequencies of the chamber.

- **Threaded Components:** The valve parts, side-chamber packing nuts, and transducer plugs are all threaded. This is to assure that an evenly distributed force is applied to all the seals. An evenly distributed hold-down force helps prevent leaking and accidental damage to the chamber (multiple hold-down bolts can be tightened unevenly). These pieces are also easy to replace if some variation of design is desired (e.g., a change in side-chamber shape or volume, a different transducer, etc.).

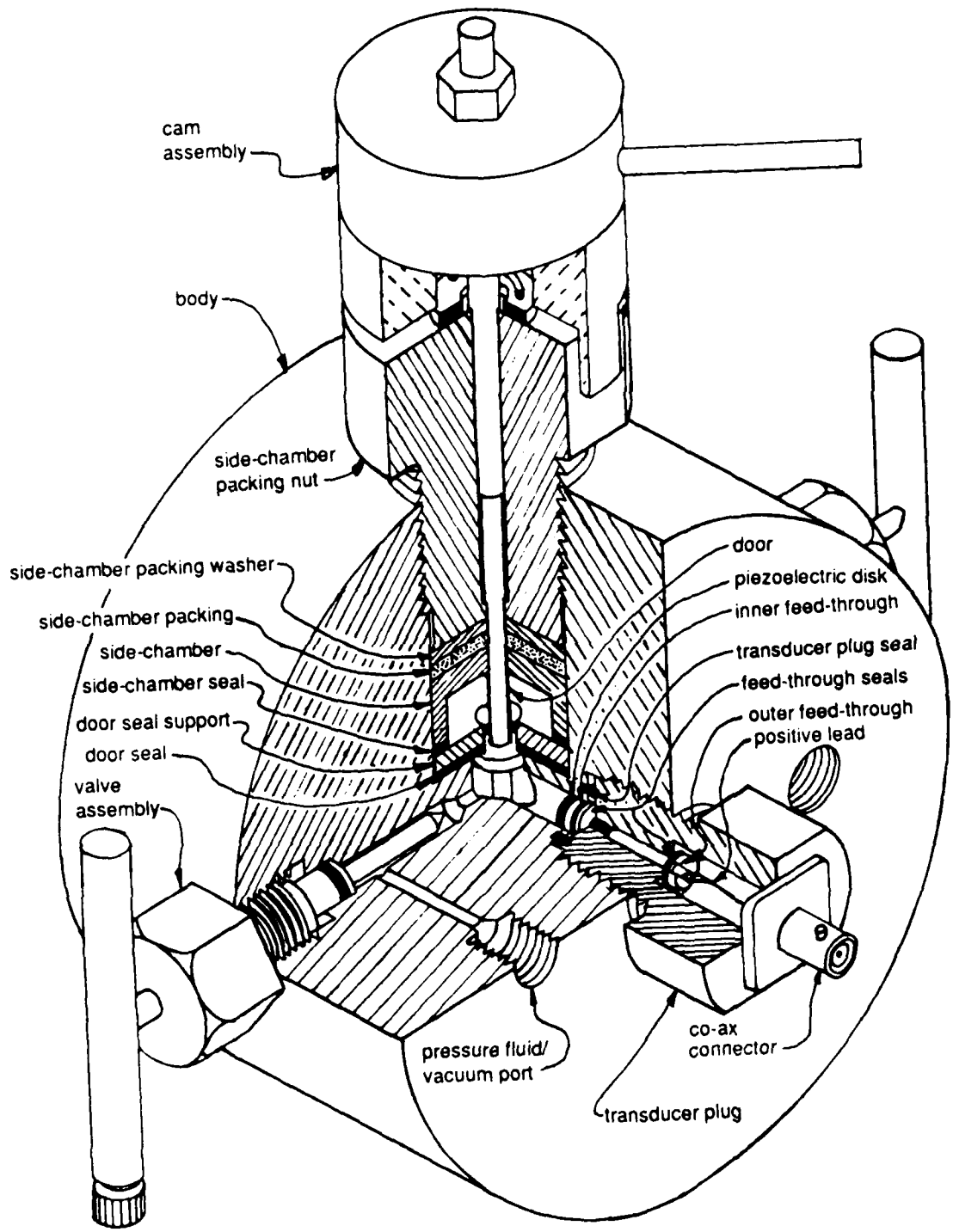


**Figure 3–1** ISOMETRIC VIEW OF ASSEMBLED CHAMBER. THREE-QUARTERS SCALE.

AS-89-1535

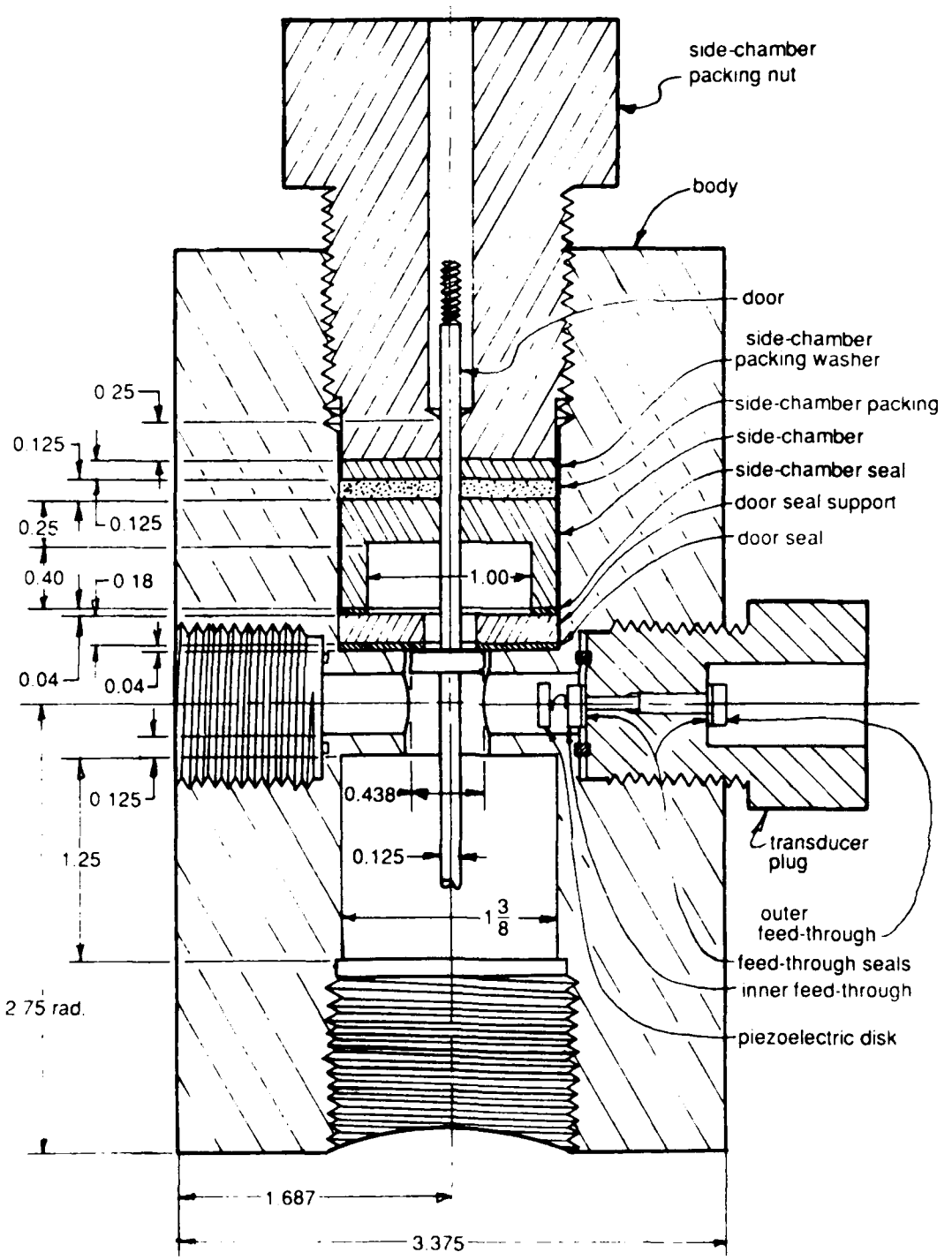


**Figure 3 2** CROSS SECTIONAL VIEW OF CHAMBER SHOWING TRANSDUCERS AND SIDE-CHAMBERS. APPROXIMATELY FULL SCALE, DIMENSIONS IN INCHES.

AS-89-1536

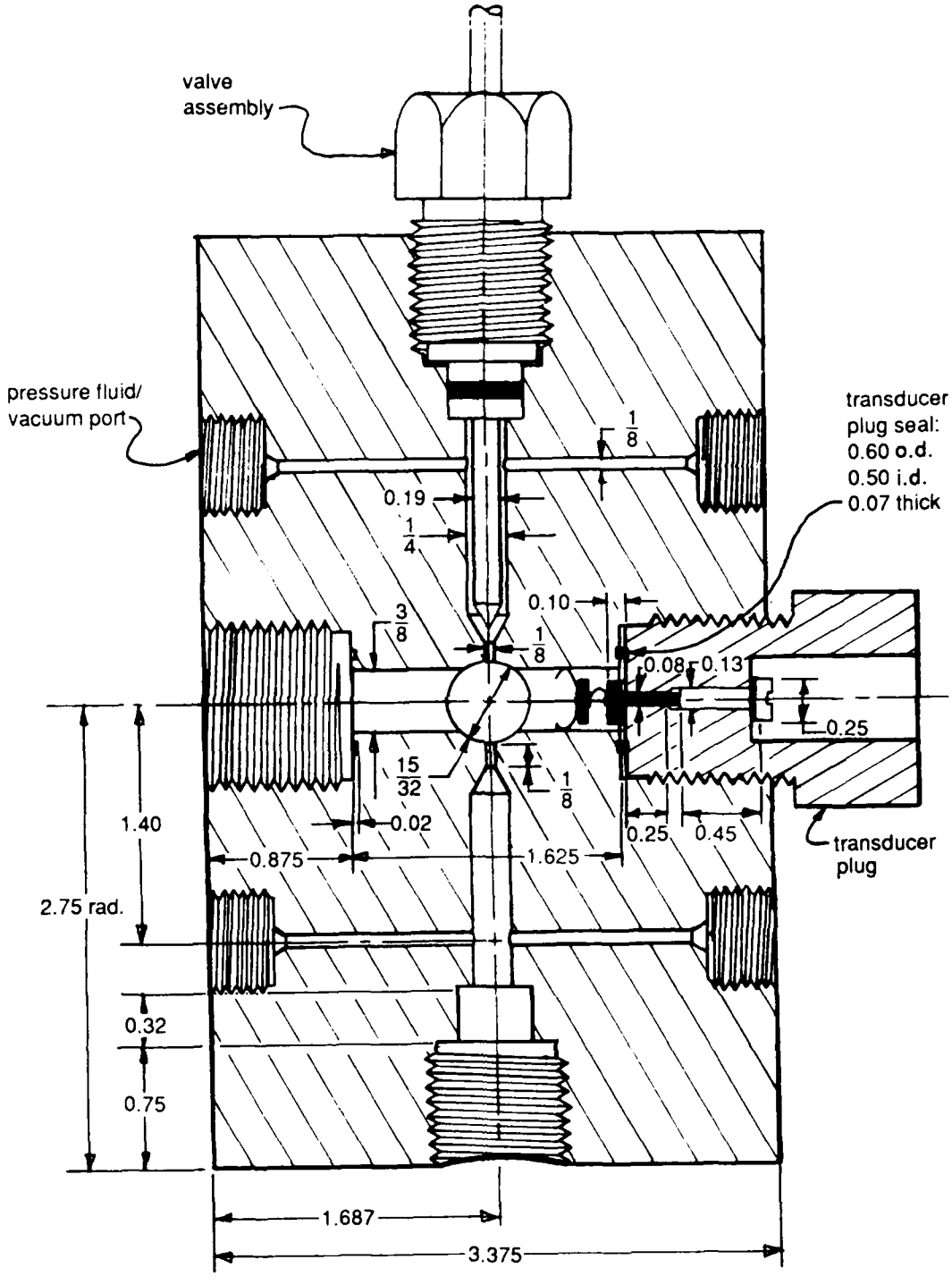


**Figure 3–3** CROSS SECTIONAL VIEW OF CHAMBER SHOWING TRANSDUCERS AND VALVES. APPROXIMATELY FULL SCALE, DIMENSIONS IN INCHES.

AS-89-1537

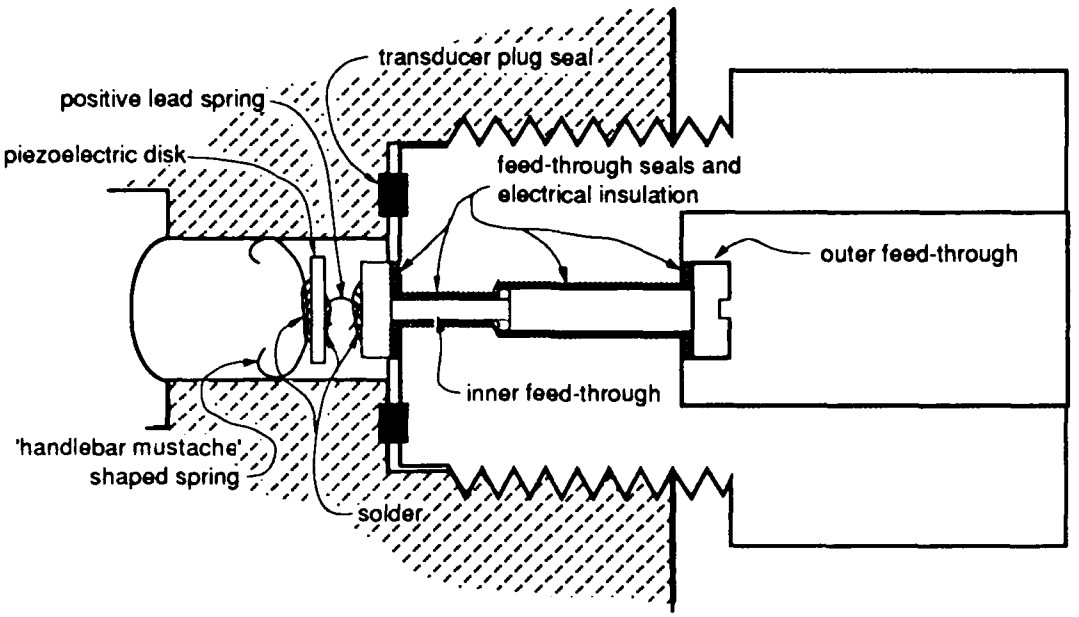


**Figure 3-4** ENLARGED CROSS SECTIONAL VIEW OF MOUNTING FOR TRANSDUCERS. SCALE IS 2:1.

AS-89-1538

- **Valves:** The valves are modeled after the non-rotating valve stem valves made by Autoclave Engineers, Inc., of Erie, Pennsylvania, except that they have longer stems. This modification allows them to seat as close as possible to the inside wall of the chamber leaving only a short distance between a closed valve stem and the bulk of the main chamber (see Figure 3–3). The short separation between valve and chamber avoids complications arising from lossy or possibly resonant fill tubes leading to external valves.

- **Building Materials and Seals:** With the exception of the feed-through connectors and the various seals, all parts of the chamber are 304 or 303 stainless steel. (The feed-throughs for the transducers were originally made of brass so they would be compatible with existing parts. Their only requirements are that they be made of a good conductor, and that the conductor is rigid enough so that at high pressures the feed-throughs will not extrude through the holes in which they sit.) Stainless steel is used in as many parts as possible because it does not react with many chemicals and it displays a large *toughness* (the area under its stress-strain curve—i.e., it deforms under load before experiencing catastrophic failure) and therefore is safer

to use for high pressure applications. Other materials include:

- **teflon seals:** Though teflon is compressible (it is advantageous to have the hardware in the chamber much more rigid than the sample), very small amounts are exposed inside the chamber in the feed-through seals and the side-chamber packing. We chose teflon because it is compliant (needed to seal the doorstems as they move through the packing), an electrical insulator (for the feed-throughs), and it is resistant to a variety of lab chemicals (cleaners such as acetone, and various pressure fluids).
- **copper seals:** Copper seals mating parts wherever possible: the side-chamber seal, the door seal, and the transducer plug seal are all copper (see Figure 3–1). Copper seals are soft enough to deform and make a good seal; they work harden enough when they seal that they do not extrude; they are relatively rigid, like the stainless parts, so they do not add to the compressibility of the chamber; and they are not reactive with any of the lab chemicals used in these measurements.
- **solder seals:** It is important that the door completely seals off the side-chambers. Unfortunately no great force can be used on the door without damaging the threads on the ends of the doorstems (see Figure 3–2). To improve this seal we melted a small amount of Pb-Sn solder on the edge of the door seal where it mates with the garage door. We then polished the solder mirror smooth and to an unobtrusive thickness. We also polished the door itself mirror smooth. The solder is soft and makes a good seal, and in this spot there is no danger of extrusion since the static pressure is the same on each side of the door. The solder also does not react with any chemicals used in the chamber. (Note, however, that if any mercury used in the fluid separator (see Section 3–4.1) is accidentally pumped into the chamber it will wet this surface. In addition, mercury will react chemically with *silver* solder).
- **stainless steel seals:** The valve stems have no special seat. The stainless steel stem simply mates to the seat machined into the stainless steel body of the chamber. The cone shaped stem, driven by the threaded sleeve, deforms enough to make a very good seal.

- **Cam Assemblies:** We designed the cam assemblies so that the user may move the door reliably and reproducibly to any of its three positions and have a sufficient force on the door to make good seals with the side-chambers'

inner seals. It rotates about a helical guide so that in the future it may easily be coupled to a stepper motor and be automated. The design is incomplete, though a functional model is in use. See Chapter 5 for more details.

- **Pressure Fluid:** The fluid we used for the measurements reported in Chapter 4 was Di(2 ethyl hexyl)sebacate, abbreviated DiSebacate. We used it because the properties are known;[19] it is inexpensive; and it is convenient to work with in that it is electrically non-conducting, clear, odorless, virtually harmless to humans, and it cleans up well with acetone. Also, this was the fluid used by McKinney and Belcher for their measurements of the compressibility of poly(vinyl acetate).[7] Unfortunately it is a commercial plasticizer and is absorbed by some samples (including many types of polyurethane). Other options include castor oil and vacuum pump oil, whose properties are also well known, but which are not as easy to work with. We also spent time investigating the use of Fluorinert (3M product FC-84) but found its sound speed was too low and compressibility too high for it to be useful. There is more on pressure fluids in Chapter 5.

The chamber in its current form conforms to all the requirements, except that at high pressures and low temperatures the teflon seal for the doorstem on the sample side-chamber leaks slightly. This occurs because at low temperatures the teflon seal is not compliant enough to make up for irregularities in the diameter of the doorstem. Data-taking occurs fast enough with the current software so that this problem does not affect the data noticeably.

## 3–4 Supporting Apparatus

Several pieces of equipment are needed to monitor, control, and process the pressure, temperature, AC signals, and, potentially, the frequency and door positions involved in a run. These parameters are monitored and, when possible, controlled with a Hewlett-Packard HP-85 desktop computer. See Figure 3-5 for a schematic of the whole apparatus.

### 3–4.1 Pressure

The pressure equipment must reproducibly achieve and maintain a specific pressure, and quantify that pressure. The equipment includes:

- **hand pump:** We use a 10,000 psi capacity hand pump to create the pressure.

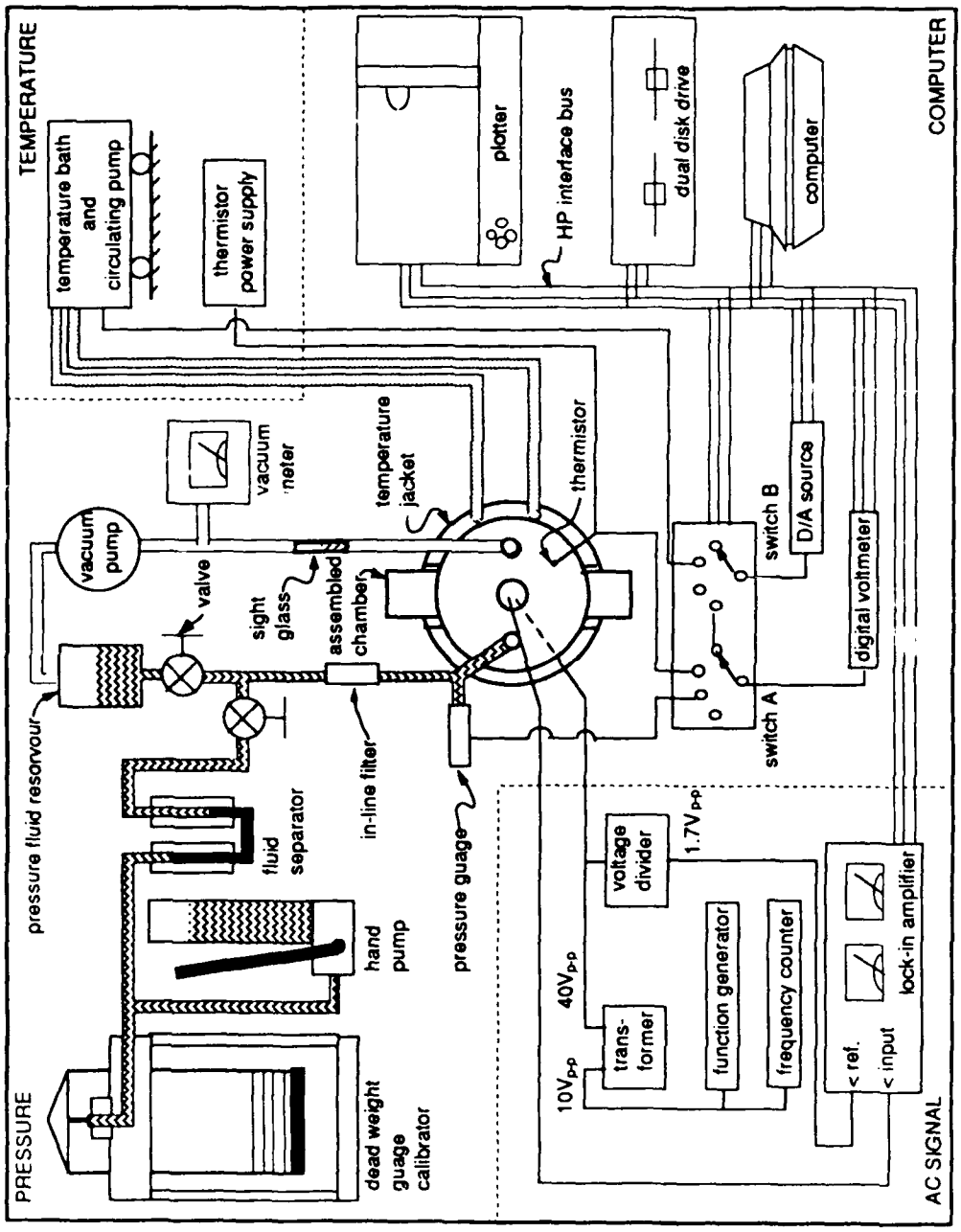


**Figure 3-5** SCHEMATIC OF COMPLETE APPARATUS. THE SCHEMATIC IS DIVIDED INTO FOUR GENERAL AREAS CORRESPONDING TO THE SUB-SECTIONS IN SECTION 3.4. THE ASSEMBLED CHAMBER CONTAINING THE SAMPLE, DOOR, ETC., IS AT THE CENTER OF THE SCHEMATIC.



AS-89-1539

- **dead weight gauge calibrator:** We keep this calibrator on line constantly (except during data taking for which the chamber is closed off). It not only allows us to calibrate the gauge, but, more importantly, it allows the fluid contained in the stroke of the piston on which the weights set to act as a "buffer." Thus the calibrator keeps the apparatus at a constant pressure while the various parts leak, expand or contract due to pressure changes, or as valves are opened and closed.

- **pressure gauge:** The pressure gauge is an Autoclave Engineers AESC 10,000 psi pressure gauge which contains an analog DC output terminal through which pressure is monitored electronically.

- **fluid separator:** A mercury-in-U-tube type fluid separator separates the pump oil in the hand pump and calibrator from the pressure fluid in the chamber.

- **vacuum equipment:** The chamber must be evacuated before it can be filled with pressure fluid so that no bubbles of air are trapped inside. There is also a pressure fluid reservoir where the fluid is degassed by evacuation prior to being loaded into the evacuated chamber. The vacuum equipment consists of a single stage vacuum pump and a thermal vacuum gauge.

### 3–4.2 Temperature

Temperature controlling equipment consists simply of a hot-or-cold temperature bath and a thermistor which is placed in a half-inch deep, $\frac{1}{8}$ inch diameter hole in the body of the chamber. The temperature bath includes heating and refrigeration equipment and a surprisingly consistent bi-metallic strip "bang-bang controller" thermostat which hangs down into the bath. A circulating pump pumps the ethylene-glycol and water mixture through insulated hoses to a tight fitting aluminum temperature jacket on the chamber. The bi-metallic strip thermostat can keep the chamber at a constant temperature with a tolerance of $\pm 0.1^{\circ}$C, but it is hard to set since it is completely uncalibrated. For later data, we replaced the bi-metallic strip with a "waiting loop" built into the software. With the waiting loop the computer checks the temperature at the thermistor between sets of program steps and while it is waiting for commands. Using a Hewlett-Packard Interface Bus (HPIB) compatible switch ("switch B" in Figure 3–5), it short- or open-circuits the thermostat leads as need be. This loop is simply a calibrated bang-bang controller. It keeps the temperature constant with a tolerance of less than $\pm 0.3^{\circ}$C.

### 3–4.3 AC Signal

We take a 10 $V_{p-p}$ signal from a Exact Electronics 505 function generator, step it up to 40 $V_{p-p}$ with a transformer, and feed it into the input transducer. An HPIB compatible PAR 5800 lock-in amplifier monitors the output. The user monitors the frequency with a digital frequency counter. The reference signal for the lock-in is tapped through a voltage divider at the 40 $V_{p-p}$ input signal rather than the low voltage side so that any phase change due to the transformer will not influence the readings of the output signal. We checked the step-up transformer for a third harmonic (which is not distinguishable from the first harmonic by the lock-in) and found no measurable third harmonic generation. The Exact Electronics function generator's frequency is controllable with a DC signal and, though it is not yet a part of the software, the frequency is intended to be computer controllable. This, along with an HPIB compatible frequency counter, would enable researchers to have data taken at several frequencies automatically.

### 3–4.4 Computer

The hardware consists of a Hewlett-Packard HP-85 desktop computer with an expanded memory; a dual disk drive; a digital volt meter, digital to analog DC source, and a multi pole switch (all to act as a multichannel D-to-A, A-to-D converter); a plotter; and plug in ROMs to operate all this equipment on the HPIB. The make-shift D-to-A, A-to-D converter is to communicate with the equipment which requires analog signals.

Software includes 6 to 10 programs stored on one of the disks (data is stored on the other disk in the dual disk drive). Currently these programs act in concert to take, store, reduce, display, and plot the data, to monitor and control temperature, and to monitor pressure. The operator is required only to change the pressure, adjust the door position, operate the valves in the body of the chamber, and supply some start up conditions such as desired temperature, the frequency, etc.

## 3–5 Procedure Summary

This is a brief summary of procedure. The data in Chapter 4 was taken using this procedure.

1. **Load Sample:** This is a labor intensive procedure: disassemble the sample side-chamber, replace the sample, reassemble the side-chamber, retorque the packing nut, and reassemble the cam onto the packing nut and doorstem.

2. **Evacuate Chamber:** Turn on the pump and open the valve on the side of the chamber where the pump is connected. Evacuate to approximately 5-10 $\mu$m of mercury (about 50 minutes with the current pump).

3. **Fill Chamber:** Fill the chamber with pressure fluid by opening valves up to the pressure fluid reservoir. Pressure fluid in the reservoir should have been degassed recently by evacuation.

4. **Seal Valve to Vacuum Pump:** When fluid appears in the sight glass of the hose to the vacuum pump from the chamber, the chamber is full. Close the valve quickly so no fluid enters the vacuum transducer.

5. **Raise Pressure:** Leave chamber at significant pressure ($\cong$4000 psi) for several hours to dissolve any small bubbles of air which may be left inside.

6. **Set Temperature:** While the chamber is waiting at a significant pressure, load and run the program "START MOR," and follow the instructions to enter the desired temperature and tolerance from the keyboard. When the temperature is within tolerance a message appears on the screen with the temperature, the tolerance, and the time the system has been within tolerance. Leave the temperature within tolerance for at least an hour before taking data (this is to assure the whole chamber is at a uniform temperature).

7. **Begin Data Taking Process:** Switch to the data taking program by pressing the indicated function key. Fill in the menu items (data, frequency, etc.).

8. **Correct Pressure:** Bring apparatus to correct pressure, wait 20-30 seconds for parts to expand or contract.

9. **Seal Chamber:** Shut the valve in the chamber which connects to the pressure apparatus.

10. **Take Data:** Follow the instructions on the screen–they include operating the cam to first close the door on the sample side-chamber, open the door, then close it on the empty side-chamber (as depicted in the schematic in Figure 2-1 on page 10). The current software averages 20 readings at each door position. The readings occur approximately $1\frac{1}{2}$ seconds apart.

11. **Judge the Data Point:** The pressure, temperature, and dynamic compressibility of the sample are displayed on the screen. If approximate values,

or values at previous pressures are known, use these to judge whether or not the reported compressibility is realistic. A huge or infinitesimal compressibility may mean that the door did not seal properly to one of the side-chambers, or that a valve was left open. As a result, the data point must be retaken. Use the appropriate function key to "save" or "try again."

12. **Other Pressures:** Follow Steps 8 to 11 for all desired pressures.

13. **Save and Plot Data:** When data taking is complete for a certain temperature, end data taking by pressing the appropriate function key. Answer questions on the screen to get various displays of the data (plots and lists on screen and paper).

14. **Other Temperatures:** At the end of plotting, etc., more questions appear in the screen. Answer appropriately to quit or go on to a different temperature. To "go on," the program re-loads and runs "START MOR." Proceed again from Step 5 as desired.

Notice that the pressure is left at a few thousand pounds per square inch between runs. We do this to assure that any dissolved air remains in solution. Air dissolved in solution has far less effect on the compressibility of the fluid in the chamber than small air bubbles do. Recall, though, from Section 2–1 that sudden changes in pressure may affect the value of a sample's compressibility. This may play a part in the values reported in Chapter 4. For all the data included in Chapter 4, we left the chamber at between 2000 and 4000 psi between runs. To begin runs, we raised the pressure to 8000 or 10,000 psi (letting the chamber set for several minutes), then took data at decreasing pressure increments until we reached atmospheric pressure. At the end of a run we again left the chamber at a pressure of a few thousand pounds per square inch.

# CHAPTER 4

## Results

### 4–1 Introduction

We tested two samples to compare values obtained with this apparatus to those obtained using the original single chamber design, as well as other methods. The samples were poly(vinyl acetate) (PVAc), and polytetrafluoroethylene (PTFE, or Teflon). We chose PVAc first to compare it with extensive data collected using the single chamber design by McKinney and Belcher,[7] and also by Lin.[3] Furthermore, we chose PVAc in order to measure a polymer in its *dispersion region* (see Section 2–1). Similarly, we chose Teflon to compare our results with data obtained by Lin,[3] and with concepts discussed by Weir,[13] Beecroft and Swenson,[16] Heydemann,[14] and Ohzawa and Wada.[15]

The rest of this chapter contains data and discussions of the data. Sections 4–2 and 4–3 are devoted to PVAc and Teflon, respectively. In Section 4–4, we discuss a set of data in which the transducers changed calibration between runs and clearly displayed the advantage of a self-calibrating apparatus.

All the data taken here was taken as described in Section 3–5. Isothermal runs were made at a range of pressures starting at 8000 or 10,000 psig and decreasing to atmospheric pressure in 500, 1000, or 2000 psi increments.

### 4–2 PVAc

We tested poly(vinyl acetate) (PVAc) to compare our results to extensive data taken by McKinney and Belcher,[7] and also to data taken by Lin[3] for a sample from the same specimen as ours. We also wished to test a sample in its dispersion region. In the dispersion region for polymers (the transition between glassy and rubbery behavior), there is commonly an increase in the real (storage) part of compressibility, $\beta_{(r)}$, and a peak in the imaginary (loss) part of compressibility, $\beta_{(i)}$. We used a sample of PVAc manufactured by Scientific Polymer Products,

Inc. Our sample came from the same specimen which Lin used for his "medium molecular weight" PVAc.[3] (Scientific Polymer Products reports the molecular mass as $M_N$ = 63,600, and $M_W$ = 194,800 where $M_N$ and $M_W$ are the number average molecular weight and mass average molecular weight, respectively.) The sample came in the form of pellets approximately 5 mm in diameter. The density is approximately 1.19 g/cm$^3$ at 24°C and atmospheric pressure, and $T_g$, the glass transition temperature, is approximately 30°C. Our sample had a mass of 3.024 g. The sample pellets had to be held together to keep them in the side-chamber both while it was being assembled, and while the door was open (see Figure 2-1). We put 20-25 pellets in a mock-up of the side-chamber and door-stem, then softened the pellets with a forced air heat gun. The pellets softened enough to stick to one-another, but not enough to deform or flow. They were left at room temperature and cooled in approximately $\frac{1}{2}$ hour. The result was an annular cylinder the size of the side-chamber and made up of small pellets with space between them—much like a small ball of small 'carameled popcorn.'

Figures 4-1 through 4-6 are plots of the real and imaginary parts of compressibility ($\beta_{(r)}$ and $\beta_{(i)}$, respectively) as a function of pressure and for several temperatures. The plots are compilations of data taken over a three month period. Notice the loss part of the compressibility has been plotted with its true sign as described in Section 2-4. Dynamic compressibility data is often reported as a magnitude only and thus appears positive when plotted. The data has not been smoothed except that points which vary considerably from the trend (indicating an obvious measurement error) have been removed. All the data is virtually linear and has been fit with straight lines. A statistical analysis of the data, or a more sophisticated curve fitting technique may yield more reliable curves, but has not been applied since this paper does not deal with such careful interpretation of the data. However, the output signal is on the order of a microvolt and is subject to electronic as well as mechanical noise. Chapter 5 contains suggestions which may lead to a higher amplitude output signal resulting in less scatter in the data. Figure 4-7 is a summary of the data plotted against pressure. Individual data points have been left out for clarity. Often data is reported plotted against temperature. Figure 4-8 is data from Figures 4-1 through 4-6 for 0 psi, 1000 psig (68 atm), 4000 psi (272 atm), and 8000 psi (544 atm). Only the data points for 0 psi are included, again for clarity. Finally, Figures 4-9 and 4-10 contain data scaled from plots reported by McKinney and Belcher,[7] and Lin,[3] respectively. Lines copied from Figure 4-8 also appear on Figures 4-9 and 4-10.

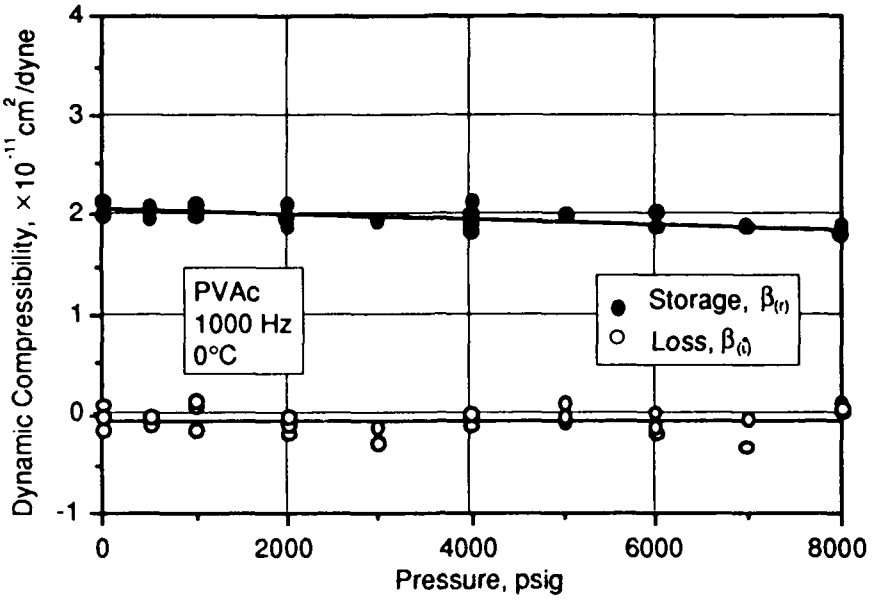


**Figure 4-1** PVAc. Dynamic Compressibility vs. Pressure. 0°C.

AS-89-1540

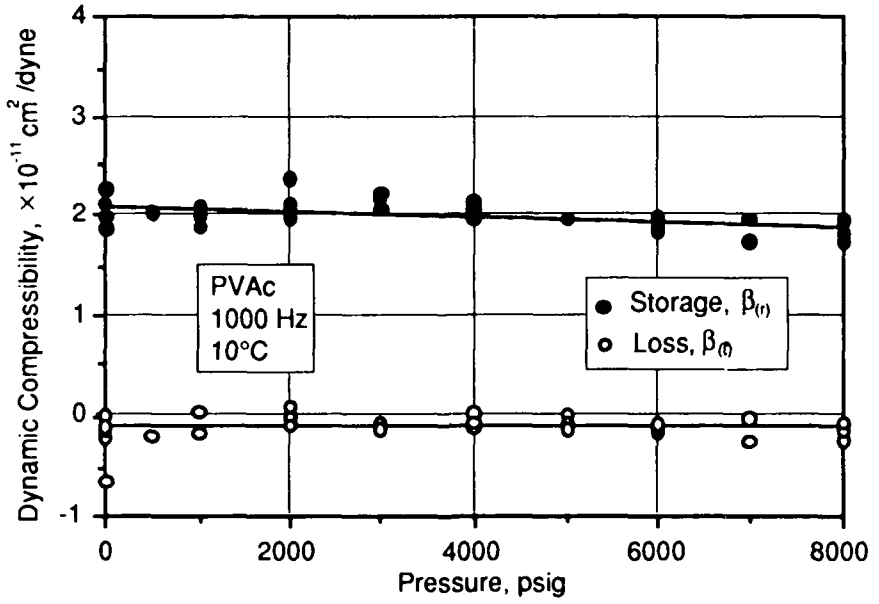


**Figure 4-2** PVAc. Dynamic Compressibility vs. Pressure. 10°C.

AS-89-1541

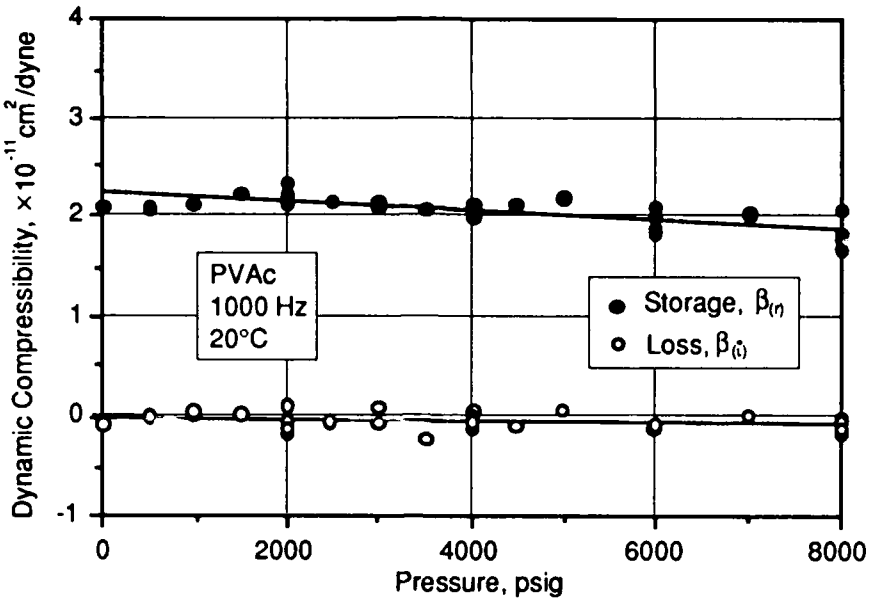


**Figure 4–3** PVAc. Dynamic Compressibility vs. Pressure. 20°C.

AS-89-1542

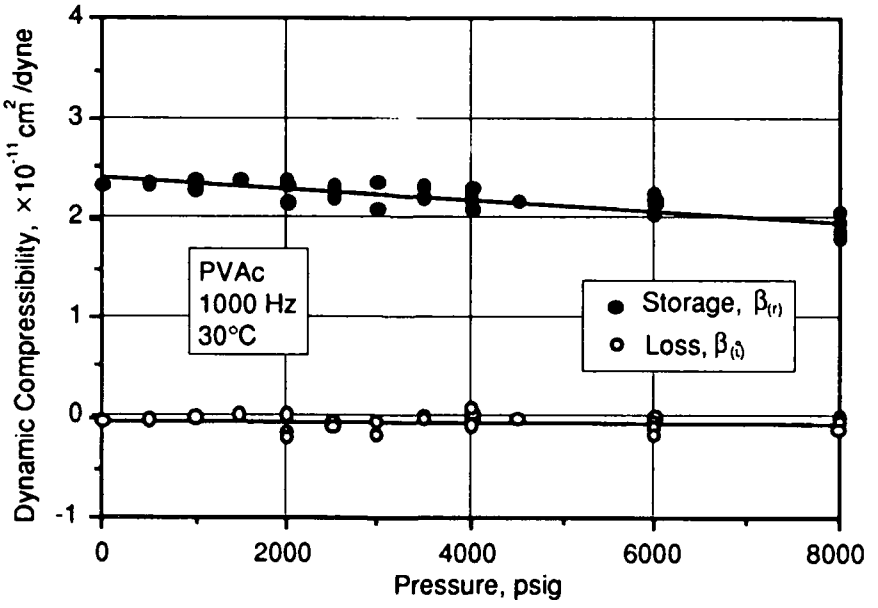


**Figure 4–4** PVAc. Dynamic Compressibility vs. Pressure. 30°C.

AS-89-1543

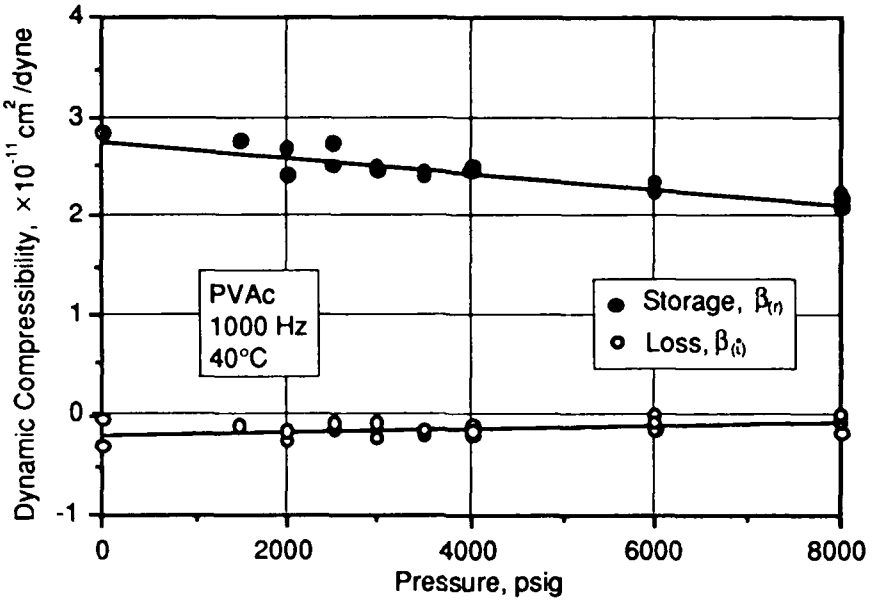


**Figure 4-5** PVAc. Dynamic Compressibility vs. Pressure. 40°C.

AS-89-1544

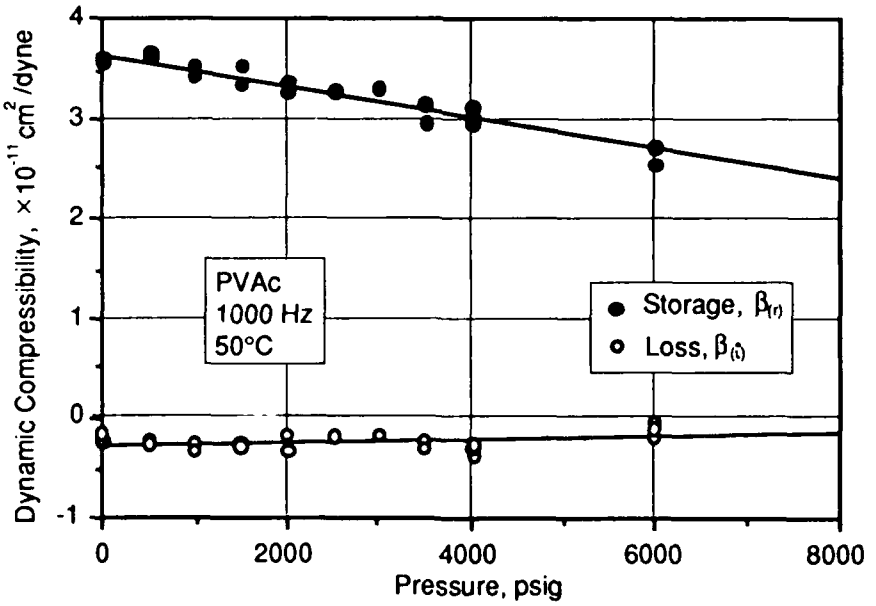


**Figure 4-6** PVAc. Dynamic Compressibility vs. Pressure. 50°C.

AS-89-1545

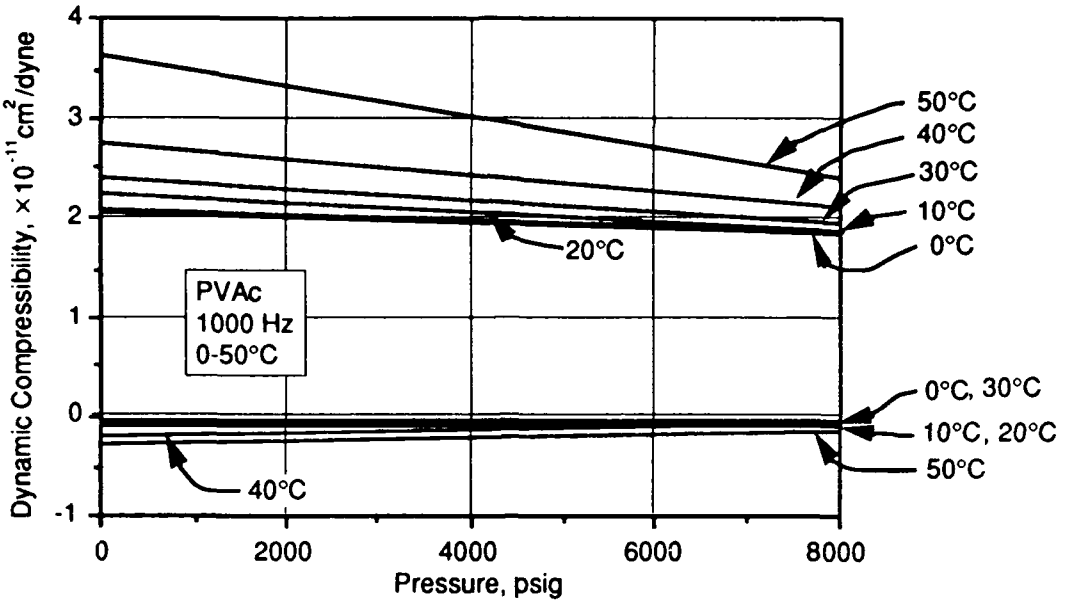


**Figure 4–7** PVAc. Summary of Dynamic Compressibility vs. Pressure.

AS-89-1546

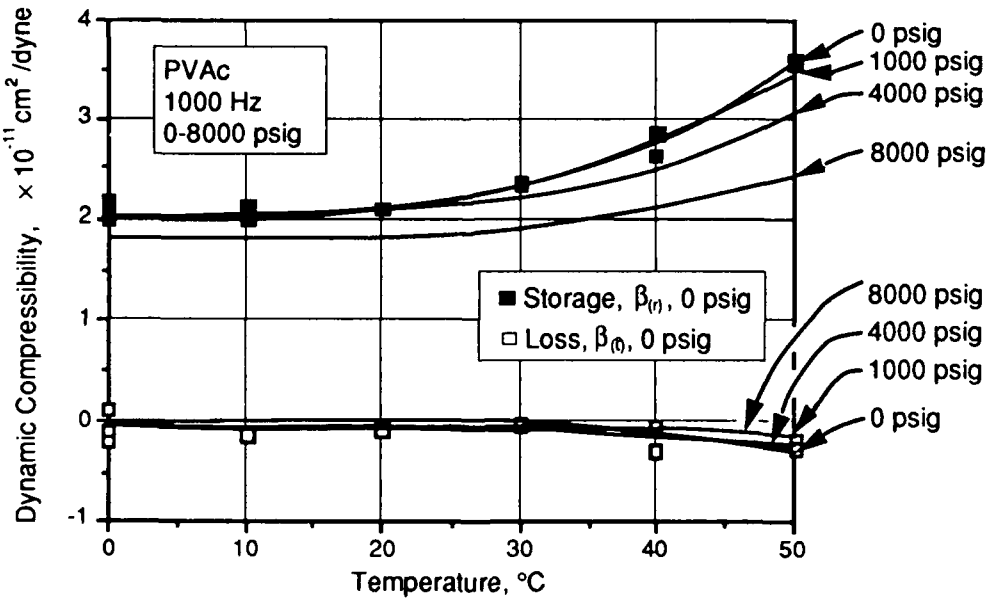


**Figure 4–8** PVAc. Dynamic Compressibility vs. Temperature. Data points shown for 0 psig only, since this data is simply transposed from the graphs above.

AS-89-1547

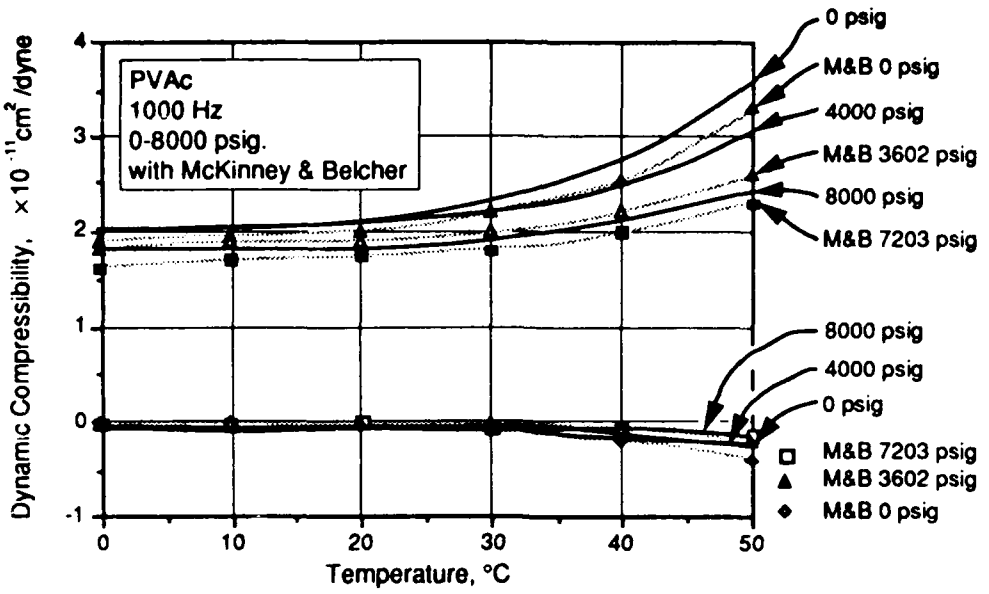


**Figure 4-9** PVAc. Summary of Dynamic Compressibility vs. Temperature. Data compared to that reported by McKinney and Belcher.

AS-89-1548

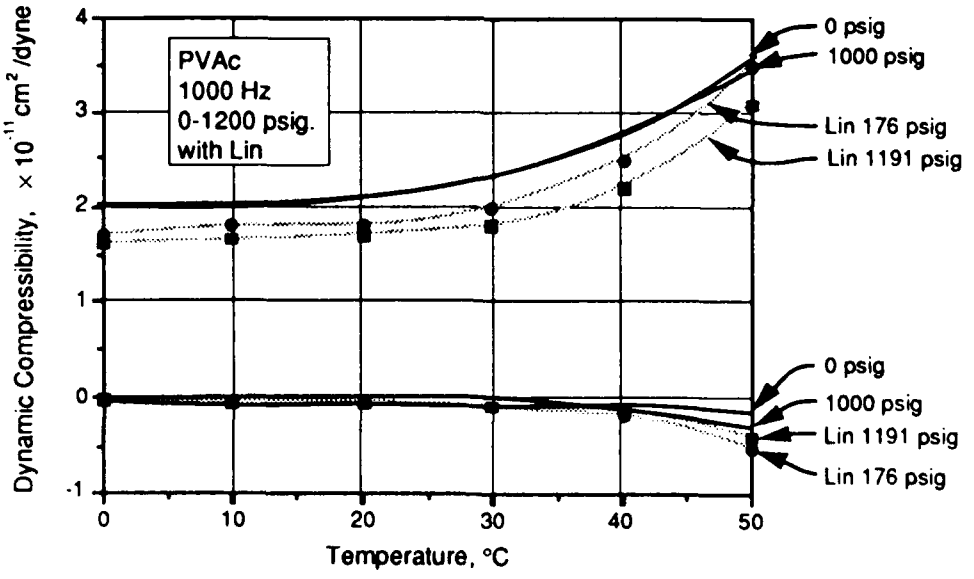


**Figure 4-10** PVAc. Summary of Dynamic Compressibility vs. Temperature. Data compared to that reported by Lin.

AS-89-1549

Even without comparing to other data, we see trends in our data that we expect (see Section 2-1). For the real (storage) compressibility we see values between about 2 and $4 \times 10^{-11} \text{cm}^2/\text{dyne}$, which is typical for polymers.[13] As the temperature rises, the compressibility generally goes up in magnitude, and at a faster rate for temperatures above $T_g$. As pressures go up, the sample generally becomes less compressible. The imaginary (loss) values are relatively small in magnitude, negative (as they should be), and on the order of $-0.1 \times 10^{-11}$ cm$^2$/dyne. They also increase in magnitude with temperature and decrease with pressure. These simple observations must be augmented with the fact that since this sample is near its $T_g$, it starts becoming *dispersive* at 20-40°C (depending on frequency and pressure). (See Section 2-1 for a brief explanation of dispersion.) If data were taken at higher temperatures we would see the loss part decrease once again in magnitude and a decrease in the slope of the $\beta_{(r)}$ versus temperature curve.[3,7] Unfortunately, our equipment was not set up for higher temperatures at the time this data was taken.

Comparing our data directly to that of McKinney and Belcher[7] (Figure 4-9), we see very similar trends, slopes, and curvatures. $\beta_{(r)}$ values are approximately 10% higher in magnitude than those reported by McKinney and Belcher, and $\beta_{(i)}$ values are smaller. Similarly, comparing to Lin's data[3] (Figure 4-10) we see the same trends, except that values of $\beta_{(r)}$ from Lin's report are lower than those reported either here or by McKinney and Belcher. These discrepancies may be due to a variety of causes. First of all, McKinney and Belcher reported that their sample may have contained a small amount of contaminant molecules. Also, though they did not mention the molecular weight of their sample, it was likely to be different than that of ours. In addition, McKinney and Belcher melted their sample at approximately 100°C. Recall from Section 2-1 that cooling rate can affect $\beta_{(r)}$—especially near $T_g$. This temperature dependence may also be a source of discrepancies between our data and that reported by Lin.[3] Ours was heated to near-melting, and let cool to room temperature, while Lin's was not heated above the maximum test temperature of 56°C. Finally, McKinney and Belcher, and Lin performed their tests at constant pressure and continually varying temperature, while this data was taken at constant temperatures and stepped pressure changes. We should also point out that we did not account for changes in the volume of our sample with changes in static pressure and temperature. McKinney and Goldstien[16] report data indicating that for the range of temperature and pressure in our work, the density of PVAc varies approximately ±2% from the average. In view of the scatter in our data, this factor is not important, though it may become so when the precision of the apparatus is improved.

In light of the variety of possible differences between this sample and others, the data reported here agrees quite well with other reported data and supports the credibility of the new chamber design.

## 4–3 Teflon

We tested polytetrafluoroethylene (PTFE, or Teflon) because, like PVAc, it had been done before.[3] In Teflon we wished to detect solid state phase changes reportedly at 19°C and 30°C.[14] This sample was cut from the same block donated by E.I. Du Pont de Nemours and Company to Lin for his measurements. $T_g$ for Teflon is usually taken to be approximately 130°C, so these tests look at Teflon's glassy states. The sample reportedly has a crystallinity of 52%.[3] The density at atmospheric pressure and 25°C is 2.151 g/cm$^3$. According to density data published by Martin and Eby,[17] and by Zoller,[18] the error due to ignoring changes in volume due to changes in static pressure and temperature is on the order of ±3%, though it may be higher. This estimate takes into account the expanded temperature and pressure ranges for this set of data (0 to 75°C and 0 to 10,000 psi, respectively). The sample was cut from a solid block to dimensions 1.5 mm (1/16 in.) smaller than the dimensions of the side-chamber, and a 6.4 mm (1/4 in.) hole was drilled in the middle for the doorstem. The final mass was 5.946 g. The sample was cut smaller than the side-chamber to allow it to be completely surrounded by pressure fluid so that true bulk compression would occur. Small pieces of wire were stuck into the sample to support it and keep it centered in the side-chamber.

Figures 4–11 through 4–18 are the dynamic compressibility of Teflon plotted against pressure for various temperatures. A summary of the fitted lines is in Figure 4–19. Notice the 20°C line appears at a different slope than, and the 30°C line is separated from, the lines of other temperatures. This change is more meaningful when we look at the compressibility plotted against temperature. Figures 4–20 through 4–23 contain original data plotted against temperature. Figure 4–24 is a composite of the curves drawn through the data. Figure 4–25 contains data for near-zero gauge pressures for our data and scaled from plots by Lin,[3] and Ohzawa and Wada.[14] Finally, Figure 4–26 contains our data at 1000 psi and Lin's at 81 atm (1191 psi).

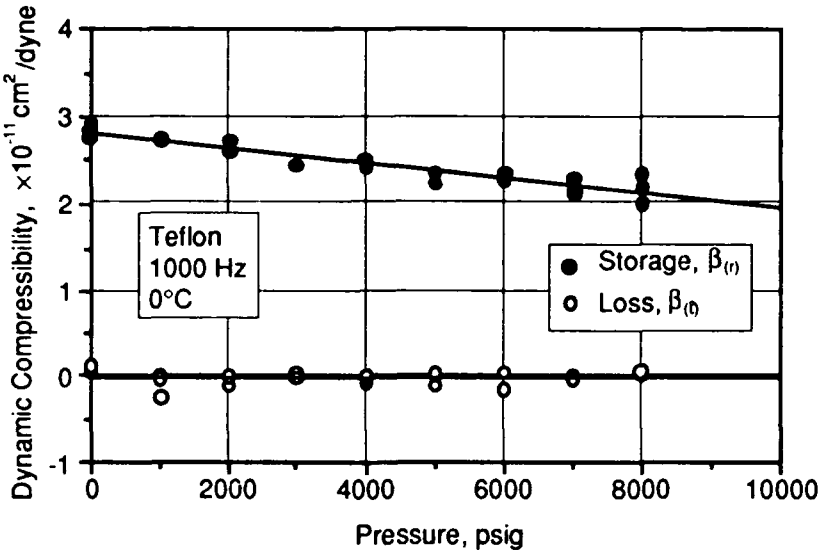


**Figure 4–11** TEFLON. DYNAMIC COMPRESSIBILITY VS. PRESSURE. 0°C.

AS-89-1550

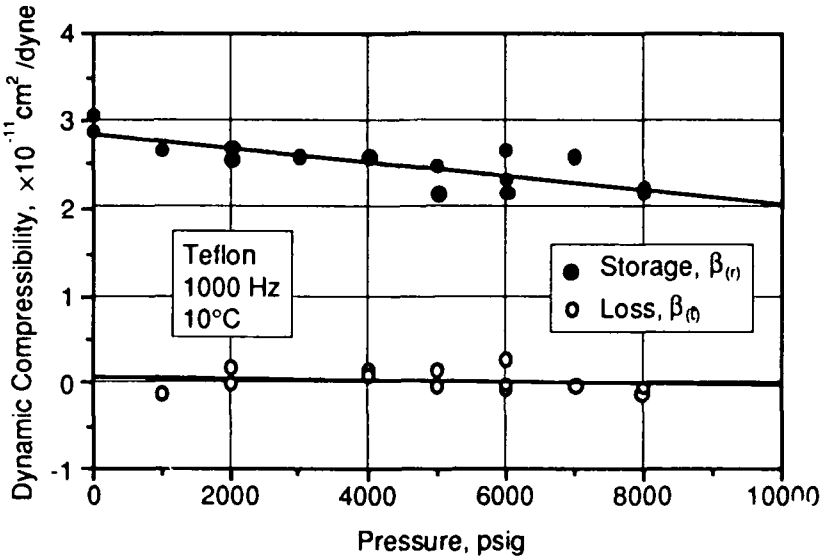


**Figure 4–12** TEFLON. DYNAMIC COMPRESSIBILITY VS. PRESSURE. 10°C.

AS-89-1551

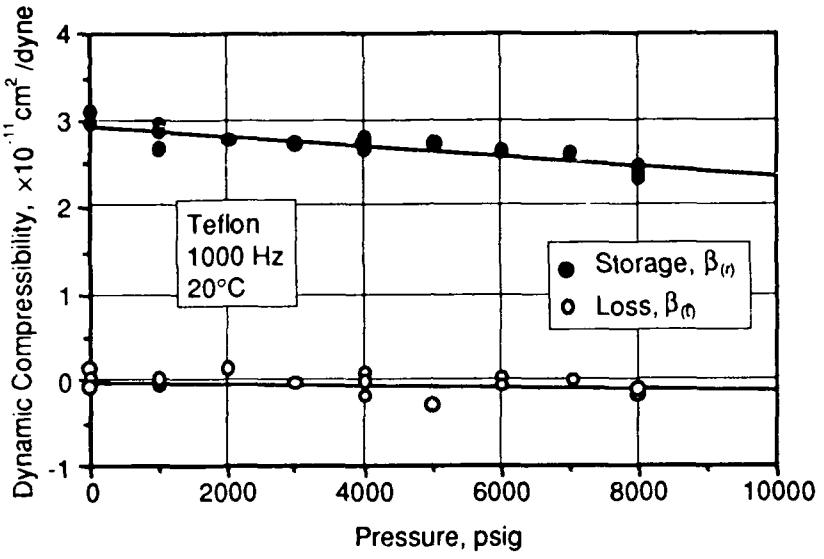


Figure 4–13 TEFLON. DYNAMIC COMPRESSIBILITY VS. PRESSURE. 20°C.

AS-89-1552

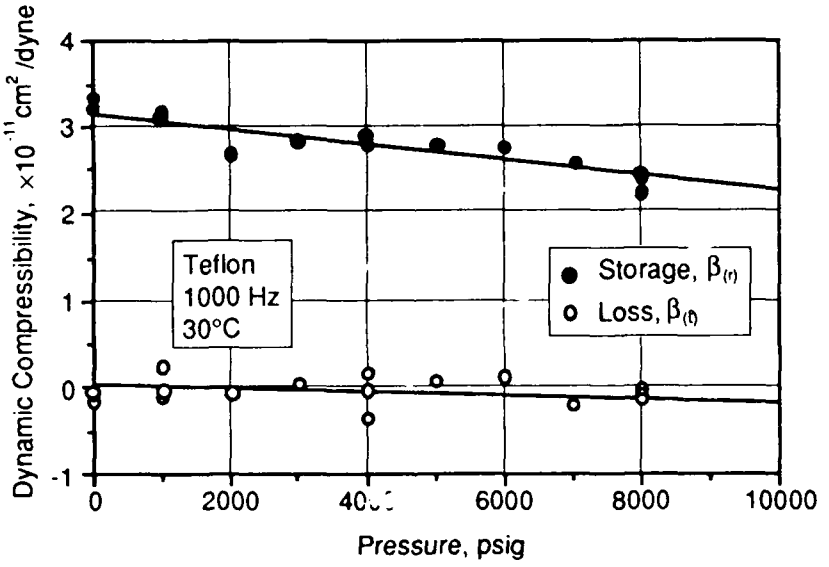


Figure 4 14 TEFLON. DYNAMIC COMPRESSIBILITY VS. PRESSURE. 30°C.

AS-89-1553

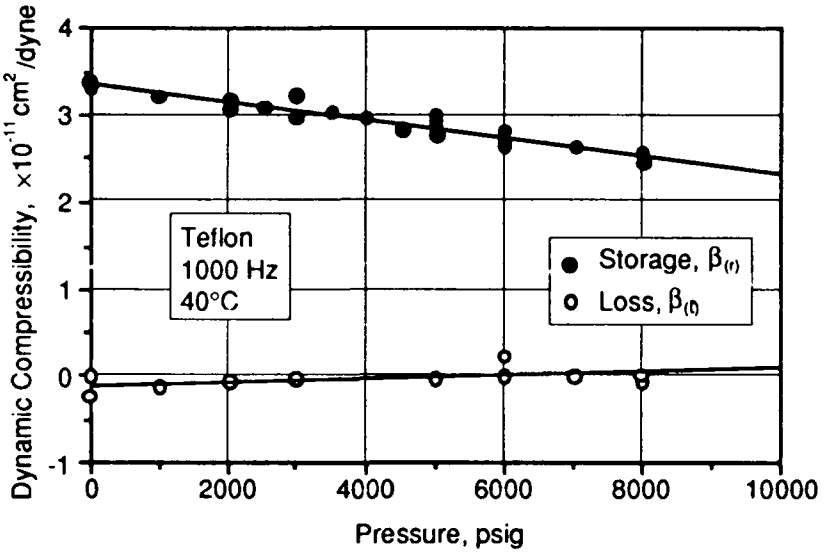


**Figure 4–15** TEFLON. DYNAMIC COMPRESSIBILITY VS. PRESSURE. 40°C.

AS-89-1554

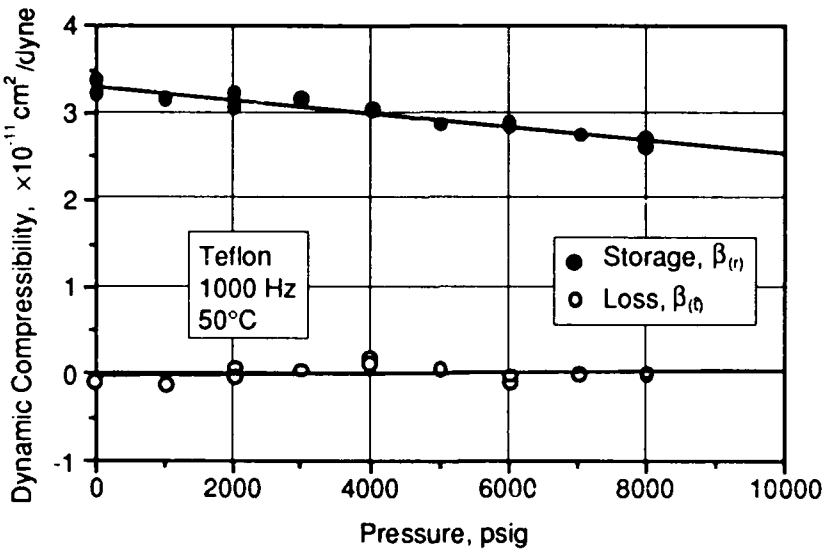


**Figure 4–16** TEFLON. DYNAMIC COMPRESSIBILITY VS. PRESSURE. 50°C.

AS-89-1555

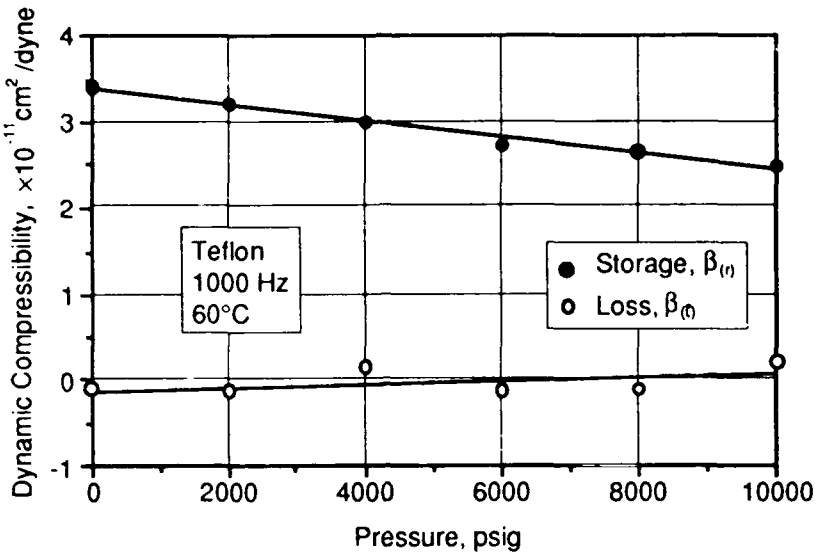


Figure 4-17 TEFLON. DYNAMIC COMPRESSIBILITY VS. PRESSURE. 60°C.

AS-89-1556

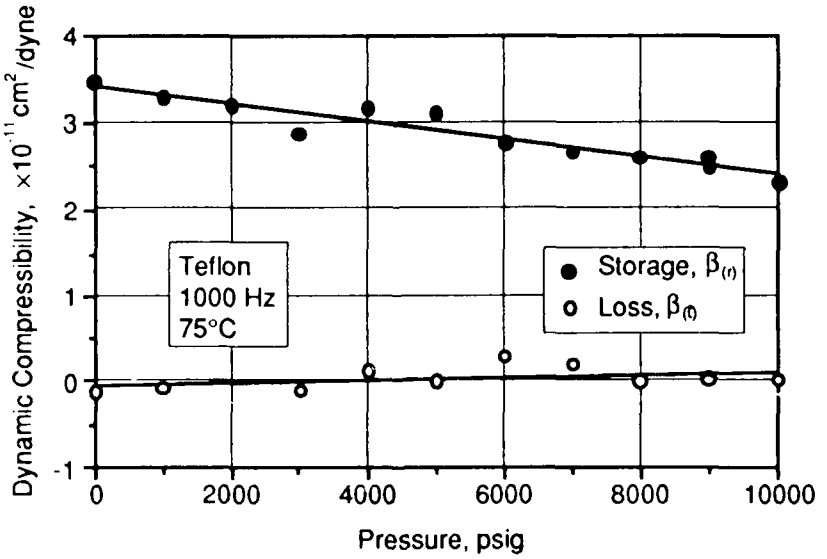


Figure 4-18 TEFLON. DYNAMIC COMPRESSIBILITY VS. PRESSURE. 75°C.

AS-89-1557

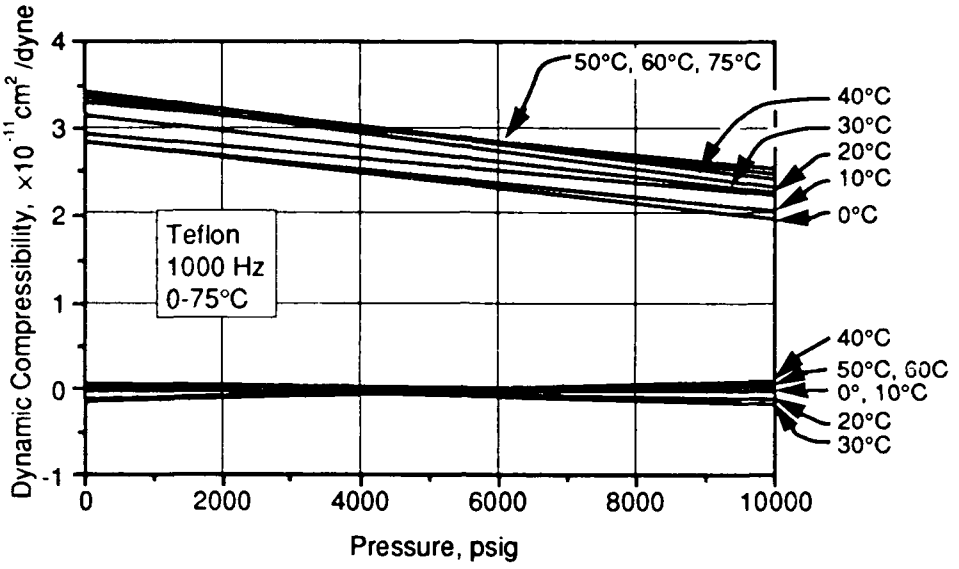


**Figure 4–19** TEFLON. SUMMARY OF DYNAMIC COMPRESSIBILITY VS. PRESSURE.

AS-89-1558

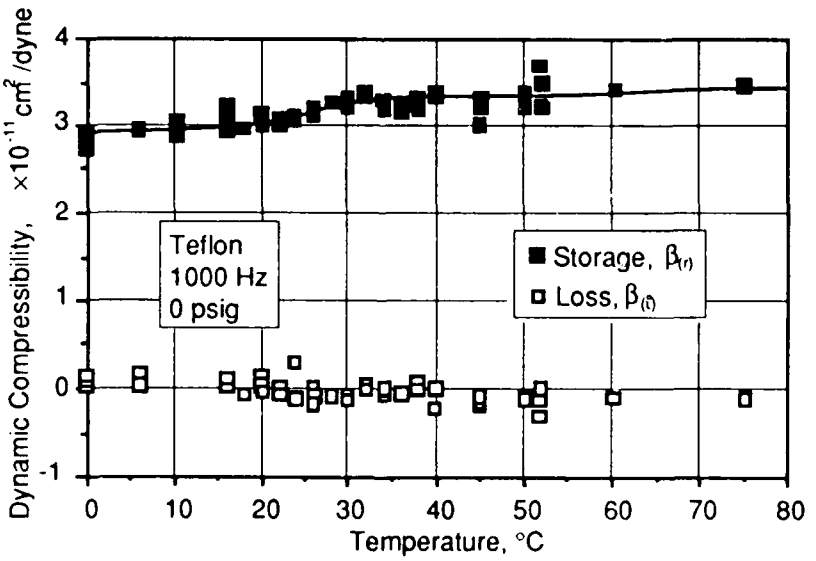


**Figure 4-20** TEFLON. DYNAMIC COMPRESSIBILITY VS. TEMPERATURE. 0 PSIG.

AS-89-1559

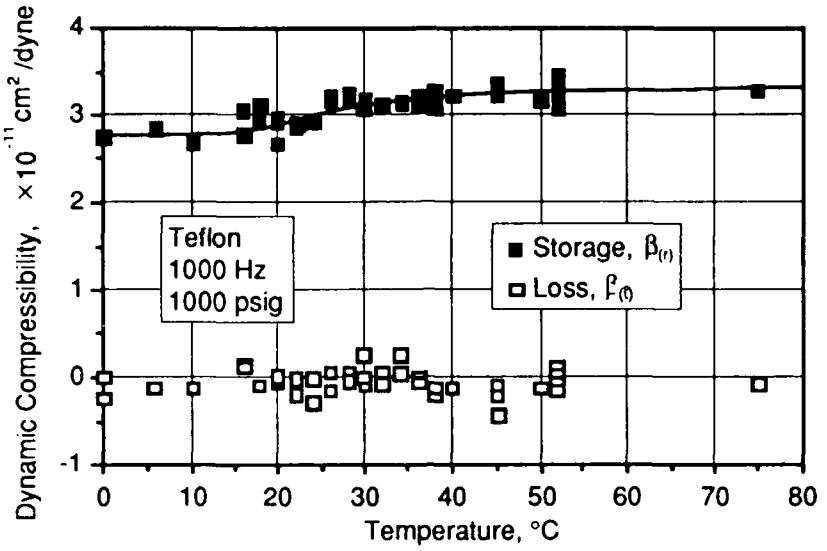


**Figure 4–21** TEFLON. DYNAMIC COMPRESSIBILITY VS. TEMPERATURE. 1000 PSIG.

AS-89-1560

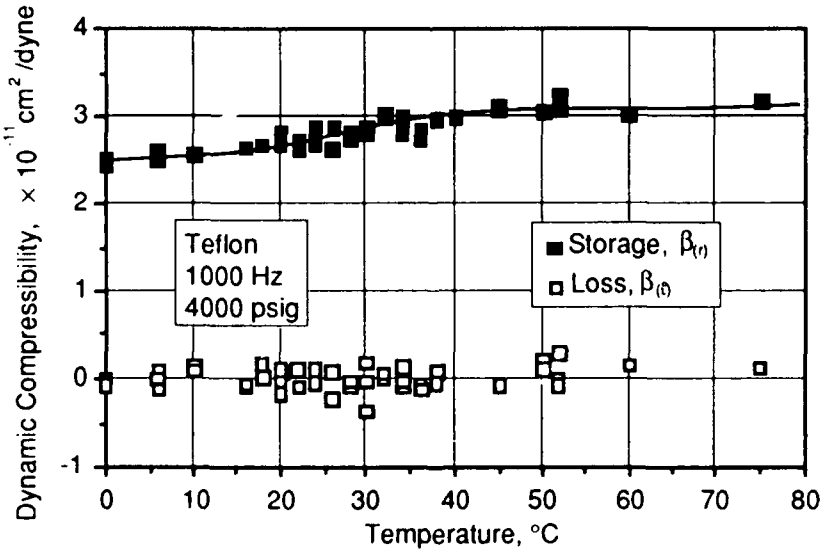


**Figure 4–22** TEFLON. DYNAMIC COMPRESSIBILITY VS. TEMPERATURE. 4000 PSIG.

AS-89-1561

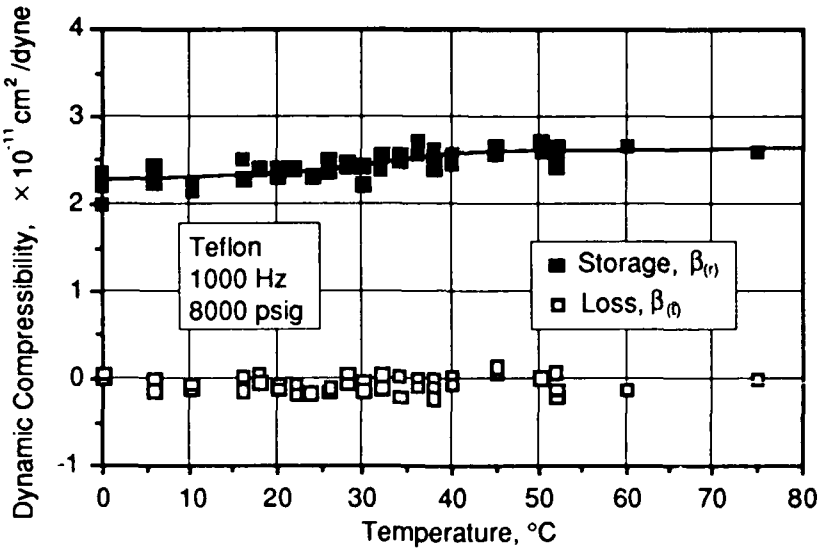


**Figure 4–23** TEFLON. DYNAMIC COMPRESSIBILITY VS. TEMPERATURE. 8000 PSIG.

AS-89-1562

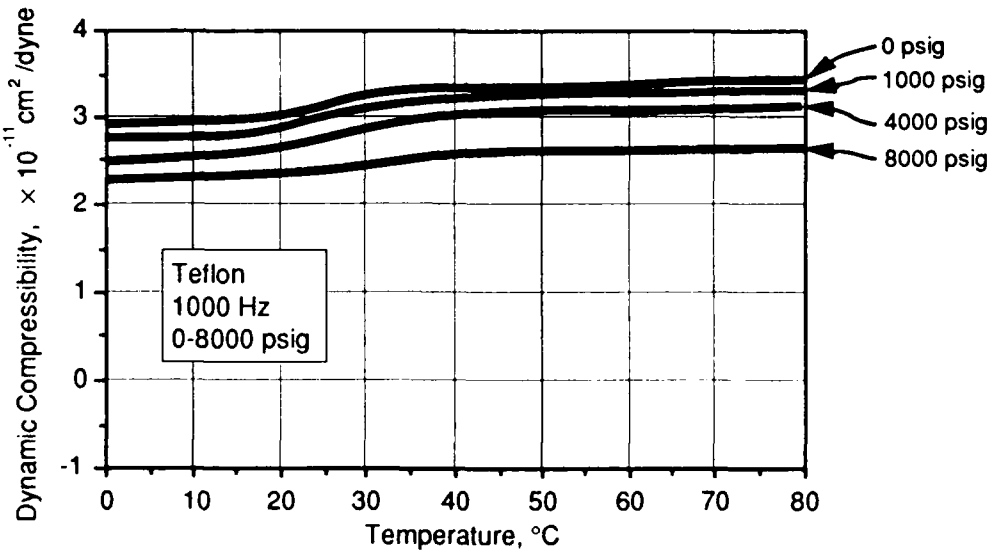


**Figure 4–24** TEFLON. SUMMARY OF DYNAMIC COMPRESSIBILITY VS. TEMPERATURE.

AS-89-1563

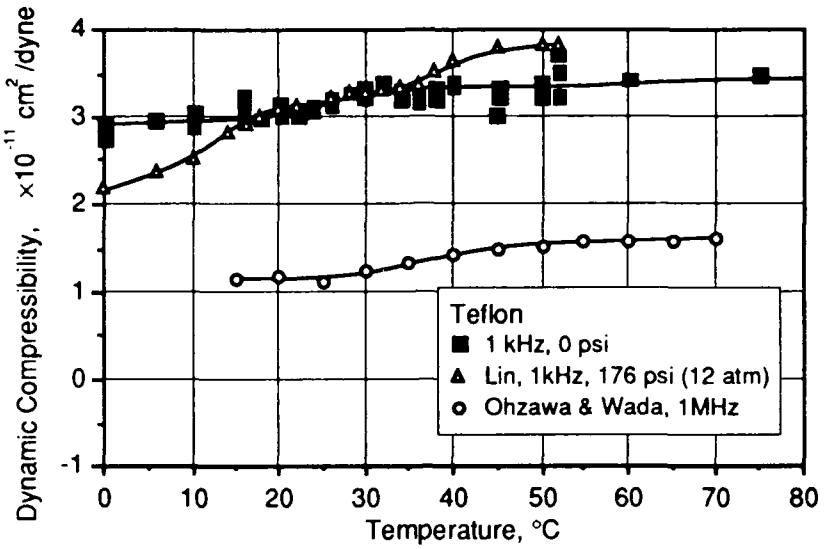


**Figure 4-25** TEFLON. DYNAMIC COMPRESSIBILITY VS. TEMPERATURE. DATA COMPARED TO THAT REPORTED BY LIN AND OHZAWA AND WADA.

AS-89-1564

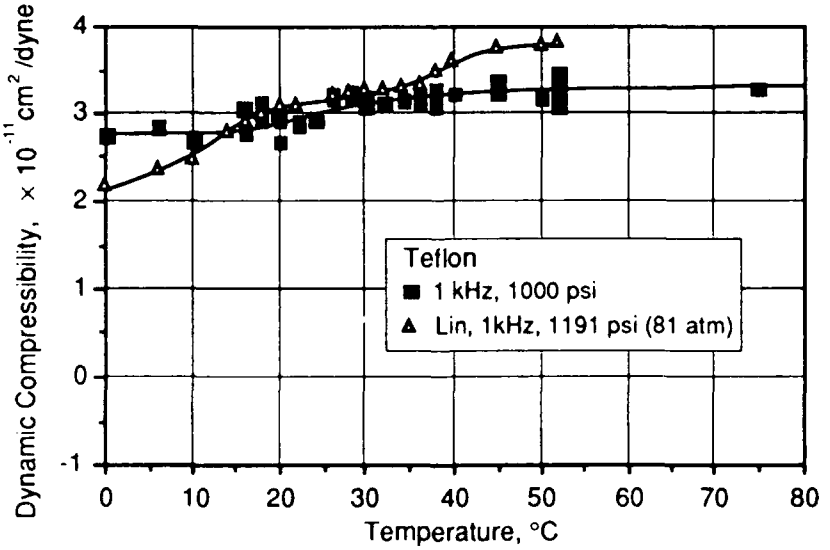


**Figure 4-26** TEFLON. DYNAMIC COMPRESSIBILITY VS. TEMPERATURE. DATA COMPARED TO THAT REPORTED BY LIN.

AS-89-1565

We again see the expected changes with temperature and pressure. The temperatures are well below $T_g$, so there is no dispersion (except possibly in the vicinity of solid state phase changes),[15] and, subsequently, the magnitude of $\beta_{(i)}$ values is rather low. However, between 20° and 30°C there is an abrupt change in slope in the $\beta_{(r)}$ versus temperature curve, and on either side of this region, the slope is about the same. The changes in slope correspond to the solid state phase changes discussed by Ohzawa and Wada,[15] Weir,[13] Beecroft and Swenson,[16] and others. The region where the transitions occur moves to higher temperatures for higher pressures. The slope change is more pronounced at lower pressures (and temperatures). This is all suggested by Weir's data and Teflon phase diagram.[13] Unfortunately, the scatter is very large for our set of Teflon runs and no general conclusions can be made for the *loss* part of the compressibility, though others have reported finding an inflection in the loss part at between 20° and 40°C.[3,15] Again, suggestions in Chapter 5 may help improve the precision so that scatter is not so much a problem.

For comparison of real (storage) compressibility values, $\beta_{(r)}$, we turn first to Ohzawa and Wada.[15] They report $\vec{K}$ (dynamic bulk modulus) versus temperature for a specimen of 100% crystallinity at 1 MHz (and presumably at atmospheric pressure). Recall $\vec{K} = 1/\vec{\beta}$. Figure 4-25 contains points scaled from Ohzawa and Wada's plot of $\vec{K}$ versus temperature at 1 MHz and 0 psig plotted as $\vec{\beta}$ versus temperature, as well as data from Lin. Only $\beta_{(r)}$ values appear. The curve made from Ohzawa and Wada's data has the same slope and changes in slope as our data does at 0 psig. The transitions occur at approximately 10°C higher temperature, and the magnitudes are about 40% lower than our data ($1.2 \times 10^{-11}$ cm$^2$/dyne rather than $3.0 \times 10^{-11}$ cm$^2$/dyne at 20°C). We should point out, however, that the facts that their sample was 100% crystallinity and their frequency was 1 MHz can contribute to their lower compressibility. They also reported that their magnitudes may be in error since their sample came in the form of suspended particles whose dimensions were not exactly known. Heydemann[14] reports data for $\beta_{(r)}$ at 20°C and atmospheric pressure for a frequency range of 2 Hz to 10 kHz. It is interesting to note that he found a value of $4.75 \times 10^{-11}$ cm$^2$/dyne that is unaffected by frequency in his range. This value is even higher than that reported here or by Lin.[3] Heydemann does not mention the crystallinity of his sample. It seems that the magnitude of $\beta_{(r)}$ for Teflon varies widely. We expect this is a function of crystallinity. Finally, let us compare Lin's data at 173 psi (12 atm) and 1191 psi (81 atm) to the present data at 0 psi and 1000 psi (68 atm), respectively. Data scaled from Lin appears in Figures 4-25 and 4-26. The real values between 20° and 30°C are identical or nearly so, but

the slope below 20°C and above 30°C on the $\beta_{(r)}$ versus temperature curves are much steeper for Lin's data. Values disagree by nearly 20% at 0°C. We have no immediate explanation for this phenomenon except that perhaps the phases on either side of the 20-30°C range are sensitive to the differences between isothermal (our) and isobaric (Lin's) testing procedures.

The real part of the dynamic compressibility data for Teflon again shows the ability of the apparatus to generate reliable data.

## 4–4 Example of the Advantage of Self-Calibration

At one point during the course of taking runs with the Teflon sample, the transducers experienced a problem in their electrical connections. The result was an effective change in their calibration constituted by a relatively large phase angle and attenuation in the output signal, $\vec{E}^{x}_{out}$. Since the change in calibration was constant for the few minutes necessary to take sets of values $\vec{E}^{T}_{out}$, $\vec{E}^{B}_{out}$, and $\vec{E}^{S}_{out}$ (the output signals with the empty side-chamber (only) on line, both side-chambers on line, and sample side-chamber (only) on line, respectively), the resulting data points were still accurate. For example, we measured the dynamic compressibility, $\vec{\beta}$, of the same Teflon sample at 1000 Hz, 20°C, and 8000 psig before, during, and after the calibration problem. The input voltage for all three cases was approximately 40 $V_{p-p}$. During an early run (in June, 1988) the signals from the output transducer were:

$$\begin{aligned} \vec{E}^{T}_{out} &= 18.19 - \mathring{\imath}\, 0.380 \quad \mu V \\ \vec{E}^{B}_{out} &= 12.15 - \mathring{\imath}\, 0.200 \quad \mu V \\ \vec{E}^{S}_{out} &= 20.28 - \mathring{\imath}\, 0.280 \quad \mu V \quad . \end{aligned}$$

When the $\vec{\beta}$ is calculated from this data using the working equations (Equations 2-4.15 and 2-4.16), we find:

$$\vec{\beta}_{(before)} = (2.36 - \mathring{\imath}\, 0.071) \times 10^{-11} \frac{\text{cm}^2}{\text{dyne}} \quad ,$$

where we used $V_s = 2.754$ cm$^3$, and $V_{MT} = 5.258$ cm$^3$, for the sample and side-chamber volumes, respectively. $\beta_f = 3.494 \times 10^{-11}$ cm$^2$/dyne is the compressibility of DiSebacate at this temperature and pressure. The following January, when the calibration problem first appeared, we took this set of data:

$$\begin{aligned} \vec{E}^{T}_{out} &= 3.278 + \mathring{\imath}\, 1.440 \quad \mu V \\ \vec{E}^{B}_{out} &= 2.430 + \mathring{\imath}\, 0.940 \quad \mu V \\ \vec{E}^{S}_{out} &= 4.170 + \mathring{\imath}\, 1.705 \quad \mu V \end{aligned}$$

$$\vec{\beta}_{(during)} = (2.32 - \mathring{i}0.148) \times 10^{-11} \frac{\text{cm}^2}{\text{dyne}} \quad .$$

Several days later we repaired the transducer and took the following data point:

$$\begin{aligned} \vec{E}^T_{out} &= 13.15 - \mathring{i}\ 0.180 \quad \mu\text{V} \\ \vec{E}^B_{out} &= 8.765 + \mathring{i}\ 0.015 \quad \mu\text{V} \\ \vec{E}^S_{out} &= 14.64 - \mathring{i}\ 0.110 \quad \mu\text{V} \end{aligned}$$

$$\vec{\beta}_{(after)} = (2.37 - \mathring{i}0.094) \times 10^{-11} \frac{\text{cm}^2}{\text{dyne}} \quad .$$

This high degree of reproducibility regardless of changes in the calibration of the transducers displays the virtues of a self-calibrating apparatus to measure dynamic compressibility.

# CHAPTER 5

## Recommendations

This Chapter is a list of suggested modifications for the apparatus. The suggestions either aim at improving the accuracy and reproducibility of the data or making the apparatus easier to use. Many of these suggestions are particular to this equipment, while some affect the basic design of the chamber itself.

- **Stack transducers:** The use of a stack of piezoelectric disks for the input transducer (rather than a single disk) may raise the signal level of the output. The stack of disks (wired in parallel) would yield a larger volume displacement for a given input voltage (there would be an accompanying increase of input current which is not a factor in our working equations). For a given input voltage amplitude, there would be a higher input pressure amplitude resulting in a higher output pressure and therefore a higher output voltage amplitude. The larger signal could raise the output level significantly without raising the level of background mechanical and electrical noise. A secondary advantage would be the decrease in volume of the main chamber, $V_{CH}$. The smaller $V_{CH}$ would lead to a larger main chamber impedance, $\vec{Z}_{CH}$, and thus lower the significance of the $\vec{Z}_{CH}$ branch relative to the $\vec{Z}_s$ (sample impedance) branch in Figure 2-3. The end result, again, is a more accurate measurement of $\vec{Z}_s$ and therefore of the sample's compressibility. Notice that an output transducer stack wired in parallel would not be useful since it would only result in an increase in electrical current in the output transducer and, again, current does not appear in our working equations. An output transducer should offer high acoustic resistance (low compressibility), and high output voltage. A larger ceramic piezoelectric disk (or, equivalently, a stack configured and wired in series) may yield a higher output signal, but one must remember that the amplitude of the mechanical part of background noise would be higher also.

A transducer stack can be mounted in much the same way as a single disk. In the case of an even number of stacked disks (both outside ends of the same polarity), a positive lead may be soldered to the feed-through. The ground can be made using two 'handlebar mustache' springs, as in Figure 5–1. This change would not require changes in the current software.

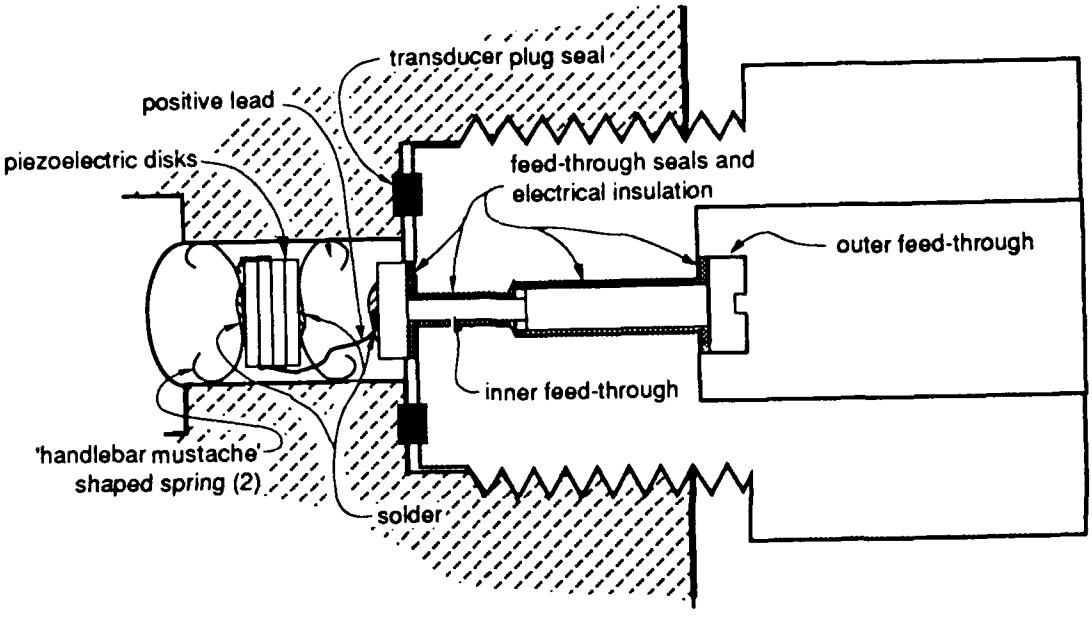


**Figure 5–1** ENLARGED CROSS SECTIONAL VIEW OF SUGGESTED MOUNTING FOR STACKED TRANSDUCERS. SCALE IS 2:1. AS-89-1566

- **HPIB compatible frequency counter:** An HPIB compatible counter would allow frequency to be measured directly through the software. With this, the software can be changed to take data for several frequencies automatically during a run. (Recall that the function generator frequency can be adjusted with a DC control voltage.) Once other changes allow more precise data to be taken, this would allow compensation for $L_n$ and $R_n$ as suggested in Subsection 2-5.3.

- **Different pressure fluids:** Any non-conducting pressure fluid whose compressibility is known as a function of temperature and pressure can be used. DiSebacate generally fits these criteria, but is a commercial plasticizer and

reacts with many forms of polyurethane. Different pressure fluids have different sound speeds (affecting upper frequency limit), viscosity (affecting $R_n$ (see Subsection 2-5.3)), and chemical make-up. All of these must be taken into account. In addition, care must be taken to remove all the old pressure fluid from the system. We found it easiest to disassemble each piece of equipment on the pressure side of the fluid separator and flush them with acetone. We also filled and emptied the pressure fluid side of the fluid separator itself several times with acetone in order to dilute residue from the old fluid. **Electrically conducting fluids:** To use electrically conducting pressure fluids, one must insulate the feed-through connector and the positive face of the transducer. One method would be to paint the feed-through and positive face of the transducer. The paint would have to be flexible enough not to chip while the positive lead/mount wire flexes—especially during assembly into the body of the chamber. Also, the paint would have to resist chemical activity with the fluid. Another possibility is a light rubber coating. The compliance of the coating would be accounted for in the impedance of the chamber, $\vec{Z}_{CH}$, which is found by experiment in the current working equations. **Use of mercury:** At first mercury seems ideal for this application: it has a very high sound speed (therefore higher frequencies may be used), and is not very compressible (making the impedance of the sample, $\vec{Z}_s$, a relatively small (and therefore important) impedance in the parallel circuit in Figure 2-3). The specific acoustic impedance of mercury, though, is approximately 20 MPa$\frac{s}{m}$, while it is only 40 MPa$\frac{s}{m}$ for stainless steel. Therefore it would be pertinent to examine the effects of coupling between the mercury and the walls of the chamber before using mercury as the pressure fluid. With mercury, the door may not be effective in closing off the side-chambers.

- **Improve fluid separator:** The fluid separator is basically a large diameter U-tube. If the mercury in the bottom is pumped too far it may get into the chamber. Also, hydraulic pump oil may get past the mercury into the pressure fluid. The mercury level can be tested by making and installing one or more short-out sensors. The sensors would consist of exposed wires protruding from electrically insulating high-pressure plugs at different heights inside the chamber. When the sensor is shorted to the fluid separator by the mercury, an alarm sounds. One such sensor is in place, but is unreliable because the mercury does not always wet the exposed stainless steel wire. Since building the sensor we have found the *tinned* wire makes the best short-out lead (tin-lead solder is wetted by mercury). This wire has a two-

fold advantage. First of all, it assures electrical contact with the mercury. Second, the wetted wire helps re-combine globules of mercury surrounded by an electrically insulating film of pressure fluid.

- **More sophisticated temperature control:** The current software temperature control loop is a thermostatic controller which responds to temperatures in the chamber via the thermistor. There is some lag between the actual temperature of the bath and the thermistor reading in the wall of the chamber, resulting in overshoot. The temperature may be kept within a smaller tolerance with a control function that accounts for this lag. In addition, the current temperature control loop is only present in the data taking and reducing programs. The printing and plotting programs simply instruct the user to turn the bath off while they are in use. Adding temperature control loops to these programs would require little modification.

- **Cam design:** The current design includes two opposing, rotating cams – one mounts on each side-chamber packing nut. They are designed to pull the doorstem (the part of the door which protrudes into the packing nut (see Figure 3–2)). The one on the sample side-chamber packing nut pulls the door shut on the sample side-chamber, and, similarly, the cam on the empty side-chamber side pulls the door shut there. The closing force is regulated by adjusting the tension on automobile valve springs inside the cams. These cams can be accidentally set to pull in both directions at once—possibly stripping the threads on the doorstem. A better cam would push and pull on one stem. Such a cam would need to include: 1) a double surface cam and follower (e.g., a grooved, helical track such as screw threads), 2) a way to adjust the closing force on both side-chambers, and 3) a way to assure the door is in the mid-position when not closed. **Materials:** The current cams are made of aluminum only because it is easy to machine. If a new cam or cams are made, they could include replaceable or more durable wear surfaces.

  Another door closing method altogether would involve hooking pneumatic pistons to the doorstems. Air under pressure (supplied by air-line facilities in the building) could drive the pistons which in turn could be used to move the door and to provide the necessary closing force. The air could be controlled by low voltage solenoid-type valves which, in turn, could easily be controlled by computer software through the low voltage DC equipment on the HPIB bus.

One should remember that too high a closing force may strip the threads on the doorstem. Also it is possible for the doorstem to bend in a buckling mode if the closing force pushes the doorstem, and to yield (and therefore reduce its cross-sectional area possibly causing the doorstem seals to leak) if the closing force pulls on the doorstem. These latter forces are rather large (on the order of 500 lbf (2200 N)) but could be obtained accidentally. Finally, notice in Figure 3-2 that the doorstem protrudes into a relatively deep hole inside the side-chamber packing nut. A longer shaft (about equal in diameter to the hole) must be attached to the doorstem in order to move the door. This is to keep any bending forces from being applied directly to the door.

# CHAPTER 6

## Summary and Conclusions

This thesis is the result of a project in which we designed and developed a new, self-calibrating apparatus to measure the adiabatic dynamic compressibility (abbreviated here as simply *compressibility*) of polymers such as those used in sonar transducers. The apparatus can determine compressibility at temperatures between approximately 0° and 80°C, pressures between atmospheric and 10,000 psig (680 atm), and frequencies which depend on the sound speed in the pressure fluid (generally less than 2000 Hz). The project is examined from three aspects: the theory behind the new design, the design of the apparatus, and the results of tests performed on sample polymers which have been tested by other researchers using other means. There is also a chapter which recommends changes that would help improve the accuracy and reproducibility of data, and make the apparatus easier to operate.

The theories and equations behind the design of the chamber are in Chapter 2. The basic approach is to use a chamber which is small compared to a wavelength. In similar designs using this approach, [3-6,14] the chamber includes input and output transducers, and a place for a sample. The input transducer, often a piezoelectric disk, is used to essentially create cyclical changes in pressure inside the chamber. The output of the output transducer is influenced by the presence of the sample, and the sample's compressibility can be determined by this influence. With this basic design, a *single chamber* design, three sets of data must be taken--one with the unknown sample in the chamber, and two others for calibration. Each set requires depressurizing and disassembling the chamber. It is often hard to get good data with this process since the properties of transducers may change when they are depressurized and pressurized again. Our chamber improves on this design in that the space for the sample is a *side-chamber*, separate from the rest of the chamber. There are two side-chambers which share a *door*. We use this door to shut off the side-chambers from the rest of the chamber--essentially removing the sample. The door allows us to

make calibration runs without opening the chamber or changing the pressure. In this sense, our chamber is *self-calibrating.* We begin Chapter 2 with an overview of dynamic compressibility in polymers. We then move on to draw a lumped element analogy between the objects in the chamber and lumped electric circuit elements. Using this analogy, we derive working equations and solve them for the compressibility of the sample. The analogy involves assumptions as to the size of the chamber relative to the wavelength, and assumptions that the side-chambers can be modeled as simple capacitors. We close Chapter 2 by using experimental data to verify the validity of these assumptions for frequencies within a practical range. The maximum operating frequency depends on the speed of sound in the pressure fluid.

The design of the chamber and supporting apparatus is described in Chapter 3. The final design involves a main-chamber straddled by two side-chambers. A single door is between them and is operated by pushing or pulling on doorstems which protrude from the door, through the wall of either side-chamber, through packing, and into the outside world. The door can close off either side-chamber or be left open. The supporting apparatus includes equipment to control static pressure, temperature, input and output signals, and computer equipment to handle data. There is vacuum and pressure equipment to evacuate, fill, and impose static pressures on the chamber using a pressure fluid. The temperature of the chamber is controlled with a temperature bath, circulating pump, and a tight-fitting aluminum temperature jacket for the chamber. The bath is controlled by computer software interacting with a thermistor imbedded in the chamber wall. The input AC signal is supplied by a function generator and stepped up through a transformer to approximately 40 $V_{p-p}$. The output is fed into a lock-in amplifier for amplitude and phase detection. The computer and accompanying software control as much of the data taking process as possible using an HPIB bus and a make-shift analog-to-digital and digital-to-analog converter system (for equipment which communicates with DC control voltages). Chapter 3 contains a brief summary of the data taking procedure. Our procedure involved isothermal measurements taken at pressures stepped in 500, 1000, or 2000 psi increments.

The results and conclusions are in Chapter 4. We measured poly(vinyl acetate) (PVAc), and polytetrafluoroethylene (PTFE, or Teflon). We compare these results and trends to data collected by Lin,[3] McKinney and Belcher,[7] and others.[13–15] PVAc data is close in magnitude to that taken by Lin,[3] and McKinney and Belcher,[7] and follows the same trends. The real part of Teflon data also is like others' and follows the same trends. We conclude that, overall, the apparatus yields reliable, useful data. In the last section of Chapter 4, we discuss a set of data which clearly displays the advantage of a self-calibrating apparatus.

# APPENDIX A

## Sound Speed in DiSebacate

The fluid used in the measurements for this report was Di(2 ethyl hexyl) sebacate, abbreviated DiSebacate. We present here some previously unpublished data from a related experiment involving the approximate plane wave sound speed, $c_o$, in DiSebacate as a function of pressure and temperature. The experimental apparatus consisted of a stainless steel bar (assumed rigid) 2.5 inches long and 2 inches in diameter with a 3/8 inch hole drilled through the 2.5 in. dimension (see Figure A–1). Piezoelectric disks, one acting as a source, the other as a detector, were mounted approximately 0.10 inch inside 0.16 inch deep recesses in two stainless steel end caps. The end caps contained two valves: one led to a hydraulic pump, the other to a vacuum pump. The whole apparatus was contained in a temperature controlling jacket. The apparatus was filled under vacuum, pressurized, and allowed to come to an equilibrium temperature overnight. The tube was excited at its second harmonic (determined by the lowest frequency at which there was a zero-phase amplitude peak). The results in Figure A–2 were found by assuming the wavelength was the distance between the ends of the recesses in the end caps, approximately 2.82 inches.

Unfortunately the original intention of this apparatus was not to determine sound speed. As a result, the 2.82 inch dimension was not measured accurately, and the data was only taken to 20°C, since higher temperatures and an accurate account of the chamber length were not important at the time this data was taken. The dimension between transducers could be off by as much as 0.1 in., or 4%, and, subsequently, the values of $c_o$ in Figure A–2 may be as much as 4% off for this reason alone. Another possible source of error is the presence of the transducer disks in the waveform, as depicted in Figure A–1. The data shows, as one might expect, that sound speed increases with pressure, and decreases with increasing temperature. At less than 2000 psig, the sound speed decreases uniformly at about 30 m/s per 10°C. If we can assume this trend continues up to 80°C (the upper limit of our data and far below the boiling point of DiSebacate

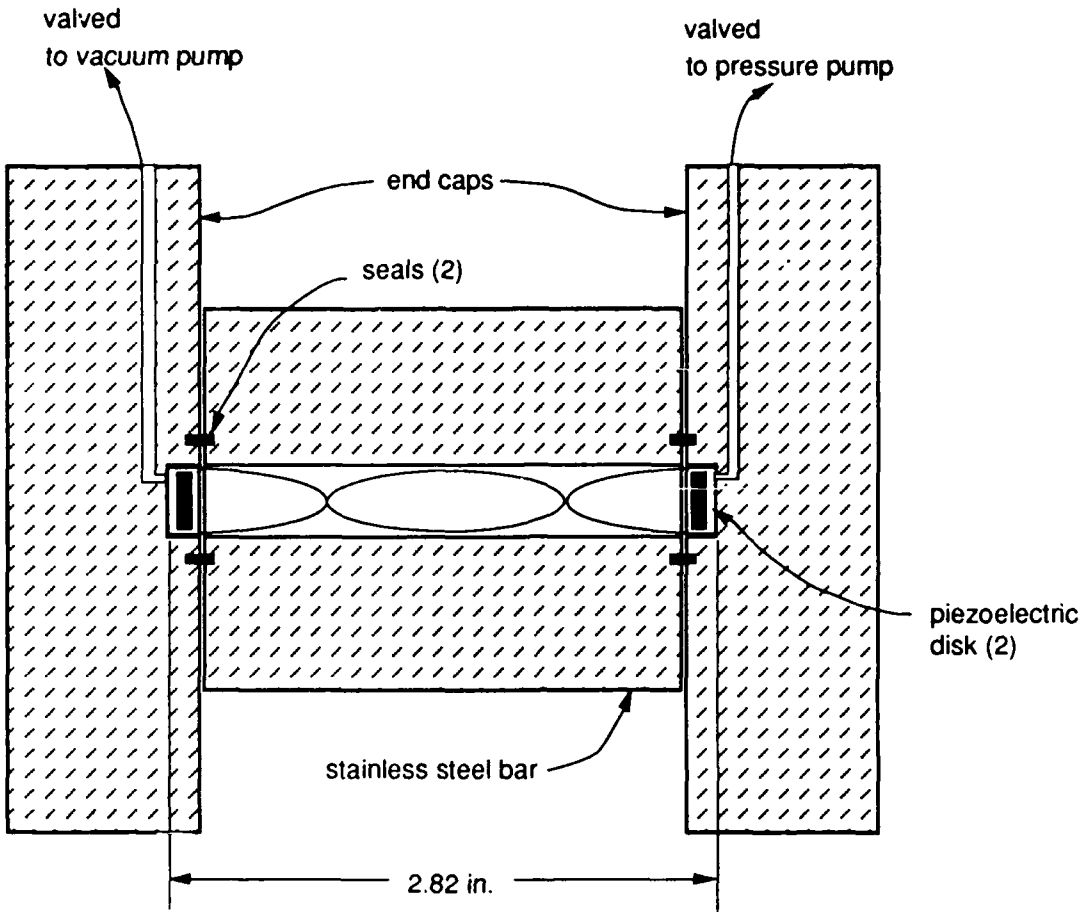


**Figure A–1** TWO-AND-ONE-HALF INCH PLANE WAVE TUBE. DRAWN TO SCALE.

AS-89-1567

which is over 200°C at room pressure), this would place the minimum sound speed at between 1200 m/s and 1300 m/s (80°C and atmosphere pressure).

As a check we use the relation between compressibility, density, and linear sound speed for non-lossy, homogeneous fluids:[12]

$$\beta = \frac{1}{\rho_o c_o^2} \quad \text{or} \quad c_o = \sqrt{\frac{1}{\beta \rho_o}},$$

(this can be calculated from Equation 1–1 since G≅0 for liquids). Manufacturers specifications show the specific gravity of DiSebacate at 25°C and atmospheric pressure is about 0.913 giving a density of $\rho_o = 0.910$ g/cm$^2$. Unpublished data from McKinney[20] reports the adiabatic compressibility as $\beta_f = 4.878 \times 10^{-11}$ cm$^2$/dyne. Using this relation and data point we find $c_o = 1501$ m/s (at atmospheric pressure and 25°C). Figure A–2 yields approximately 1433 m/s at 20°C

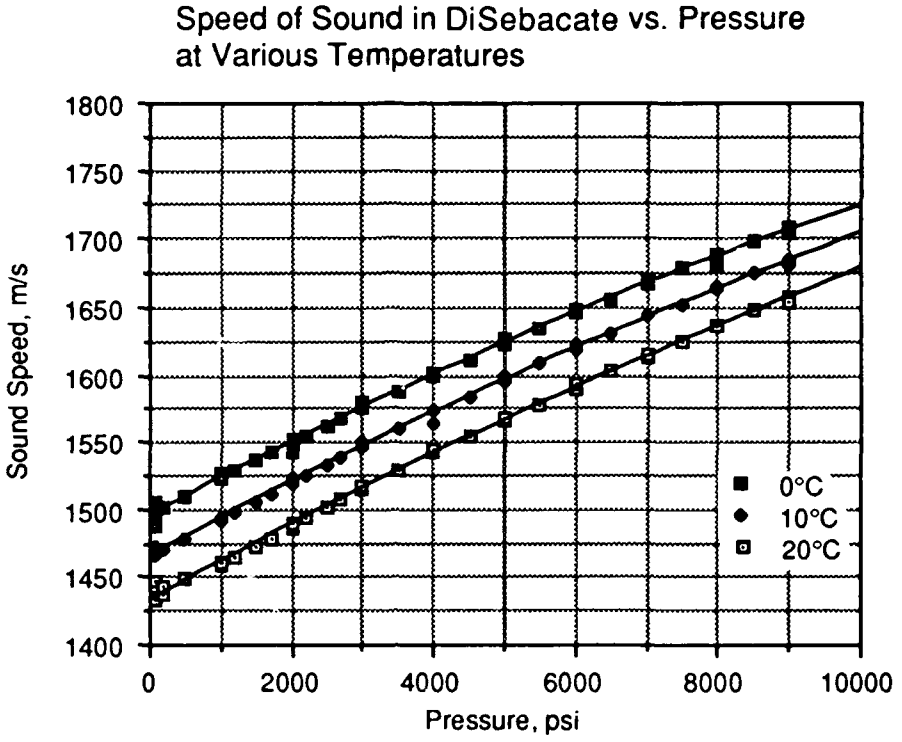


**Figure A–2** APPROXIMATE LINEAR, ADIABATIC SOUND SPEED IN DI(2 ETHYL HEXYL)SEBACATE AS A FUNCTION OF PRESSURE AT VARIOUS TEMPERATURES

AS-89-1568

and atmospheric pressure. Extrapolating to 25°C gives us 1418 m/s, a 6% discrepancy.

## REFERENCES


[1] Lawrence E. Kinsler *et al., Fundamentals of Acoustics, 3rd ed.* (John Wiley & Sons, Inc., New York, 1982).

[2] Harkrishan Singh and A. W. Nolle,"Pressure Dependence of the Viscoelastic Behavior of Polyisobutylene," J. Appl. Phy. 30, No. 3, 337 (1959).

[3] Tien-Sheng Lin, "Dynamic Compressibility of High Polymers," Applied Research Laboratories Technical Report No. 85-12 (ARL-TR-85-12), Applied Research Laboratories, University of Texas at Austin (1985).

[4] John E. McKinney, Seymour Edelman, and Robert S. Marvin, "Apparatus for the Direct Detection of Dynamic Bulk Modulus," J. Appl. Phys. 27, 425 (1956).

[5] Hajime Tanaka, Toshio Nishi, and Yasaku Wada, "New Instrument for Measuring Complex Adiabatic Compressibility and Adiabatic Pressure-Induced Temperature Variation in the Frequency Range from 0.5 Hz to 2 kHz," Rev. Sci. Instrum. 57, No. 10 (1986).

[6] Jay Burns, Peiter S. Dubbelday, and Robert Y. Ting, "Bulk Modulus of Elasticity of Various Elastomers: Theory and Experiment," NRL Report No. 5991, Naval Research Laboratory, Washington, D.C. (1987).

[7] John E. McKinney and Harriet Vera Belcher, "Dynamic Compressibility of Poly(Vinyl Acetate) and Its Relation to Free Volume," J. Res. Nat. Bur. Stand. 67, 43 (1963).

[8] Kenneth M. Ralls, Thomas H. Courtney, and John Wulff, *An Introduction to Materials Science and Engineering* (John Wiley & Sons, Inc., New York, 1976).

[9] John D. Ferry, *Viscoelastic Properties of Polymers* (John Wiley & Sons, Inc., New York, 1980).

[10] Warren P. Mason, Ph.D., *Electrical Transducers and Wave Filters, 2nd ed.* (D. van Nostrand Co., Inc., New York, 1948).

[11] John E. McKinney and Robert Lindsay, "Density and Compressibility of Liquids," in *American Institute of Physics Handbook, 3d ed.*, ed. Dwight E. Gray (McGraw-Hill Book Company, Inc., New York, 1972).

[12] Charles E. Weir, "Transitions and Phases of Polytetrafluoroethylene (Teflon)," J. Res. Nat. Bur. Stand. 50, 95 (1953).

[13] P. Heydemann, "The Dynamic Compressibility of High Polymers in the Frequency Range from .1 c/s to 60kc/s," Acustica 9, 446 (1959).

[14] Yoshiyuki Ohzawa and Yasaku Wada, "Mechanical Relaxations and Transmitions in Polytetrafluoroethylene," Japan. J. Appl. Phys. 3, 436 (1964).

[15] R. I. Beecroft and C. A. Swenson, "Behavior of Polytetrafluorocthylene (Teflon) under High Pressures," J. Appl. Phys. 30, 1793 (1959).

[16] J. E. McKinney and M. Goldstien, "PVT Relations for Liquid and Glassy Poly(vinyl acetate)," J. Res. Nat. Bur. Stand. 78A, 331 (1974).

[17] G. M. Martin and R. K. Eby, "Effect of Low Pressures on the Room Temperature Transitions of Polytetrafluoroethylene," J. Res. Nat. Bur. Stand. 72A, 467 (1968).

[18] P. Zoller, "The Specific Volume of Poly(tetrafluoroethylenc) as a Function of Temperature (30°-372°C) and Pressure (0-2000 kg/cm$^2$)," J. Appl. Poly. Sci. 22, 633 (1978).

[19] J. E. McKinney, personal communication. Dynamic compressibility data for Di(ethyl hexyl)sebacate. The data were based on measurements of equilibrium $P$, $V$, $T$ values and of specific heat at constant (effectively zero) pressure. The adiabatic compressibility at zero pressure was obtained from these results by standard thermodynamic formulae. The ratio of adiabatic to isothermal compressibility at a given temperature was considered to be the same (to sufficient accuracy) at pressures up to 1000 atm as for zero pressure.

29 November 1989

# DISTRIBUTION LIST FOR ARL-TR-89-53 UNDER ARL:UT INDEPENDENT RESEARCH AND DEVELOPMENT PROGRAM

| Copy No. | |
|---|---|
| | Superintendent<br>Naval Research Laboratory<br>Underwater Sound Research Division<br>P.O. Box 568337<br>Orlando, FL 32856-8337 |
| 1 | Attn: J. Blue |
| 2 | R. Ting |
| 3 | P. S. Doubleday |
| 4 | C. M. Thompson |
| 5 | Library |
| | Commanding Officer<br>Naval Ocean Research and Atmospheric Laboratory<br>Stennis Space Center, MS 39529-5000 |
| 6 | Attn: Library |
| | Office of the Chief of Naval Research<br>Department of the Navy<br>Arlington, VA 22217-5000 |
| 7 | Attn: M. Orr |
| 8 | Library |
| | Office of the Chief of Naval Research<br>Office of Naval Technology<br>Department of the Navy<br>Arlington, VA 22217-5000 |
| 9 | Attn: Library |
| | Commander<br>Naval Sea Systems Command<br>Department of the Navy<br>Washington, D.C. 20362-5101 |
| 10 | Attn: J. Koegler (Code 55N) |
| 11 | E. Plummer (Code 63D1) |
| 12 | Library (Code 9961) |
| | Commander<br>Naval Air Systems Command<br>Department of the Navy<br>Washington, D.C. 20361-5460 |
| 13 | Attn: Code 933B |
| | Director<br>Naval Research Laboratory<br>Washington, D.C. 20375 |
| 14 | Attn: R. D. Corsaro (Code 5135) |
| 15 | Library |

Distribution List for ARL-TR-89-53 under ARL:UT Independent Research and Development Program
(cont'd)

| Copy No. | |
|---|---|
| | Commanding Officer<br>Naval Ocean Systems Center<br>San Diego, CA 92152-5000 |
| 16 | Attn: Library |
| | Commanding Officer<br>Naval Surface Warfare Center<br>White Oak Laboratory<br>Silver Spring, MD 20910 |
| 17 | Attn: Library |
| | Commanding Officer<br>Naval Surface Warfare Center<br>10901 New Hampshire Ave.<br>Silver Spring, MD 20903-5000 |
| 18 | Attn: W. M. Madigosky |
| | Commander<br>David Taylor Research Center<br>Bethesda, MD 20084 |
| 19 | Attn: J. J. Dlubac (Code 1945) |
| 20 | B. Douglas (Code 0113) |
| 21 | R. Loesch (Code 1908) |
| 22 | S. J. McKeon (Code 1908) |
| 23 | J. M. Niemiec (Code 1945) |
| 24 | S. C. Schreppler (Code 1945) |
| 25 | Library |
| | Commanding Officer<br>Naval Oceanographic Office<br>Stennis Space Center, MS 39522-5001 |
| 26 | Attn: Library |
| | Commanding Officer<br>Naval Air Development Center<br>Warminster, PA 18974 |
| 27 | Attn: Library |

Distribution List for ARL-TR-89-53 under ARL:UT Independent Research and Development Program
(cont'd)

| Copy No. | |
|---|---|
| | Office in Charge<br>Naval Underwater Systems Center<br>New London Laboratory<br>New London, CT 06320 |
| 28 | Attn: A. Bruno (Code 44) |
| 29 | R. Kasper (Code 44) |
| 30 | M. Moffett (Code 3111) |
| 31 | B. McTagget |
| 32 | R. P. Radlinski (Code 311) |
| 33 | E. Recine (Code (2133) |
| 34 | M. Ricciuti (Code 332) |
| 35 | Library |
| | Superintendent<br>Naval Postgraduate School<br>Monterey, CA 93943 |
| 36 | Attn: Library |
| | Commanding Officer<br>Naval Coastal Systems Center<br>Panama City, FL 32407 |
| 37 | Attn: Library |
| 38 | Commanding Officer<br>Naval Intelligence Support Center<br>Washington, D.C. 20390 |
| 39-50 | Commanding Officer and Director<br>Defense Technical Information Center<br>Cameron Station, Building 5<br>5010 Duke Street<br>Alexandria, VA 22314 |
| | Officer in Charge<br>Naval Underwater Systems Center<br>Newport Laboratory<br>Newport, RI 02840 |
| 51 | Attn: B. Sandman (Code 8215) |
| | Applied Research Laboratory<br>The Pennsylvania State University<br>P.O. Box 30<br>State College, PA 16801 |
| 52 | Attn: Library |

Distribution List for ARL-TR-89-53 under ARL:UT Independent Research and Development Program
(cont'd)

Copy No.

Applied Physics Laboratory
The University of Washington
1013 N.E. 40 St.
Seattle, WA 98105
53 Attn: Library

Marine Physical Laboratory
Scripps Institution of Oceanography
The University of California, San Diego
San Diego, CA 92093
54 Attn: Library

Bell Telephone Laboratories, Inc.
Whippany Road
Whippany, NJ 07961
55 Attn: Library

Vector Research
Suite 1200
6903 Rockledge Dr.
Bethesda, MD 20817
56 Attn: W. T. Reader

Department of Physics
Kalamazoo College
Kalamazoo, MI 49007
57 Attn: W. M. Wright

Vibron Limited
1720 Meyerside Dr.
Mississauga, Ontario LST 143
CANADA
58 Attn: S. J. Lind

Atlantic Applied Research Corp.
1129 Middlesex Turnpike
Burlington, MA 01803
59 Attn: S. A. Africk

Cambridge Acoustical Associates, Inc.
54 Cambridge Park Dr.
Cambridge, MA 02140
60 Attn: M. C. Junger

Distribution List for ARL-TR-89-53 under ARL:UT Independent Research and Development Program
(cont'd)

| Copy No. | |
|---|---|
| | Department of Mechanical Engineering<br>The University of Texas at Austin<br>Austin, TX 78712 |
| 61 | Attn: M. Averkou |
| 62 | C. Darvennes |
| 63 | M. Hamilton |
| | Department of Physics<br>The University of Texas at Austin<br>Austin, TX 78712 |
| 64 | Attn: A. W. Nolle |
| 65 | Signal Physics Group, ARL:UT |
| 66 | Garland R. Barnard, ARL:UT |
| 67 | David T. Blackstock, ARL:UT |
| 68 | Charles E. Bradley, ARL:UT |
| 69 | Jimmy F. Byers, ARL:UT |
| 70 | J. T. Cloer, Jr., ARL:UT |
| 71 | George P. Coble, ARL:UT |
| 72-82 | David E. Edmonds, ARL:UT |
| 83 | Glen E. Ellis, ARL:UT |
| 84 | Marshall E. Frazer, ARL:UT |
| 85 | Harlan G. Frey, ARL:UT |
| 86 | James A. Hawkins, ARL:UT |
| 87 | T. G. Muir, ARL:UT |
| 88 | Michael V. Smith, ARL:UT |
| 89 | Ronald O. Stearman, ARL:UT |
| 90 | James E. Stockton, ARL:UT |
| 91 | Deborah A. Summa, ARL:UT |
| 92 | James A. TenCate, ARL:UT |
| 93 | Jacqueline N. Tjøtta, ARL:UT |

Distribution List for ARL-TR-89-53 under ARL:UT Independent Research and Development Program
(cont'd)

| Copy No. | |
|---|---|
| 94 | Sigve Tjøtta, ARL:UT |
| 95 | J. Kenneth Vaughan, ARL:UT |
| 96 | Reuben H. Wallace, ARL:UT |
| 97 | Joseph F. Willman, ARL:UT |
| 98 | Library, ARL:UT |
| 99-111 | Reserve, ARL:UT |